Development of a fabric-based plasmonic sensor for point-of-care diagnostics

By Dalal Saleh Alhatab

A Thesis Submitted to
Saint Mary's University, Halifax, Nova Scotia
In Partial Fulfilment of the Requirements for the Degree of
Masters of Science in Applied Science

April, 2017, Halifax, Nova Scotia

Approved: Dr. Christa L. Brosseau
Associate professor
Supervisor

Approved: Dr. Marc Lamoureux
Associate professor
Committee member

Approved: Dr. Dong Zhongmin
Professor
Committee member

Approved: Dr. Shine (Xu) Zhang
Research chair
External examiner

Date: April 18, 2017

ABSTRACT

Development of a fabric based plasmonic sensor for point-of-care diagnostics

By Dalal Saleh Alhatab

Recently, the demand for new diagnostic techniques for detecting disease biomarkers at the patient point-of-care (POC) has increased. This project focuses on our recent progress towards a fabric-based plasmonic sensor which can be used in conjunction with surface-enhanced Raman spectroscopy to detect target biomarkers in bodily fluids. Building off of our recent success in this area, we have been exploring a variety of different fabric materials for this purpose. This project focused on detecting 6-thiouric acid which has the potential to be an important urine biomarker for the action of 6-mercaptopurine (MP), an immunosuppressive drug. In addition, detection of levofloxacin (fluoroquinolone-antibiotic; widely used for the treatment of bacterial infections, guanine and 2-deoxyguanosine (models of 8-oxo-2-deoxyguanosine, a cancer biomarker) also were performed in this research. Detection of these urine biomarkers focused on the use of electrochemical surface-enhanced Raman spectroscopy (EC-SERS) as well as the fabric-based SERS substrate.

April, 18, 2017

Dedication

I would like to dedicate this work to my husband Khaled Aljermi. There is no doubt in my mind that without his continued support I could not have completed this process. A special feeling of gratitude to my loving parents, Saleh Alhatab and Zohra Khalifa whose words of encouragement and push for tenacity ring in my ears. My brothers and sisters have never left my side and are very special. I dedicate this work to my wonderful children Lamaa, Mohamed, and Jana for being there for me throughout the entire Master's program.

Acknowledgments

I would like to thank Dr. Christa Brosseau for being my research supervisor, and for giving me the opportunity to complete my master's degree in her research group. I would also like to thank Dr. Marc Lamoureux and Dong Zhongmin for being on my supervisory committee and Dr. Shine Xu Zhang for being my external examiner.

I would like to thank Dr. Brosseau group members, especially; Osai Clarke for helping me throughout my master's program and Marwa Yasmin for spending a lot of time training me on Raman Spectroscopy. Also, I would like to thank Xiang Yang for helping me image my samples using SEM.

I would give special thanks to my best friends Dalal, Najwan, Aisha, and Huda for all their support and encouragement.

Finally, I would like to thank the department of Chemistry and the Faculty of Graduate Studies and Research at Saint Mary's University, and the Libyan government for providing me with a scholarship.

Table of Contents page

Abstract II

Dedication III

Acknowledgments IV

Table of Contents VI

List of Figures XI

List of Tables XVII

List of Abbreviations XVIII

Table of Contents

Chapter 1 Introduction……....1
1.1 Preamble 1
1.2 Objectives of the thesis 2
1.3 Scope of thesis 3
Chapter 2 Literature Review……..….....4
2.1 Point-of-care diagnostics 4
2.1.1 Introduction 4
2.1.2 Advances in point-of-care platforms 5
2.1.3 Current limitations 7
2.2 Wearable sensors 8
2.2.1 Design and applications 8
2.2.1.1 Motivation for wearable sensors 11
2.2.1.2 Wearability criteria 11
2.2.1.3 Smart textiles and fabric-based sensors 12
2.2.2 Current limitations 13
2.3 Plasmonic sensors 14
2.3.1 Introduction to plasmonics 14
2.3.2 Applications of Plasmonics 15
2.3.3 Plasmonic sensor design 16
2.3.4 Nanomaterials: Synthesis and Characterization 17
2.3.5 Plasmonic sensors 21
2.3.6 Surface-Enhanced Raman Spectroscopy 22
2.3.6.1 Raman Spectroscopy 22
2.3.6.2 SERS 24
2.3.6.3 Electrochemical SERS sensors 26
2.4 Target biomarkers 29
2.4.1 Choice of biomarkers for SERS-based sensing 29
2.4.2 6-Thiouric acid: A biomarker for chemotherapeutics 29
2.4.3 Levofloxacin: A ubiquitous antibiotic 31

2.4.4 Guanine and 2-deoxyguanosine: A model of 8-oxo-2-deoxyguanosine, a cancer biomarker 32
Chapter 3 Theory and Techniques……34
3.1 Introduction 34
3.2 Electrochemistry: Principles and Applications 34
3.2.1 Introduction..... 34
3.2.2 Double-layer models of the electrified interface 35
3.3 Raman Spectroscopy 37
3.3.1 Theory of Raman Spectroscopy..... 37
3.3.2- Surface-Enhanced Raman Spectroscopy (SERS)..... 39
3.3.3-Electrochemical Surface-Enhanced Raman Spectroscopy (EC-SERS) 41
Chapter 4 Material and Methods…….....44
4.1 Reagents and solutions 44
4.2 Instrumentation..... 45
4.2.1 Electrochemistry 45
4.2.1.1 Preparation of sustainable fabric-based electrode 48
4.2.2 Raman Spectrometer and SERS setup 48
4.2.3 UV-VIS spectrophotometry..... 49
4.3 Selection of Fabric for Sensor Platform 49
4.4 Modification of fabric for SERS 50
4.4.1 AgNP synthesis and characterization 50
4.4.2 Modification of fabric with AgNPs 51
4.4.3 Characterization of plasmonic fabric sensors 51
Chapter 5 Result and Discussion……...52
5.1 Nanoparticle characterizati..... 52
5.1.1 UV-vis spectroscopy..... 52
5.1.2 SEM and TEM of silver nanoparticles 53
5.2 Electrochemical SERS (EC-SERS) investigation of target biomarkers..... 53
5.2.1 Introduction..... 53
5.2.2 EC-SERS of biomarkers of interest..... 54
5.2.2.1 EC-SERS of 6-thiouric acid on SPE 54
5.2.2.2 EC-SERS of levofloxacin on SPE 62
5.2.2.3 EC-SERS of guanine on SPE..... 66

5.2.2.4 EC-SERS of 2-deoxyguanosine on SPE 70
5.2.3 ...Conclusion……70
5.3 Fabric-Based SERS 74
5.3.1 Introduction 74
5.3.2 Fabric selection and characterization 74
5.3.3 Evaluation of SERS performance for 4,4'-bipyridine 76
5.3.3.1 Normal Raman of 4,4'-bipyridine (4,4'-bipy) 76
5.3.3.2 SERS of 1.0 mM 4,4'-bipy, one layer AgNPs on the selected fabrics. 78
5.3.3.3 SEM of fabrics modified with one layer of AgNPs 81
5.3.3.4 SERS of 4,4'-bipy on fabric samples modified with 3 layers of AgNPs... 81
5.3.3.5 SEM of fabrics modified with 3 layers of AgNPs 83
5.3.4 Evaluation of SERS performance of 4-ATP 84
5.3.4.1 Normal Raman of 4-ATP 84
5.3.4.2 SERS of 4-ATP on the selected fabric samples 86
5.3.4.3 SERS of 1.0 mM 4-ATP 3 layers AgNPs with KCl treatment (5 fabrics). 88
5.3.4.4 SERS of 1.0 mM 4,4'-bipy; 3 layers of AgNPs with KCl treatment 91
5.3.4.5 Comparison between blend fabric and silk-based "Fab-Chip" 95
5.3.5 SERS of biomarkers on modified blend fabric 96
5.3.5.1 SERS of 6-thiouric acid on blend fabric 97
5.3.5.2 SERS of levofloxacin on blend fabric 100
5.3.5.3 SERS of guanine on blend fabric 101
5.3.5.4 SERS of 2-deoxyguanosine on blend fabric 103
5.3.6 Conclusion 104
5.4 EC-SERS of biomarkers on Fabric-based electrode 104
5.4.1 Achira fabric-based-electrode characterization 104
5.4.2 EC-SERS of 1.0 mM 4-ATP on Achira fabric-based-electrode 107
5.4.4 EC-SERS of biomarkers on blend fabric-based electrode 112
5.4.4.1 Blend fabric-based-electrode characterization 112
5.4.4.2 EC-SERS of 1.0 mM 6-TUA 114
5.4.5 Conclusion 117
Chapter 6 Conclusions and Future work……..……..118
Chapter 7 References……...121

List of Figures

Figure # **Description** **Page #**

Figure 2.2.1: An example of a smart shirt.[30] 11

Figure 2.2.2: Baby garment prototype for ECG measurement. (Left) inside showing the textrodes; (right) outside.[38] 13

Figure 2.1: Real and imaginary dielectric functions for gold, silver and silicon.[44] 22

Figure 2.4.1: Molecular structure of (a) 6-thiouric acid (b) levofloxacin, (c) guanine 30

Figure 2.4.2: Metabolism of azathioprine (TPMT = thiopurine methyltransferase; XO = xanthine oxidase). 31

Figure 3.1: Illustration of the electrical double layer according to Bockris / Devanthan / Mueller model. 36

Figure 3.2: Types of scattering: Rayleigh, Stokes, and anti-Stokes.[53] 37

Figure 3.3: Schematic illustration of localized surface plasmon resonance on metal nanospheres.[115] 41

Figure 4.2.1: Screen-printed-electrode (left), and Achira fabric-based-electrode (right) ... 46

Figure 4.2.2: Photo of the setup used for EC-SERS, including the flat-walled vial, AgNP-modified screen printed electrode, and USB connector (left), and Achira fabric-based electrode in an electrochemical cell 47

Figure 4.2.3: Schematic setup of the electrochemical surface enhanced Raman spectroscopy setup. The inset shows an SEM image of the Ag deposited onto the working electrode of a disposable screen printed electrode. 47

Figure 4.2.4: Sustainable fabric-basedelectrode 48

Figure 5.1.1: UV-vis spectrum of AgNP colloidal sol. 52

Figure 5.1.2: (a) SEM image of silver nanoparticle (b) TEM image of silver nanoparticle 53

Figure 5.2.1: Normal Raman spectrum of 6-TUA powder, collected for 30 seconds at 785 nm excitation, laser power was 55 mW (a) before, (b) after baseline correction 54

Figure 5.2.2: (a) SERS spectrum, recorded in air (30 second acquisition, 785 nm excitation) for an untreated AgNP electrode (b) SERS spectrum of electrode in (a) after incubation in 0.5 M KCl for 30 minutes, followed by rinsing with distilled water. 57

Figure 5.2.3: EC-SERS spectra obtained for 1.0 mM 6-TUA at an applied voltage of -1.0 V vs Ag/AgCl for (a) AgNP electrode treated with potassium chloride and (b) untreated AgNP electrode. Acquisition time was 30 seconds at 785 nm excitation..... 57

Figure 5.2.4: EC-SERS spectra for 1.0 mM 6-TUA drop coated at open circuit potential and three selected applied potentials. Each spectrum acquisition time was 30 seconds at 785 nm excitation. Laser power was 46.5 mW. Supporting electrolyte was deaerated..... 59

Figure 5.2.5: EC-SERS spectra of 1.0 mM 6-TUA in synthetic urine at open circuit potential and several selected applied potentials. Each spectrum acquisition time was 30 seconds at 785 nm excitation 60

Figure 5.2.6: Comparison of EC-SERS signal for 1.0 mM 6-TUA at an applied potential of -1.0 V vs Ag/AgCl for (a) 0.1 M NaF as supporting electrolyte and (b) synthetic urine as supporting electrolyte. Each spectrum acquisition time was 30 seconds at 785 nm. 60

Figure 5.2.7: Comparison of EC-SERS signal obtained at -1.0 V vs Ag/AgCl in 0.1M NaF as supporting electrolyte for (a) 1.0 mM 6-TUA and (b) 1.0 mM 6-TUA. Each spectrum acquisition time was 30 seconds; laser power was 46.5 mW, at 785 nm excitation. 62

Figure 5.2.8: Normal Raman spectrum of levofloxacin powder. The spectra were measured at 22.3 mW for a time interval of 30 seconds using 785 nm excitation. 63

Figure 5.2.9: EC-SERS spectra for 1.0 mM levofloxacin at open circuit potential and applied potentials. Each spectrum acquisition time was 30 seconds at 785 nm excitation. Supporting electrolyte was 0.1 M NaF. Laser power was 46.5 mW..... 65

Figure 5.2.10: EC-SERS of 1mM levofloxacin at OCP (black) and at -1.0V (red). The spectra were measured at 46.5 mW for a time interval of 30 seconds using 785 nm excitation. 65

Figure 5.2.11: EC-SERS of 1.0 mM levofloxacin at OCP, normal Raman , and at -1.0V. The spectra were measured at 46.5 mW for a time interval of 30 seconds using 785 nm excitation. 66

Figure 5.2.12: Normal Raman of guanine powder. Spectra were measured at 10.6 mW for a time interval of 30 seconds using 785 nm excitation. 67

Figure 5.2.13: EC-SERS spectra for 1.0 mM guanine at OCP and applied potentials. Each spectrum acquisition time was 30 seconds, 46.5 laser power, at 785 nm excitation. Supporting electrolyte was 0.1 M NaF. 69

Figure 5.2.14: Comparison between normal Raman spectra of guanine powder and EC-SERS spectrum of guanine solution at -1.0V. Each spectrum acquisition time was 30 seconds, 46.5 laser power, at 785 nm excitation. 70

Figure 5.2.15: Normal Raman of 2-deoxyguanosine. The spectra were measured at 22.3 mW for a time interval of 30 seconds using 785 nm excitation. 70

Figure 5.2.16: EC-SERS spectra for 1.0 mM 2-deoxyguanosine at OCP and applied potentials (0.0V to -1.0V). Each spectrum acquisition time was 30 seconds at 785 nm excitation. Supporting electrolyte was 0.1 M NaF. 71

Figure 5.2.17: Comparison between the normal Raman of 2-deoxyguanosine powder and the EC-SERS signal at -0.7V. Both spectra were collected at 46.5 mW for a time interval of 30s using 785 nm excitation. 71

Figure 5.3.1: Normal Raman of untreated blend fabric. The spectrum was collected at 46.5mW, for a time interval of 60 seconds using785 nm excitation. 75

Figure 5.3.2: SEM image of white cotton fabric untreated with silver nanoparticles..... 75

Figure 5.3.3: Normal Raman spectra for 4,4’-bipy powder. The spectrum was collected at medium power (10.6 mW) for a time interval of 30 seconds using 785 nm laser line. ... 78

Figure 5.3.4: SERS of 1 mM of 4,4’-bipy, 1 layer AgNPs, 30s on (a) white cotton, (b) hemp, (c) bamboo, (d) blue cotton, (e) blend (37% silk, 35% hemp, 28% org.cotton). Laser power was 10.6 mW, all spectra were collected in a time of 30s. 80

Figure 5.3.5: Scanning electron microscopy (SEM) of fabric modified with one layer of AgNPs under (a) low and (b) high magnification. SEM images were conducted using

Tescan MIRA3 LMU Field Emission under high vacuum mode at 10 kV, and at a scanning speed of 32.00 µs / pixel 81

Figure 5.3.6: SERS of 1 mM of 4,4'-bipy, 3 layer AgNPs, 10.6 mW, 30s (a) blue cotton, (b) hemp, (c) blend, (d) white cotton. (Drop coating 10µL of AgNPs). 83

Figure 5.3.7: SEM images of blend fabric samples modified with 3 layers AgNPs at (a - c) low and (d) high magnification. SEM images were conducted using Tescan MIRA3 LMU Field Emission SEM under high vacuum mode at 10 kV, and at a scanning speed of32.00 µs / pixel 84

Figure 5.3.8: Normal Raman of 4-ATP powder. Spectrum was collected at 22.3 mW laser power for 30s at 785 nm excitation. 85

Figure 5.3.9: SERS spectra of 1mM 4-ATP drop coated on fabric samples (a) blend, (b) blue-cotton, (c) bamboo, (d) white-cotton. Peaks due to citrate are labelled with an asterisk (*). 87

Figure 5.3.10: SERS spectra obtained for 1.0 mM 4-ATP on blend fabric substrate (a) fabric substrate treated with potassium chloride and (b) untreated fabric. Acquisition time was 30 seconds at 785 nm excitation. Asterisks denote peaks due to citrate. 89

Figure 5.3.11: SERS spectra of 1.0 mM 4-ATP on (a) blend (b) bamboo (c) blue-cotton (d) white-cotton, (e) hemp with KCl treatment. Each spectrum acquisition time was 30 seconds at 785 nm excitation, power at the sample was 22.3 mW. 90

Figure 5.3.12: (a) SERS of 1.0 mM 4-ATP on fabric platforms treated with 0.5M KCl, using a 785nm laser line (30 s, 10.6 mW). Each spectrum is the average of 10 spectra collected from 10 different spots on the same SERS substrate (b) peak intensity of 1600 cm^{-1} peak for all five fabrics. 91

Figure 5.3.13: SERS spectra of 1.0 mM 4,4'-byp on blend fabric (a) treated with KCl, (b) untreated with KCl. The spectra were measured at 10.6 mW for a time interval of 30 seconds using 785 nm excitation 92

Figure 5.3.14: SERS spectra of 1.0 mM 4,4'-byp on (a) blend, (b) bamboo, (c) b-cotton after KCl treatment. Each spectrum acquisition time was 30 seconds, laser power was 22.3 mW, at 785 nm excitation. 94

Figure 5.3.15: (a) SERS of 1.0 mM 4,4'-byp on fabric platforms treated with 0.5M KCl, using a 785nm laser line.(30 s, 10.6 mW) Each spectra is the average of 10 spectra

collected from 10 different spots on the SERS substrate (b) peak intensity of 1600 cm^{-1} peak. 95

Figure 5.3.16: SERS of 1.0 mM 4-ATP on blend fabric and Fab-chip. The spectra were measured at 10.6 mW for a time interval of 30 seconds using 785 nm excitation. 96

Figure 5.3.17: SERS of 1mM 6-TUA drop coated on blend fabric. The spectra were measured at 22.3 mW for a time interval of 30 seconds using 785 nm excitation. 97

Figure 5.3.18: SERS of 1.0 µM 6-TUA drop coated on blend fabric for seven different spots. The spectra were measured at 22.3 mW for a time interval of 30 seconds using 785 nm excitation. 98

Figure 5.3.19: SERS of 1.0 nM 6-TUA drop coated on blend fabric for seven different spots. The spectra were measured at 22.3 mW for a time interval of 30 seconds using 785 nm excitation. 99

Figure 5.3.20: (a) SERS of different concentrations of 6-TUA drop coating on blend fabric. Each line represents the average of 10 spots, the spectra were measured at 22.3 mW for a time interval of 30 seconds using 785 nm excitation. (b) peak intensity of 10 spots 100

Figure 5.3.21: SERS of 1.0 mM levofloxacin in synthetic urine (a) after KCl treatment, (b) without KCl treatment. Spectra were measured at 10.6 mW for a time interval of 30 seconds using 785 nm excitation. 100

Figure 5.3.22: SERS of 1.0 mM guanine (10 different spots). The spectra were measured at 10.6 mW for a time interval of 30 seconds using 785 nm excitation. 101

Figure 5.3.23: Comparison between normal Raman of guanine powder and SERS of 1.0 mM guanine on blend fabric. 101

Figure 5.3.24: SERS of 1.0 mM 2-deoxyguanosine. The spectra were measured at 10.6 mW for a time interval of 30 seconds using 785 nm excitation. 102

Figure 5.4.1 Fabric based-electrode provided by Achira Labs. 105

Figure 5.4.2: Achira Labs fabric-based electrode modified with three layers of AgNPs (2µL per layer) 106

Figure 5.4.3: SEM image of fabric-based-SPE, (a) at low magnification, (b) at low magnification. SEM images were conducted using Tescan MIRA3 LMU Field Emission SEM under high vacuum mode at 10 kV, and at a scanning speed of 32.00 µs / pixel. 106

Figure 5.4.4: (a) SERS of 10 different spots 1.0 mM of 4-ATP on AChira fabric-based-electrode modified with AgNPs and treated with 0.5 M KCl solution. Spectra were measured at 10.6 mW for a time interval of 30s, using 785 nm excitation. (b) The average of 10 spots..... 108

Figure 5.4.5: EC-SERS spectra for 1.0 mM 4-ATP at open circuit potential and applied potentials. Each spectrum acquisition time was 30 seconds at 22.3 mW, and 785 nm excitation. Supporting electrolyte was 0.1 M NaF. (a) cathodic direction, and (b) anodic 108

Figure 5.4.6: SEM images and EDX spectra of AgNPs modified fabric-based-SPE after EC-SERS measurement. SEM images were conducted using Tescan MIRA3 LMU Field Emission SEM under high vacuum mode at 10 kV, and at a scanning speed of 32.00 µs / pixel.5.4.3 EC-SERS of 6-TUA on Achira Fabric-based electrode..... 109

Figure 5.4.7: EC-SERS spectra for 1.0 mM 6-TUA at open circuit potential and applied potentials. (a) Cathodic, and (b) anodic direction. Each spectrum acquisition time was 30 seconds at 46.5 mW and 785 nm excitation. Supporting electrolyte was 0.1 M NaF. . 110

Figure 5.4.8: Comparison between SERS signal of 1.0 mM 6-TUA collected on (a) blend fabric (b) EC-SERS signal at OCP on fabric-based-electrode (Achira Labs) and (c) EC-SERS signal at OCP on SPE, using 785 nm excitation, laser power was 46.5 mW..... 1111

Figure 5.4.9: Comparison between EC-SERS of 1.0 mM 6-TUA at -1.0 V collected from (a) SPE and (b) fabric-based electrode. The spectra were measured at 46.5 mW for a time interval of 30 seconds using 785 nm excitation. 112

Figure 5.4.10: Blend fabric-based-electrode modified with 3 layers of AgNPs. 113

Figure 5.4.11: SEM image of blend fabric-based-electrode modified with AgNP. (a) before EC-SERS (a), and after EC-SERS (b). SEM images were conducted using Tescan MIRA3 LMU Field Emission SEM under high vacuum mode at 10 kV, and at a scanning speed of 332.00 µs / pixel. 114

Figure 5.4.12: EC-SERS spectra for 1.0 mM 6-TUA at open circuit potential and applied potentials. Each spectrum acquisition time was 30 seconds (46.5 mW) at 785 nm excitation. Supporting electrolyte was 0.1 M NaF. (a) Cathodic, (b) Anodic. 115

Figure 5.4.13: Comparison between SERS of /EC-SERS of 1.0 mM 6-TUA at OCP (a) on blend fabric, (b) on Achira fabric-based electrode, (c) screen-printed electrode and (d) blend fabric-based electrode (made from conductive inks). Each spectrum acquisition time was 30 seconds (46.5 mW) at 785 nm excitation..... 116

Figure 5.4.14: EC-SERS signal of 1.0 mM 6-TUA at -1.0 V, on (a) screen-printed-electrode, (b) fabric-based-electrode (Achira Labs) and (c) blend fabric-based-electrode (made from conductive inks). Spectra were measured at 46.5 mW, in a time interval 30s, using 785 nm excitation. 116

List of Tables

Table #	Description	Page #
Table 1	Vibrational mode assignments for both the normal Raman spectrum and the SERS spectra for 6-thiouric acid. Assignments were made based on calculated frequencies as well as reported literature values	**55**
Table 2	Vibrational mode assignments for both the normal Raman spectrum and the SERS spectra for levofloxacin	**64**
Table 3	Band assignment for the normal Raman (powder) and SERS spectra for guanine.	**68**
Table 4	Vibrational mode assignments for both the normal Raman spectrum and the SERS spectra for 2-deoxyguanosine.	**71**
Table 5	Type of fabrics and their compositions.	**76**
Table 6	SERS band assignments for 4,4'-bipyridine	**77**
Table 7	SERS peaks for p-ATP on silver substrates	**86**

List of Abbreviations

4,4’-bipy	4,4’-bipyridine
6-MP	6-mercaptopurine
6-TUA	6-thiouric acid
8-OHdG	8-Hydroxy-2′-deoxyguanosine
Ag/AgCl	silver-silver chloride electrode
AgNPs	Silver nanoparticles
AZA	Azathioprine
CAGR	compound annual growth rate
CE	counter electrode
CE	chemical enhancement
CM	Chemical Mechanism
DLS	dynamic light scattering
EC	Electrochemical
ECG	electrocardiogram
EC-SERS	Electrochemical SERS
EDS	Energy Dispersive X-ray Spectra
EEC	electroencephalogram
EF	Enhancement Factor
ELISA	enzyme-linked immunosorbent assays
EM	Electromagnetic Mechanism
EM	electron microscopy
GSR	galvanic skin response
HIV-1	human immunodeficiency virus
ICS	immunochromatographic strip
ihp	inner Helmholtz plane
IR	infrared spectroscopy
LOD	limit of detection
LSP	Localized Surface Plasmon
LSPR	Localized Surface Plasmon Resonance
MDR	multi-drug resistant
NaF	Sodium fluoride
NPs	nanoparticles
OCP	Open Circuit Potential
ohp	Outer Helmholtz plane
PPG	photoplethysmography
PSP	Propagating Surface Plasmon
PZC	Potential of Zero Charge
RE	reference electrode
SCE	saturated calomel electrode
SEM	Scanning Electron Microscopy
SERS	Surface Enhanced Raman Spectroscopy
SIDS	Sudden Infant Death Syndrome

SPM	scanning probe microscopy
SPR	Surface Plasmon Resonance
SP	Surface Plasmon
SPEs	Screen Printed Carbon Electrodes
SPR	Surface Plasmon Resonance
TB	tuberculosis
TEM	transmission microscopy
UV-VIS	Ultraviolet-visible spectroscopy
XRD	x-ray diffraction
ROS	reactive oxidative species
UVRR	UV resonance Raman scattering
WE	working electrode

Chapter 1 Introduction

1.1 Preamble

Earlier diagnosis of disease is key to timely and effective treatment. Recently, demand for the monitoring of human disease using new techniques is growing, and in particular technology that can be used at the patient point-of-care is attractive. Next generation diagnostic and monitoring capabilities could be achieved by wearable sensors which are currently under development.[1] Such wearable sensors, generally made from conductive fabric materials (termed *e-textiles*), are already in existence, however at present they are only capable of monitoring physical information, such as heart rate, blood pressure, and body temperature.[2,3] However, wearable chemical sensors that monitor or detect biomarkers in the bodily fluids of the wearer, have also gained much attention recently.[4,5] Wearable chemical sensors that are being explored or suggested include cloth diapers which can monitor disease markers the urine, or exercise clothing which could monitor a patient's response to medication through their sweat.[6] Such a fabric-based sensor needs to be coupled to an instrumental read-out, which could include electrochemical, optical or piezoelectric signals. This thesis work seeks to explore the extent to which surface-enhanced Raman spectroscopy, or SERS, can be coupled to a fabric-based sensor platform for sensitive and selective monitoring of chemical biomarkers. SERS is particularly attractive for this application as it is based on the inelastic scattering of light from the sample, and corresponds to vibrational transitions specific to the molecular structure of the analyte, thus providing a chemical "fingerprint" capable of identification of the analyte.[7]

This thesis seeks to develop novel surface enhanced Raman spectroscopy (SERS) substrates from sustainable fabrics such as bamboo, cotton, hemp, and various blends. Signals for three target biomarkers are evaluated in artificial urine, and compared to electrochemical SERS investigations. Finally, the potential of fabric-based electrodes for on body electrochemical SERS based sensing is explored.

1.2 Objectives of the thesis

The objective of this thesis is to develop sensitive, cost effective and wearable SERS substrates from fabrics such as cotton, hemp and bamboo. This fabric "chip" could then be incorporated into clothing and other textiles to monitor disease biomarkers found in bodily fluids such as sweat or urine. A critical part of this project involves the functionalization of the fabric chip with plasmonic nanoparticles, and evaluating the ability of the sensor to support effective SERS enhancement. This first objective will be evaluated using two common SERS probes: 4,4'-bipyridine (4,4'-bipy) and 4-aminothiophenol (4-ATP); both of which are a strong Raman scatterers and bind strongly to the enhancing metal nanoparticle.

More specifically, this thesis is focusing on using the fabric chip described above to detect the following biomarkers in artificial urine:

1- 6-thiouric acid (6-TUA); a metabolite of the immunosuppressive drug azathioprine
2- Levofloxacin; an antibiotic drug used to treat bacterial infections such as respiratory and urinary tract infections.

3- Guanine; a model of the cancer biomarker 8-oxo-2-hydroxyguanosine

In addition, investigations toward the use of fabric-based electrodes are included in this thesis work.

1.3 Scope of thesis

This thesis consists of 6 chapters. Chapter 1 provides a brief introduction to the research conducted and the objectives of the thesis. Chapter 2 consists of a literature review of the important aspects of this project including point of care diagnostics, wearable sensors, smart textiles, plasmonic sensors and the target biomarkers chosen for study. Chapter 3 provides the background theory for the techniques used in this project including Electrochemistry, Raman Spectroscopy, SERS, and electrochemical SERS (EC-SERS). Chapter 4 summarizes the experimental procedures including the instrumentation and nanoparticle synthesis and characterization. The major experimental results are provided in Chapter 5, and includes EC-SERS of the biomarkers (6-thiouric acid, levofloxacin, guanine, and 2-deoxyguanosine). Next, fabric selections are evaluated and characterized, and once modified with plasmonic nanoparticles, SERS results are presented and discussed. In addition, investigation of the performance of fabric-based electrodes using EC-SERS is presented. Lastly, conclusions and future work are highlighted in Chapter 6. Chapter 7 includes the references cited in this thesis work.

Chapter 2 Literature Review

2.1 Point-of-care diagnostics

2.1.1 Introduction

Throughout the 20th century, and continuing today, most diagnostic testing in the healthcare field has been performed in centralized laboratories in order to make use of sophisticated instrumentation.[8] Unfortunately, this instrumentation has also traditionally been expensive, large and has the requirement of a trained operator. As a result, there has been an increasing push towards the ability to conduct such analysis in a more time and cost effective manner using portable instrumentation.[8] This is especially the case in developing nation countries which often lack modern laboratory facilities and instrumentation.[8] In such resource limited settings, there is a great need for diagnostics which are simple, do not require a stable power source, do not utilize expensive reagents and which can be operated by someone with no technical training, even someone who may be illiterate.[9] In order to overcome these issues, the development of rapid and easy-to-use point-of-care (POC) tests which can detect biomarkers that are associated with various diseases are highly sought after.[9] This emerging area enables more widespread monitoring of health parameters for disease prevention and treatment.[10] POC devices are designed to be used at the patient point-of-care, which eliminates extensive diagnostic testing at central laboratories and hospitals, and improves loss to follow-up, since patients can be directed to treatment during the same clinical visit.[10] POC devices are being developed to achieve a reliable and accurate diagnosis, which plays a fundamental role in healthcare decisions and choice of treatment.[9] POC devices currently in heavy use

include the lateral flow assay (i.e. home pregnancy test) and the electrochemical-based in-home blood glucose monitor.[9,11]

POC diagnostics allow the primary care team to receive the desired results in a more timely fashion. The result is then used to make a decision and take appropriate action, which will lead to an improved health outcome for the patient.[9] Also, POC tests have the ability to lower medical costs. For instance, home diagnosis for streptococcal pharyngitis (strep throat) in children would reduce costly doctor visits and lessen transmission. Commercially available POC tests range from simple platforms, such as the in-home blood glucose monitor,[12] to highly complex POC platforms such as that used in detecting infectious disease.[8] These complex POC tests are based on a variety of antibody-based detection methods, including agglutination, enzyme-linked immunosorbent assays (ELISA) and lateral flow immunochromatography.[11]

2.1.2 Advances in point-of-care platforms

Much research conducted in the early 1990's focused on applications of point-of-care sensors and diagnostics. POC devices are effective for the detection, prevention, and treatment of various diseases such as infectious diseases,[8] viral and bacterial respiratory tract infections,[13] and cancer.[14] POC testing technologies can be divided into two main categories; the first category consists of small handheld devices, providing qualitative and/or quantitative analysis.[15] The second category includes larger, often bench-top devices which are essentially laboratory instruments which have been reduced in size, cost, and complexity.[15] Examples of these large POC devices include critical care analysers, and small haematology and immunology analysers.[15] The major

technologies in the first category include glucose biosensor strips and lateral flow tests.[11,15] The blood glucose meter is a POC tool used to monitor the blood glucose of diabetic patients at home. The ability to measure blood glucose in the home setting has given diabetic patients the ability to better control their blood sugar levels and avoid potential complications.[12] Lateral flow (LF) devices are the most established point-of-care testing platforms due to their simplicity, specificity and low cost.[9] LF tests use a membrane or modified paper strip to indicate the presence of protein markers such as pathogen antigens or host antibodies.[16] In the U.S., lateral flow tests are used for diagnosis in a small number of indications; the home pregnancy test being the most well-known example.[16] Initially, rapid tests for infectious diseases such as human immunodeficiency virus (HIV-1 and HIV-2), tuberculosis (TB), and hepatitis B were introduced in a dipstick format in developing countries.[9] In the late 1980s, the first immunochromatographic strip (ICS) lateral flow format was introduced for disease diagnosis. From that time, the technology of POC testing has continued to develop. Most lateral flow tests used today are based on microfluidic technology.[9] Over the last two decades, microfluidic technologies have experienced significant growth in the field of diagnostics.[9]

POC diagnostics also are used in lower cost environments because they require less complex infrastructure and training.[9] According to a 2013 UPMC Center for Health Security report, point-of-care (POC) tests offer a number of possible advantages over other diagnostic approaches; this includes lower cost, ruggedness and the capacity to generate accurate and reliable results rapidly.[9] The overall global diagnostics market

was projected to exceed $50 billion in 2014[9]; however, POC tests represent only a small portion of this market, at present. The global market for point-of-care diagnostics is expected to reach $27.5 billion by 2018 at an estimated compound annual growth rate (CAGR) of 9.3% from 2013-2018.[9]

2.1.3 Current limitations

A major issue in POC diagnostics is the detection of biomarkers related to certain diseases in bodily fluids, because such fluids are incredibly complex. In addition, finding cheap techniques to analyze these markers is also problematic. Some tests require the use of molecular tags, which can be very expensive and can have stability issues. Portable measurement techniques are also required, and in particular instruments which are battery operated and hand-held.

In addition to these challenges, there is another central challenge which has to date not been addressed. In all cases currently, the use of a POC test requires that a sample be taken of a bodily fluid (blood, urine, etc) and that the measurement be completed sometime afterwards. This time delay could be as short as a few minutes, or as long as several hours. Recently there has been an increasing interest in wearable technology, and e-textiles which can monitor physical parameters such as heart rate and blood pressure are already in existence. What is not currently available, however, is the ability to do on-body chemical sensing. Such a technology, coupled with remote signal transmission, would be a very valuable tool for continual patient monitoring. The focus of this thesis work is to explore this possibility through the development of new plasmonic sensor technology.

2.2 Wearable sensors

Currently, the design and development of wearable sensor systems for health monitoring has gained significant attention within the scientific and industrial communities.[18] Wearable sensor technology has been used in different fields including healthcare, information processing, public safety, acoustic sensing, entertainment (gaming), pressure sensing, military applications, and position tracking.[18] Wearable sensors have been used for both health monitoring and prognosis. Most of these wearable sensors are capable of measuring significant physiological parameters such as heart rate, blood pressure, body and skin temperature, oxygen saturation, and respiration rate.[18,19] Wearable sensors have been traditionally developed by integrating biochemical sensors in fields such as in analytical chemistry, materials science, microfluidics and electrical engineering. Physical sensors directly embedded into clothes are already marketed, such as smart vest, which is used to monitor heart rate, blood pressure and body temperature.[18] Another example of wearable sensors are infant wearables, which can track everything from an infant's breathing, movement, and sleep position to the temperature, humidity, and noise and light levels of the baby's local environment.

2.2.1 Design and applications

Wearable sensors typically rely on wireless, miniature sensors enclosed in patches or bandages, or in items that can be worn, such as a ring or an undergarment. Wearable sensors have diagnostic as well as monitoring applications. Current capabilities include physiological and electrolyte sensing, as well as motion sensing.[18,20,21] Physiological monitoring could also help in both diagnosis and treatment of a wide number of

neurological, cardiovascular and pulmonary conditions which can cause seizures, hypertension, dysrhythmias, and asthma.[18] Wearable sensors are designed for various applications including health and wellness monitoring, safety monitoring, home rehabilitation, and assessment of treatment efficacy.[18]

A focal application of wearable sensors is for health and wellness monitoring, which includes both short term monitoring and long term monitoring. Short term monitoring consists of the monitoring of daily lifestyle activities. Giansanti et al.[22] developed an accelerometer-based device designed for step counting in patients with Parkinson's disease. Sazonov et al.[23] developed an in-shoe pressure and acceleration sensor system that was used to classify activities such as sitting, standing, and walking. Aziz et al.[24] used wearable sensors to monitor the recovery of patients after abdominal surgery using a wireless body sensor network. The device consists of wearable sensors (vital signs, motion) combined with miniaturized computers wirelessly linked to one another which will allow continuous monitoring of patients in any environment.[24] Many recent advancements have highlighted the importance of activity monitoring for wellness applications, and have suggested that such monitoring could increase exercise compliance in obese populations.[25] Similarly, long-term monitoring of several physiological parameters has great potential to improve diagnosis and treatment of cardiovascular disease.[17] Several devices are available for such long term monitoring which have the ability to monitor heart rate, blood pressure, oxygen saturation, respiratory rate, body temperature and galvanic skin response.[19]

Another application of wearable sensors is in safety monitoring. Several devices have evolved for safety monitoring such as fall detection and emergency response.[18] Some devices designed for safety monitoring are commercially available, such as The Life Alert Classic by Life Alert Emergency Response Inc.[26] and the AlertOne medical alert system [27]. Another device in this category is the My Halo™ by Halo Monitoring™. This system is worn as a chest strap and detects falls while concurrently monitoring heart rate, skin temperature, wake / sleep patterns, and activity levels.[28] Another design developed by Bourke et al.[18] detects falls using a tri-axial accelerometer embedded in a custom-designed vest. Additionally, smart phone applications are an emerging technology used for fall detection.[18]

Another application of wearable sensors is in the detection of epileptic seizures which has gained considerable attention from researchers and clinicians. The sensors that are used to detect epileptic crises (EC) are called electroencephalogram (EEC) sensors.[29] Furthermore, wearable sensors can be worn to monitor individuals working in hostile environments in response to emergency situations. The Pro-TEX project is an example of such sensor technology.[25] This project developed smart garments for monitoring emergency-disaster personnel, which focuses on smart garments to monitor firefighters and their environment during fire interventions. Smart garments in this context mean garments integrating a network of sensors, microprocessors, energy sources, and communication tools. In addition, these garment-based sensors are also used to measure environmental variables such as temperature and exposure to chemicals (toxic gases, chemical agents, corrosive vapors).[25]

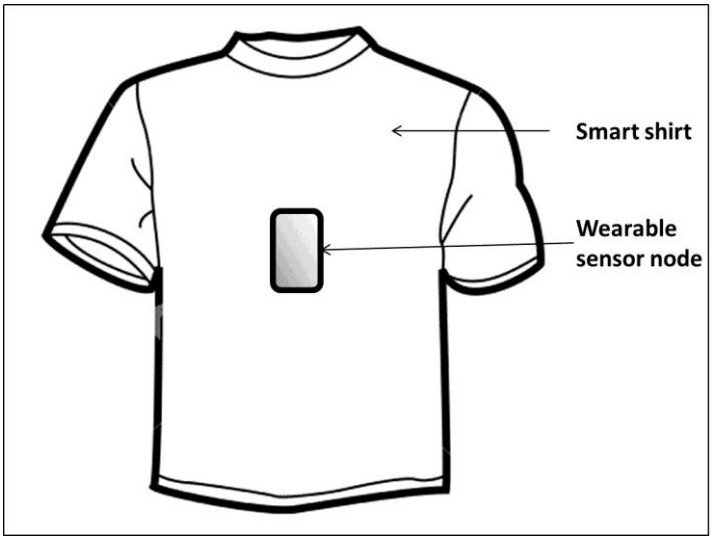

Figure 2.2.1: An example of a smart shirt adapted from reference [30].

2.2.1.1 Motivation for wearable sensors

The interest in wearable sensors originates from the need to monitor patients over extensive periods of time. Remote monitoring systems and wearable sensors have the potential to relieve and solve some problematic patient access issues. For example, approximately 20% of Americans live in rural areas, but only 9% of available physicians work in such areas.[18] Much research and literature describes the difficulties patients face in rural areas when it comes to monitoring their health status and obtaining treatment. Compared to those in urban areas, those in rural areas travel 2 to 3 times farther to see a physician, see fewer specialists, and can expect less hopeful outcomes for treatment of emergency conditions, such as diabetic coma, stroke, and heart attack.[31,32]

2.2.1.2 Wearability criteria

There are numerous criteria that should be taken into account when designing a wearable sensor, including the size and weight of the sensor. For example, the sensor

should be small enough so that it does not affect a person's movement or action.[25] In addition, the wearable sensor should be cost effective so as to ensure wide public access to these technologies. Moreover, to increase the system's operational lifetime, the power consumption needs to be minimized. In addition, the functionality of a wearable sensor must satisfy a specific clinical need to measure parameters important to the health of the individual.[29] Ultimately, performance and cost should balance with functionality and reliability of a device to encourage acceptance of any wearable device into daily life.[33]

2.2.1.3 Smart textiles and Fabric-based sensors

Smart textiles have received significant attention in the last decade for their use in wearable technologies.[34] Currently, close and continuous monitoring methods which can assist physicians with health monitoring of patients are in a high demand for diseases that are generally difficult to detect without continuous monitoring, such as cardiovascular disease.[35] Much research has been conducted on developing wearable sensors, often made of conductive fabric material.[36] Currently, wearable sensors are focused primarily on physiological monitoring, while very few focus on obtaining chemical information residing on the skin or in the bodily fluids of the wearer, which could provide further insight into overall health.[37]

Research has been reported on the fabrication of smart textiles with conductive fibers and on analyses of the applications of soft sensors as components of e-textiles.[38] An example of a smart textile in this regard is a piezo-resistive sensor which is being developed for a smart training shoe. Once the textile is integrated with read-out electronics, it will be capable of measuring the step rate during training and the

information will be easily prompted on the display of a smart watch.[38] Another example of this kind of textile was reported by Pandian et al. in which the authors describe a Smart Vest, which is a wearable physiological monitoring system.[39] They integrated a variety of sensors within the garment fabric which was capable of collecting several biosignals. The parameters measured by this vest include electrocardiogram (ECG), photoplethysmography (PPG), heart rate, blood pressure, body temperature, and galvanic skin response (GSR).[38] Also, a baby vest (Figure 2.2.2) was recently developed for the continuous monitoring of the electrocardiogram (ECG) of children demonstrating an increased risk of Sudden Infant Death Syndrome (SIDS).[40] The sensors and the antenna are made out of textile materials. All electronics are mounted on a flexible circuit to facilitate integration into the baby's clothing.

Figure 2.2.2: Baby garment prototype for ECG measurement. (Left) inside showing the textrodes; (right) outside reproduced with permission.[38]

2.2.2 Current limitations

In a world where the development of cost-efficient and non-invasive techniques for diagnosing and monitoring disease is of great interest, wearable sensors could

provide an alternative to traditional methods of analysis. Although there are many advantages and benefits to using wearable sensors, there are several limitations of this technology. For example, sporadic contact between the garment and the wearer during movement can lead to reduced accuracy and precision, thus affecting the reliability of the results.[18] In addition to new fabric materials, it is also important to develop new sensing technologies which can be combined with existing fabrics. This thesis work will focus on the development of a fabric-based plasmonic sensor for wearable sensor applications.

2.3 Plasmonic sensors

2.3.1 Introduction to plasmonics

Plasmonics is the study of the interaction between certain nanoscale metals and incident electromagnetic radiation.[41] When these metals (typically the coinage metals, Ag, Au and Cu) are organized into nanoscale structures, unique physical properties occur that are not observed in bulk materials.[41] For instance, the optical properties of bulk gold are different from nanoscale gold; bulk gold appears yellow in color while gold nanospheres are red.[42] The nanoparticles are so small (less than the wavelength of the incident light) that electrons are not free to move as they are in bulk gold, but instead are confined in nanometer dimensions; this is referred to as *quantum confinement*. Due to this movement restriction, these particles interact differently with light.[42] Specifically, the oscillating electric field of the incident light causes the surface electrons in the metal to oscillate collectively, producing a large electric field in the immediate vicinity of the particle.[42] This phenomenon leads to a resonance condition

known as a surface plasmon resonance (SPR), which is either a localized surface plasmon (LSP) or a propagating surface plasmon (PSP), depending on the dimensions of the nanometal.[41] LSPR is observed when the nanometal is nanoscale in more than one dimension, such as a sphere, whilst PSP is observed when the nanometal is nanoscale in only one dimension, such as a nanofilm.[41]

2.3.2 Applications of Plasmonics

The study of these light-metal interactions is a recent field known as "plasmonics",[41-43] which is related to the localization, guidance, and manipulation of electromagnetic waves beyond the diffraction limit and down to the nanometer-length scale. A key component of plasmonics is metal nanoparticles, including Au, Ag, and Cu that are highly efficient at absorbing and scattering light.[44] Metal nanoparticles exhibit unique optical properties due to the excitation of localized surface plasmons, which makes them highly sensitive probes for detecting small biomolecules. This field has attracted much attention due to its potential application in optical devices, sensors, medical diagnostics and therapeutics.[44] In addition, many applications of plasmonics have been developed over the past decades including LSPR sensing and surface-enhanced Raman spectroscopy (SERS).[43] In LSPR sensing, the dielectric environment around a plasmonic nanoparticle changes due to the interaction of analyte molecules with the nanoparticle surface.[44] This change leads to a shift in the resonant frequency of the LSPR, which can be readily monitored using high resolution UV-vis instrumentation. The wavelength shift in the LSPR can then be determined and correlated to analyte concentration. LSPR sensing relies on careful modification of the nanoparticle surface,

often with a capture agent such as an antibody or a nucleic acid which will bind specifically to the analyte of interest.[44]

Another very useful application of plasmonic nanoparticles is in surface-enhanced Raman spectroscopy, or SERS.[44] In SERS, the relatively weak Raman signal of an analyte can be increased by up to 10^{10} orders of magnitude,[45] simply by ensuring that the analyte is on or in very close proximity to the metal surface. In SERS, the enhanced electromagnetic field generated by the LSPR of a plasmonic nanostructure contributes largely to this strong enhancement, although a chemical enhancement mechanism is also at play.[44] In general, the enormous enhancement in signal allows SERS to be a very useful vibrational spectroscopic tool, capable of single molecule detection in some cases.[45] Since SERS is a major focus of this thesis work, this technique will be further outlined in Chapter 3.

2.3.3 Plasmonic sensor design

Recently, plasmonic sensor technologies have improved and some of these sensors are now commercially available. In addition, researchers have made use of the localized plasmonic heating character for purposes of drug delivery.[46] Conventional drug delivery protocols call for the encapsulation of a drug in a coating that prevents interaction with non-target cells.[46] When the drug arrives at the target region the drug can then be released at a desired rate. This can be improved by having a polymer coating that is temperature activated.[46] Various researchers have focused on the development of new types of plasmonic nanostructures for improving sensitivity, selectivity, and detection limits, relative to non-plasmonic sensing systems.[43] Moreover, current advances in

nanoparticle synthesis technology and micro and nano-fabrication technologies provide a new way to overcome the limitations of conventional surface plasmon resonance (SPR) sensors, which include improving performance (sensitivity and selectivity) while also increasing throughput.[43]

Work in the biosensor field is currently expanding along two main paths: miniaturization and improvement of the limit of detection (LOD) in complex fluids.[47] Attempts to miniaturize optical biosensors, for example, have included a surface plasmon resonance (SPR) biosensor integrated with a cell phone for the detection of ß2 macroglobulin, a biomarker for many ailments including cancer, inflammatory disorders, and kidney disease.[47] In terms of plasmonic sensors, the size, shape and surface chemistry of the metal nanoparticles is paramount to function.[44] As a result, very careful attention is paid to both the synthesis and characterization of these materials.

2.3.4 Nanomaterials: Synthesis and Characterization

Nanotechnologies involve designing and producing objects or structures at a very small scale: nanoscale objects by definition have at least one dimension that is on the order of 100 nanometers (100 millionth of a millimeter) or less.[48] Nanomaterials can include nanoscale spheres, cubes, rods, and fibers. Nanomaterials are used in a variety of applications including healthcare, electronics, cosmetics, textiles, information technology and environmental protection.[48]

A central focus of this thesis work is on nanoparticles, more specifically, silver nanoparticles (AgNPs), which are used for various applications such as in diagnostic

applications, antibiotic applications, conductive applications, and optical applications.[48] AgNPs play a significant role in cancer therapy as they have a notable anti-proliferative effect and induce apoptosis-mediated cell death both in drug sensitive and in multi-drug resistant (MDR) cancer cells.[49] For example, AgNPs can be designed with proteins that specifically detect drug resistant cells with overexpressed transporter proteins on their surface.[50] AgNPs also find widespread use in antimicrobial applications.[51,52] Introduction of silver nanoparticles into bacterial cultures induces a high degree of structural and morphological changes, which can lead to cell death. As the silver nanoparticles come in contact with the bacteria, they adhere to the cell wall and cell membrane.[51] It has been noted that the introduction of silver nanoparticles has shown to have synergistic activity with common antibiotic already used today, such as; penicillin, erythromycin, clindamycin, and vancomycin against *E. coli* and *S. aureus*.[51] In addition, silver nanoparticles have been used in medical equipment as it has been shown that silver nanoparticles drastically lower the bacterial count on medical devices.[52] Furthermore, silver nanoparticles play a significant role in plasmonic applications such as SERS , near-field optical microscopy, and LSPR based sensing.[44]

Nanoparticle synthesis can proceed through two general approaches: top-down and bottom-up.[48] Both approaches play a significant role in modern industry and nanotechnology. The top-down approach refers to a physical breakdown of a bulk material into nanoscale components. This approach can be classified into two categories; mechanical or chemical. Mechanical strategies include milling, extrusion and grinding. Chemical strategies include evaporation, sputtering, and chemical etching techniques.

Such top-down approaches can introduce imperfection and crystallographic damage to the resulting materials.[48] In addition, such processes may introduce impurities and structural defects to the nanomaterial surface, which can have a significant impact on the physical properties and surface chemistry of the resulting nanomaterials.[48]

The bottom-up approach refers to building a nanomaterial from the "bottom up", which means starting with individual atoms or ions and using these as building blocks to create larger structures.[48] Bottom-up approaches are popular for nanoparticle synthesis, as they generally allow for the fabrication of nanostructures with few defects and a more homogeneous chemical composition. Precipitation and chemical reduction are the two most widely used bottom-up synthetic routes with the latter being the most common.

Several characteristics should be considered for any practical application of nanoparticles regardless of the fabrication method. These characteristics include: identical size of all particles (uniformity of size) and identical shape (morphology).[48] While identical size and shape are not often obtainable, near-identical (near-monodisperse) is certainly optimal. The most common way of producing a nanomaterial using the bottom-up approach is via the reduction of metal ions in aqueous solution using a strong reducing agent.[48] The result is a colloid wherein a nanoscale solid is suspended in a liquid – this is referred to as a sol. There are two mechanisms by which metal nanoparticles can be formed via reduction; 1) nucleation and growth 2) seed-mediated growth.[48] In the standard nucleation and growth mechanism, nanoparticles are produced when the metal cations have been reduced to elemental nuclei, and these zero valent nuclei then grow into nanoparticles. In seed-mediated growth, these same zero valent

nuclei typically serve as "seeds" and are introduced to a growth solution composed of metal ions and capping agents that will facilitate the growth onto the surface of the seed.[48]

Capping agents are used in colloidal synthesis to stabilize the nanostructures in several ways: imposing size constraints, controlling morphology and protecting nanostructures from aggregation. Some examples of typical capping agents include oleic acid, oleyamine, trioctylphosphine and dodecanethiol. The strong binding properties of these capping agents to the metal surface allows for the synthesis of near-monodisperse nanoparticles that can be readily self-assembled into highly ordered patterns.[48]

Many types of metal precursors, reducing agents, chemicals and procedures are used in the synthesis of metallic nanoparticles in an effort to control the reduction reactions and the properties of the initial nuclei.[48] The precursors, for example, consist of inorganic salts, elemental metals, and metal complexes. Common examples include Ni, Co, $HAuCl_4$, H_2PtCl_6, $RhCl_3$, and $PdCl_2$. Examples of commonly used reducing agents include sodium citrate, citric acid, hydroxylamine hydrochloride, carbon monoxide, sodium carbonate, aqueous methanol, and formaldehyde.[48] Characterization of nanostructures is most often completed using electron microscopy (EM), such as scanning electron microscopy (SEM), transmission microscopy (TEM), and scanning probe microscopy (SPM).[48] In addition, other characterization methods for metal nanoparticles include x-ray diffraction (XRD), dynamic light scattering (DLS) and zeta potential determination.

2.3.5 Plasmonic sensors

For nanoscale metallic structures, such as metallic nanoparticles and rods, incident light with an appropriate wavelength can be used to excite a localized oscillation of charge on the metal surface, a process that is referred to as localized surface plasmon resonance LSPR, as described previously.[44,45] The magnitude of the LSPR is strongly dependent on nanoparticle size, shape and the local dielectric environment.[44] The nanoscale coinage metals (Au, Ag, Cu) are optimal for enhancing the local field as they spontaneously amplify the scattering and absorption of incident photons on their surface.[44]

In terms of plasmonics, it is important to choose a metal that can support a strong surface plasmon at the desired resonance wavelength. The ability of a metal nanoparticle to support a surface plasmon is dependent on its dielectric properties.[44] The dielectric function is often used to characterize the optical properties of bulk materials as a function of the frequency of incident electromagnetic radiation, and is denoted by the symbol ε, which for a metal represents a complex function, composed of real and imaginary components, denoted as ε_r and ε_i, respectively.[44] The dielectric function of a material reflects the unique interaction between its electrons and incident light. According to Mie theory, only metals are capable of supporting LSPRs, since only metals have electrons which are free to oscillate.[44] Mie theory can be used to calculate the extinction cross-section (C_{ext}) of a metal which is a measure of a particular metals ability to both absorb and scatter incident light at a certain wavelength, λ, as highlighted in Equation 1. When C_{ext} is large, the metal supports a strong SP, and this only occurs for metals which have a

negative real component and a small, positive imaginary component of the complex dielectric function.[44] As shown in Figure 2.1, in the visible wavelength regime this is only true for certain metals such as Ag, Au and Cu. Silver is the most widely used plasmonic metal, capable of supporting LSPR across the entire visible spectrum and into the infrared (300 to 1200 nm).[44]

$$C_{ext} = \frac{24\pi^2 R^3 \varepsilon_m^{\frac{3}{2}}}{\lambda}\left[\frac{\varepsilon_i}{(\varepsilon_r+2\varepsilon_m)^2+\varepsilon_i{}^2}\right] \qquad [1]$$

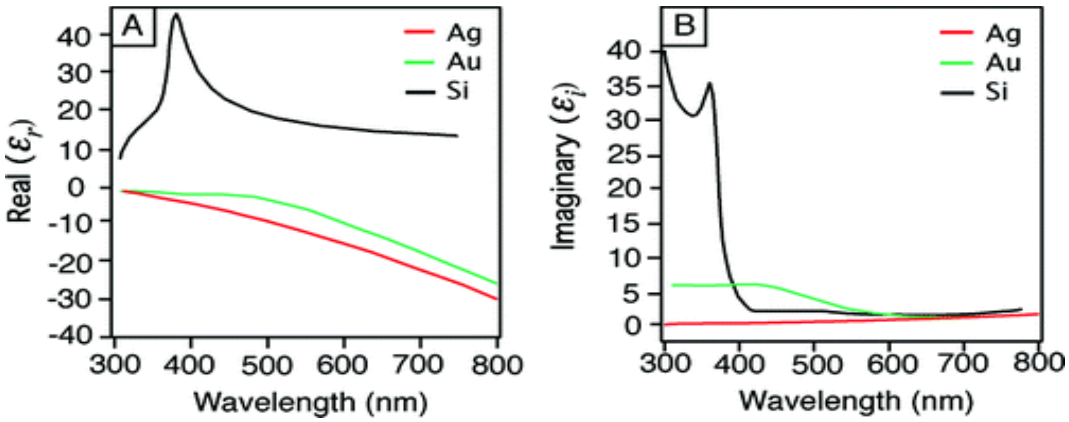

Figure 2.1: Real and imaginary dielectric functions for gold, silver and silicon. Used with permission.[44]

2.3.6 Surface-Enhanced Raman Spectroscopy

2.3.6.1 Raman Spectroscopy

Raman spectroscopy is a vibrational technique based on the inelastic scattering of monochromatic light, usually from a laser source. When light is inelastically scattered, the frequency of the photons change upon interaction with a sample.[53] The scattering process happens between a photon and a molecule. The incident radiation assumes a

different frequency after the interaction, and that frequency change is characteristic of the molecular vibrations present in the molecule. The shift in frequency of the scattered photons can be greater or less than that of the incident photons.[53] The direction of the shift is dependent on whether the molecule is in the vibrational ground state or an excited state.[54] If the molecule was in the ground state then the incident photons would lose energy, resulting in scattered radiation that was lower in frequency that the incident light, this is termed Stokes scattering.[53-55] The opposite occurs when the molecule is in an excited state, and is referred to as anti-Stokes scattering. Since the majority of Raman investigations are done at room temperature, where the population of the excited state is low, most Raman spectrometers are designed to collect only the Stokes scattered light.[55]

There are several factors that can affect the intensity of Raman active vibrations:[54] 1) more polar chemical bonds are less vulnerable to electron cloud distortion, and are thus weakly scattering 2) bending vibrations are usually weaker than stretching vibrations 3) the band intensity increases with bond order 4) intensity is typically increased with atomic number since larger electron clouds allow for greater polarizability 5) symmetric vibrations are generally more intense than anti-symmetric vibrations and lastly 6) crystalline materials are more Raman active than non-crystalline materials.[54]

Raman spectroscopy offers many advantages over other spectroscopic techniques such as infrared spectroscopy (IR). One of the main advantages is that water molecules are weak scatterers which can be very useful when analyzing biological samples that are prepared in aqueous solutions since water will not interfere.[56] Also, carbon dioxide, glass, and alcohols are weak Raman scatters and therefore cause less interference with the

analyte signal compared to IR. Other advantages include the simplicity in obtaining a Raman spectrum, minimal sample preparation and modification required, non-destructive nature, and rapid analysis time. In addition, portable, hand-held instrumentation is widely available. [56,57]A significant disadvantage of Raman spectroscopy includes an interference with fluorescence when certain samples are irradiated by the energetic laser beam, resulting in a significant background.[53] The main disadvantage of Raman spectroscopy; however, is that the Raman Stokes scattering is relatively weak, and only a small amount of the incident light (~one in one million photons) is scattered inelastically.[58] As a consequence, only strongly scattering molecules present as bulk solids, liquids, or gases exhibit useful normal Raman spectra. Some of these disadvantages can be overcome by using surface-enhanced Raman spectroscopy (SERS) which is a variation of normal Raman spectroscopy.

2.3.6.2 SERS

SERS is a sensitive technique for molecular identification that overcomes many limitations of normal Raman spectroscopy such as fluorescence interference and an inherently weak signal.[59] SERS is associated with the enhancement of the electromagnetic field surrounding small metal particles, which gives rise to large electric field enhancements at the surface and allows one to obtain a spectroscopic fingerprint of any molecules located near this metal surface. For these reasons, SERS is a powerful and sensitive technique that has been gaining in popularity since its discovery in the late 1970's.[59]

Recently, there have been increasing literature reports that highlight the use of SERS in detecting disease biomarkers in bodily fluids (e.g. blood, urine, saliva, and serum). For example, Zhang et al. reported the SERS-based detection of hypoxanthine as a biomarker for prostate cancer and free heme as a biomarker for acute kidney dysfunction.[60] Moreover, there has been a significant increase in the number of publications focusing on the detection of biomolecules in biologically relevant fluids and/or patient samples by SERS. Granger et al. was able to detect serum carbohydrate antigen as a biomarker for pancreatic adenocarcinoma, which is a devastating form of cancer.[59] This work reported on an immunoassay array coupled with SERS as a sensitive readout method. The authors suggested that this technique can be used to detect this form of cancer at an early stage. Kim et al. investigated the detection of multiple biomarkers by SERS using a gold-patterned microarray chip as a substrate.[62] In this study, human and rabbit immunoglobulin were tested as model protein markers to confirm the efficacy of their SERS-based immunoassay. Zhang et al. were able to use SERS to detect an anthrax biomarker using a portable Raman spectrometer.[61] Particularly, they studied and detected calcium dipicolinate, a biomarker for *Bacillus subtilis* spores. One of the aims of their research was to develop a portable Raman spectrometer as a portable screening tool, since many field-sensing applications require portability and flexibility.[63] Lee et al. developed a SERS-based immunoassay by using a gold array-embedded gradient microfluidic chip platform for cancer biomarkers.[62] As seen from the literature, different biomarkers were detected using different substrates such as microfluidic chips,[64] modified silver electrodes,[60] silver films,[66] gold patterned microarray chips[64],

electrochemical SERS sensors[56] and other platforms modified with silver and gold nanoparticles.

2.3.6.3 Electrochemical SERS sensors

Electrochemical SERS (EC-SERS) methods are based on combining a Raman spectrometer with an electrochemical set-up, including a potentiostat and a three-electrode system. The working electrode of the electrochemical cell is modified such that it is rendered SERS-active. SERS is a sensitive technique, and by combining it with electrochemistry one can improve and enhance the selectivity and signal intensity.[56,67,68] Various examples in the literature are based on spectroelectrochemical methods for studying adsorbates on SERS active electrodes such as 2-amino-5-(4-pyridine)-1,3,4-thiadiazole,[67] pyridine[68]and DNA.[69]

Recently our group has reported on a portable version of EC-SERS, which consists of a small benchtop Raman spectrometer, a laptop computer, and a portable USB potentiostat.[54] Zhao et al. used this EC-SERS set-up to detect uric acid, a urine biomarker of preeclampsia.[66] In this work, Zhao et al. were able to obtain quantitative detection of uric acid in both 0.1 M NaF and synthetic urine. The electrode was modified by multilayers of gold and silver to achieve a better enhancement of the SERS signal. Using this same system, Karaballi et al. developed an EC-SERS DNA aptasensor for direct detection of tuberculosis via DNA hybridization.[70]

2.3.6.4 Fabric-based SERS sensors.

SERS enhancement is observed from analytes adsorbed onto SERS active substrates. The more SERS-active the substrate, the more SERS enhancement can be obtained. One of the challenges related to the SERS technique is to develop an effective substrate.[71] Many substrates have been designed and explored, including metal nanoparticle films, porous substrates, and bimetallic nanostructures.[76] Fabrication of these substrates tends to be time consuming and expensive. Recently, researchers have focused their attention on flexible SERS substrates, such as paper-based SERS sensors, because they are inexpensive and environmentally friendly.[71] Additionally, fabric-based SERS substrates also have been investigated because of their flexibility and wearability. Recently in our group, Robinson et al. modified a traditional Indian fabric called zari with silver nanoparticles, and investigated the SERS performance of this substrate using 4,4'-bipyridine as a standard SERS probe, and a strong signal was obtained.[71] This modified fabric sensor was termed a "fab-chip", and represents the first reported fabric-based SERS substrate using a woven textile. Kim et al.[72] reported the possibility of using modified cotton fabrics to observe the exchange reaction between benzenethiol and 4-nitrobenzenethiol by SERS. Recently, Ballerini et al.[73] investigated the detection of various analytes by SERS on modified cotton threads. These threads have the potential of being incorporated into apparel, such as military uniforms, for the detection of biohazards. More recently, Liu et al.[74] produced a silk fabric modified with gold nanoparticles as a flexible SERS substrate.

In a further exploration, Kurouski et al. investigated commercial fabric-based substrates as low cost 3-D SERS platforms,[75] and demonstrated LSPR profiles were based on the experimental near-field responses of 3-D SERS substrates. This study presented the use of wavelength scanned surface-enhanced Raman excitation spectroscopy (WS-SERES) to investigate the near-field SERS properties of the commercial 3-D SERS platforms.[75] They found that the near-field properties of 3-D SERS substrates are primarily determined by the presence of nanoparticle dimers, trimers, and higher order nanoparticle clusters.

In the current thesis work, different types of commonly available sustainable fabrics were selected in this research to investigate the optimal fabric to be used as a fabric-based SERS substrate. This fabric can then be developed for use as a wearable sensor at the patient point-of-care for on-body monitoring of disease biomarkers in bodily fluids. These fabric chips were modified with silver nanoparticles, and the SERS performance was evaluated for several important biomakers. For comparison, EC-SERS measurements for the same biomarkers were completed in order to evaluate the effect of applied potential on the SERS signal. A final aim of this project was then to combine the two concepts and investigate the performance of a fabric-based-electrode using EC-SERS. This technology can be used in the future for rapid monitoring of disease biomarkers found in bodily fluids (i.e. sweat or urine) at the patient point-of-care.

2.4 Target biomarkers

2.4.1 Choice of biomarkers for SERS-based sensing

The biomarkers that were chosen for this thesis work were all urine biomarkers, and included 6-thiouric acid (6-TUA), levofloxacin, and guanine. Each biomarker will be described in detail below.

2.4.2 6-Thiouric acid: A biomarker for chemotherapeutics

6-Thiouric acid (TUA) (structure shown in Figure 2.4.1a) has the potential to be an important urine biomarker for the action of the immunosuppressive drug Azathioprine® (AZA). This drug is widely used in chemotherapy treatment for leukemia patients,[76,77] which is the most common form of childhood cancer.[78,79] One of the treatment options for leukemia is a bone marrow transplant,[78,80] which requires the use of drugs such as azathioprine (AZA) for immunosuppression in order to prevent transplant rejection. AZA is a prodrug form that is quickly converted to 6-mercaptopurine (6-MP), the active metabolite. Monitoring of 6-MP is typically done through analysis of human serum, using techniques such as fluorescence sensors, liquid chromatography, and electrochemical methods.[81-87] Though these methods have proven to exhibit high selectively and sensitivity, they are often combined with complex sample treatment, expensive equipment and complicated techniques.[81] Therefore, advances in the detection of this particular drug is warranted. 6-MP is metabolized into three main compounds (Figure 2.4.2): 6-thioguanine, 6-thiouric acid, and 6-methyl-mercaptopurine. One of the metabolites, 6-thioguanine, is the active component which is responsible for the immunosuppression. The other two metabolites, 6-thiouric acid (6-TUA) and 6-methyl-

mercaptopurine are produced from the action of xanthine oxidase and thiopurine methyltransferase, respectively, and are inactive products.[88] 6-TUA is excreted in the urine[82] and quantitative detection at low concentrations would offer a valuable tool for assessing the effectiveness of 6-MP in patients.

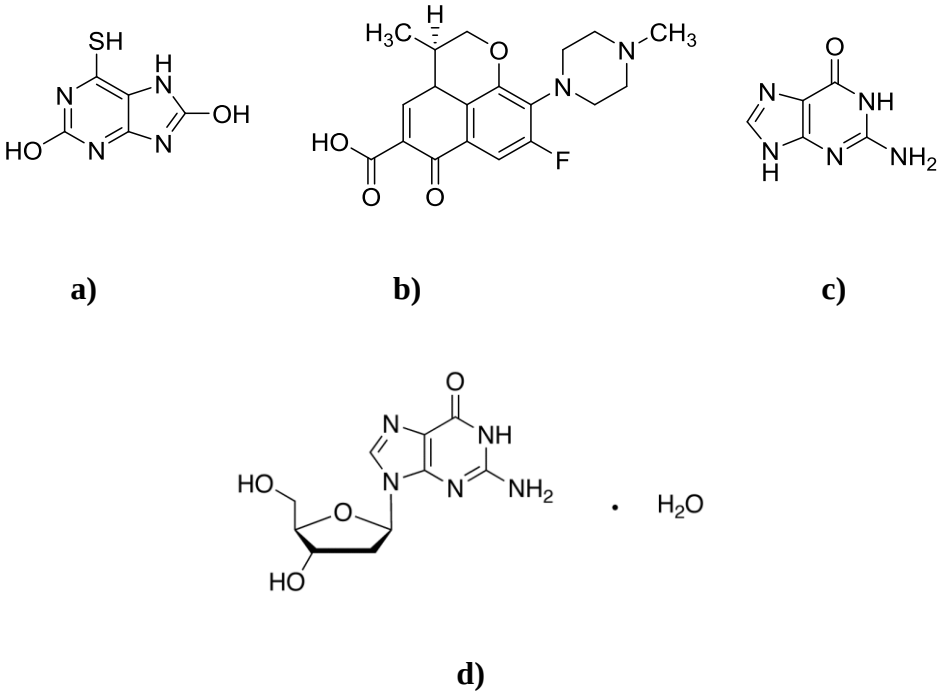

Figure 2.4.1: Molecular structure of (a) 6-thiouric acid (b) levofloxacin, (c) guanine.

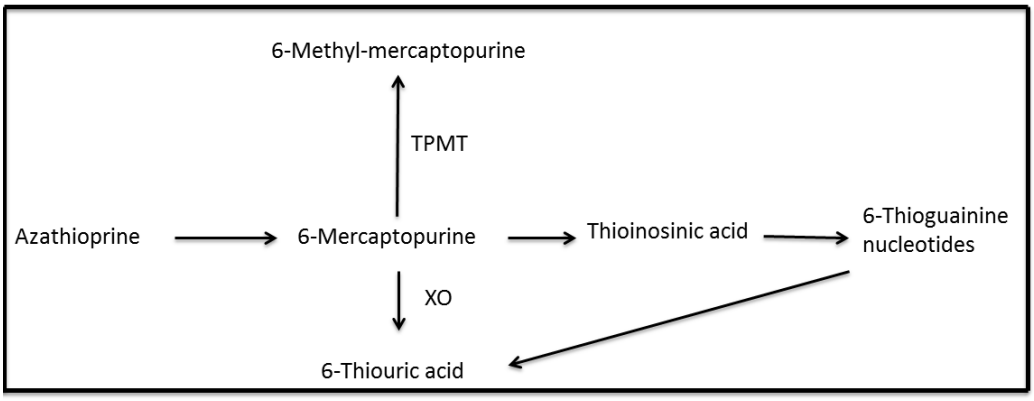

Figure 2.4.2: Metabolism of azathioprine (TPMT = thiopurine methyltransferase; XO = xanthine oxidase). Adapted from reference [88].

2.4.3 Levofloxacin: A ubiquitous antibiotic

Levofloxacin (Figure 2.4.1b) is classified as a fluoroquinolone antibiotic, and is widely used for the treatment of bacterial infections, particularly respiratory and urinary tract infections.[89-92] Levofloxacin can be used to treat a variety of infections including lung, skin, sinus, and urinary tract infections, including hospital and community-acquired pneumonia, acute bacterial sinusitis, complicated and uncomplicated skin infections, and acute pyelonephritis.[92] Levofloxacin undergoes limited metabolism in the human body, and more than 85% of the administrated dose is excreted into urine as unchanged drug.[91] Consequently, its clearance rate can be easily monitored by determining its concentration in urine. Djabarouti et al.[91] reported the use of the HPLC assay as a fast analysis of levofloxacin in human plasma. Another study by Liang et al.[92] presented the use of liquid chromatography with UV and fluorescence for detection and quantitation of levofloxacin in human plasma. Hidi et al.[90] employed lab-on-chip surface enhanced Raman spectroscopy to detect levofloxacin in artificial and human urine. The levofloxacin

concentration that was detected in these studies was in the range between 0.45 and 1.8 mM.

2.4.4 Guanine and 2-deoxyguanosine: A model of 8-oxo-2-deoxyguanosine, a cancer biomarker

8-Hydroxy-2′-deoxyguanosine (8-OHdG) is commonly identified as a biomarker of oxidative DNA damage.[93] Oxidative stress is a physiological condition that results when an imbalance exists between reactive oxidative species (ROS) and natural antioxidant enzymes.[94-97] When the production of ROS is increased, numerous biomolecules, such as DNA, lipids and proteins can be damaged due to oxidation. Recent studies have linked exposure to toxins, such as heavy metals and pesticides, to increased ROS production, which induces oxidative stress.[93,98] Oxidative stress is also associated with aging, atherosclerosis, hypertension, renal failure, immune alterations, neurodegeneration, diabetes, radiation damage, cancer, and numerous other degenerative conditions.[98,99,100] It is therefore of great interest to be able to assess oxidative damage.

8-OHdG is the most commonly used marker of oxidative DNA damage,[93] and its concentration in urine is thought to represent the extent of whole body oxidative DNA damage.[98] 8-OHdG is a sensitive marker of the DNA damage due to hydroxyl radical attack at the C8 of guanine. This damage, if left unrepaired, has been proposed to contribute to mutagenicity and cancer.[98] For example, higher levels of 8-OHdG are noted in *Helicobacter pylori*-associated chronic atrophic gastritis as well as gastric cancer.[100] There are many clinical diseases that are associated with increased urinary 8-OHdG

production, including *Helicobacter pylori* infection, colorectal tumor, breast cancer, bladder/prostate cancer, lung cancer, atherosclerosis, diabetes, and smoking.[99]

Presently, the most common analytical methods used for measuring 8-OHdG in urine are chromatography and enzyme linked immunosorbent assays (ELISA).[101] Both of these methods have associated drawbacks. Chromatographic methods require specialized equipment, have high labour costs and require pre-treatment of the urine sample.[101,102] ELISA, although the fastest, simplest and more inexpensive technique for the determination of this biomarker [103], requires long incubation periods, and results obtained by ELISA have been shown to be inaccurate.[101,104] Due to its highly conjugated structure, 8-OHdG can be examined using ultraviolet (UV) spectroscopy and Raman spectroscopy. These two techniques were combined by Kundu and Loppnow, who employed UV resonance Raman scattering (UVRR) to show how the UVRR spectrum of 8-OHdG differs significantly from that of deoxyguanosine.[98] Furthermore, Jayanth et al. demonstrated that the resonance Raman spectra of nucleobases, specifically guanine, are highly sensitive to modifications such as oxidation.[105] Raman spectroscopy has the potential to offer a low cost and sensitive method for monitoring 8-OHdG in urine. In this thesis work, guanine and 2-deoxyguanosine (their structures in Figure 2.4.1c and 2.4.1d respectively) will be used as a model of 8-OHdG, due to the relatively high cost of 8-OHdG.

Chapter 3 Theory and Techniques

3.1 Introduction

This section provides the necessary theoretical background for concepts central to this thesis work as well as an introduction to the instrumentation used in this project. This chapter begins with a focus on the principles and applications of electrochemistry, and then moves on to discuss the theory behind Raman spectroscopy, SERS and EC-SERS.

3.2 Electrochemistry: Principles and Applications

3.2.1 Introduction

Electrochemistry is the study of chemical processes that cause electrons to move, thereby facilitating oxidation-reduction reactions. An electrochemical cell consists of electrolyte, and at least two electrodes (a cathode and an anode at which the reduction and oxidation reactions occur, respectively). There are two main measurement techniques used in electrochemistry: potentiometric and potentiostatic.[106] The electrolyte is an aqueous salt solution which is allows the electrical current to flow. During the electrochemical measurement, oxygen may be present, which can pose an interference. To overcome this issue and remove the oxygen, the electrolyte is generally purged with ultrapure argon or nitrogen prior to measurement.[106]

The majority of electrochemical cells used in voltammetric measurements consist of three electrodes: a reference electrode (RE), a counter electrode (CE), and a working electrode (WE).[106] The RE has a constant potential that is not affected by the applied potential. The most commonly used REs include the silver-silver chloride electrode

(Ag/AgCl) and the saturated calomel electrode (SCE).[106] The CE is made from a solid conductive material, such as platinum or graphite, and its role is to complete the electrical circuit; acting as an anode when the WE is acting as a cathode and *vice versa*.[106] The WE is where the redox reaction of interest takes place. Electroanalysis is highly dependent on the material of the WE, and there are some characteristics that need to be considered such as: reproducibility, cost, availability, toxicity, potential window, and electrical conductivity.[106] Carbon is one of the most widely used working electrode materials in electroanalysis, and is suitable for various sensing and detection applications because it has a demonstrated chemical inertness, a broad potential window, a low background current, and is inexpensive. Other common choices for working electrode materials include gold and platinum.[106]

3.2.2 Double-layer models of the electrified interface

A double layer is an interfacial region that forms when an electrode is immersed in an electrolyte solution, and is used to describe the array of charged particles at the surface of an electrode.[107] The electrical properties of such a layer are important, since they significantly affect the electrochemical measurement. A positively charged electrode will attract a layer of negatively charged ions, and *vice versa*; this structure is termed the electrical double layer.[107]

The concept of the existence of the double layer at an electrified interface was first described by Helmholtz in 1879.[107] This early model had several limitations however, and was too simplistic. For example, the Helmholtz model did not take into account the role of the solvent. The model used by most researchers at present was

described by Bockris / Devanthan / Mueller in 1963.[108,109] This model describes the specific adsorption of ions and the role of solvent at the interface, and takes into consideration the interaction between the electrode and dipolar solvents (i.e. water).

A classic, simplified model of the double layer formed at the metal electrode surface is presented in Figure 3.1. There is a layer of adsorbed water molecules on the electrode surface.[110] Since it has been assumed that there is excess of negative charge at the metal phase, the hydrogen atoms of adsorbed water molecules are oriented towards the metal surface.[110] As shown in Figure 3.1, the double layer model consists of an inner layer and an outer layer. The inner layer close to the electrode surface is called the inner Helmholtz plane (ihp); this region contains solvent molecules and adsorbed ions.[110] The other region is the outer Helmholtz plane (ohp) which is an imaginary plane that passes through the center of solvated ions that are non-specifically adsorbed.[109,110]

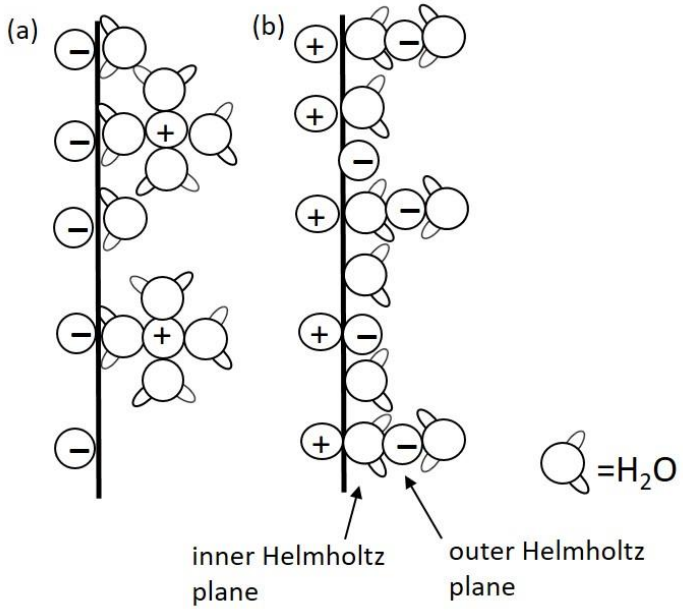

Figure 3.1: Illustration of the electrical double layer according to Bockris / Devanthan / Mueller model. Adapted from reference [109].

3.3 Raman Spectroscopy

3.3.1 Theory of Raman Spectroscopy

Raman spectroscopy is a spectroscopic technique based on the inelastic scattering of monochromatic light.[53] This technique is commonly used in chemistry to provide qualitative and quantitative information about an analyte. When the light or source radiation is focused onto the sample, the photons can be scattered either elastically or inelastically by the sample.[53] The first prediction of inelastic scattering was in 1923 by Adolf Smekal; however, the first observation was in 1928, reported by Sir Chandrasekhara Venkata Raman and Kariamanickam S. Krishnan. The complete theory of the Raman effect was published a few years later by Georg Placzek in 1934.[53]

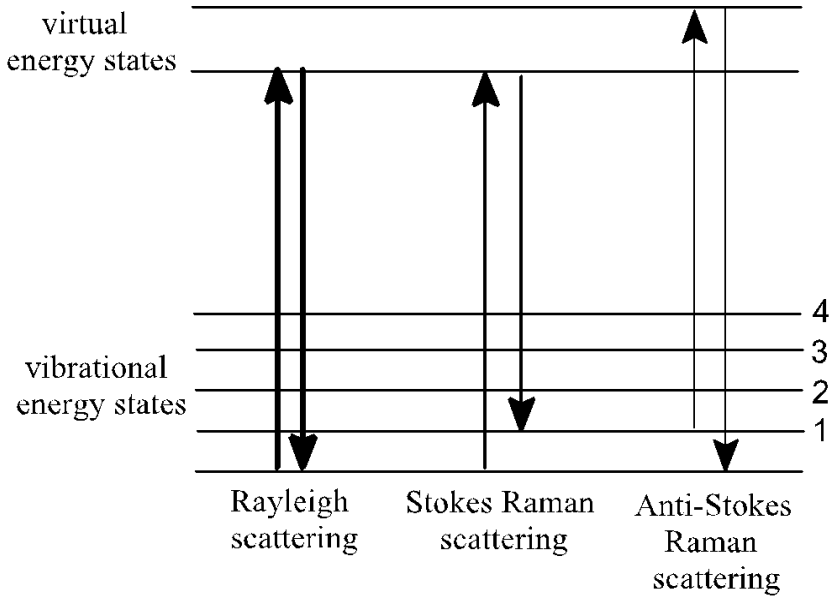

Figure 3.2: Types of scattering: Rayleigh, Stokes, and anti-Stokes. Adapted from reference [53].

As seen in Figure 3.2, three different types of scattering can occur, which are referred to as Rayleigh, Stokes and anti-Stokes scattering. Rayleigh scattering, also known as elastic scattering, does not provide any vibrational information about the molecule because there is no net energy gain or loss.[53,54] In Rayleigh scattering, the molecule is excited by photons to the virtual state and returns to the same vibrational state from which it started, and emitted photons have the same energy and the same wavelength as the initial photons.[54] The second type of scattering is Stokes scattering, which provides useful vibrational information about the molecules. The molecule is excited to a virtual level, and then relaxes back to the original vibrational state by emitting a photon that has less energy, and therefore a longer wavelength than the initial photon.[55] Anti-Stokes scattering occurs when the molecule is initially in an excited state. Hence, the molecule will reach a virtual energy state and return to the ground state by emitting photons that have a higher energy and shorter wavelength than the initial photon. Since most molecules are in the gound state at room temperature, Stokes scattering is more commonly observed than anti-Stokes scattering, and hence most Raman spectrometers are designed so as to only collect the Stokes-scattered radiation.[54]

There are many advantages of using Raman spectroscopy including ease of use, small sample requirement, non-destructive nature, rapid analysis time, and also portable instrumentation is widely available.[54,56,57] Raman spectroscopy is a similar vibrational spectroscopic method to infrared spectroscopy (IR). Both IR and Raman spectroscopy provide a molecular fingerprint for a target molecule, which is useful for detection in a complex sample. Moreover, Raman spectroscopy has advantages over infrared

spectroscopy (IR), as Raman scattering is very weak for water, which is very useful when analyzing biological samples that are prepared in aqueous solutions because water will not interfere. Also, carbon dioxide, alcohols and glass are also weak scatterers.[57] However, there are some limitations for Raman spectroscopy, such as photodecomposition of the sample, which may occur due to high laser power. As well, the Raman signal is relatively weak, since only approximately 1 in one million photons are inelastically scattered. Another disadvantage is that some compounds fluoresce when exposed to the laser beam. A technique has been developed to overcome these limitations called Surface-Enhanced Raman Spectroscopy (SERS). SERS is the subject of this thesis work, and is described in detail below.

3.3.2- Surface-Enhanced Raman Spectroscopy (SERS)

Surface-enhanced Raman spectroscopy (SERS) is a selective and sensitive technique for molecular identification that overcomes many limitations of normal Raman spectroscopy (fluorescence interference and weak signal).[59] In SERS, the Raman signal for a desired analyte can be increased by 10^6-10^{10} times simply by incorporating coinage metal nanoparticles into the system. This level of signal enhancement makes single molecule detection a possibility, as has been illustrated for certain systems.[59]

In 1974, research conducted by Fleischmann et al.[111] showed that pyridine exhibited an increase of its Raman signal when adsorbed onto an electrochemically roughened silver electrode surface. Further observation by Jeanmaire and Van Duyne examined some factors that would affect the intensity of the Raman signal, such as surface roughness, electrolyte composition of the solution and an intrinsic

electromagnetic effect.[112] However, Albrecht and Creighton reported that a charge-transfer effect was the reason behind this enhancement.[113] It is now understood that there are two primary mechanisms underlying the SERS enhancement: an electromagnetic (EM) and a chemical enhancement (CE).[59,114] Theoretical predictions estimate that the chemical mechanism contributes ~10^2 to the overall enhancement, while the electromagnetic enhancement contributes the most to SERS, approximately 10^4-10^{10}.[59,114] Therefore, the metal surface is carefully designed and roughened on the nanoscale for optimal electromagnetic enhancement. Electromagnetic enhancement results from the collective oscillation of conduction electrons when an incident electric field interacts with a metallic surface.[114,115] Laser excitation of a roughened metal surface gives rise to a collective oscillation of conduction electrons in that surface, which generates a localized surface plasmon resonance (LSPR) as shown in Figure 3.3. When a surface plasmon is present, the Raman signal will be enhanced. The chemical enhancement mechanism is related to the chemical interactions between the metal and adsorbed molecule. These interactions lead to an enhancement of signal up to (10^2).[114-116]

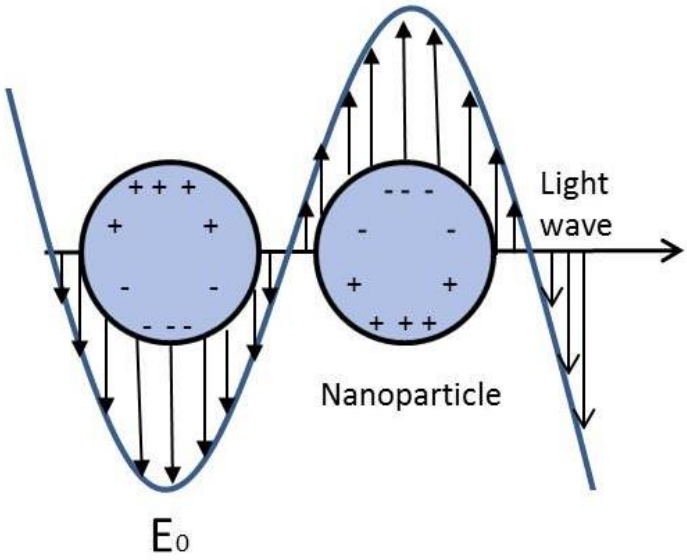

Figure 3.3: Schematic illustration of localized surface plasmon resonance on metal nanospheres. Adapted from reference [115].

Surface-enhanced Raman scattering (SERS) has been used for a wide range of sensing applications, including biosensing and environmental analysis.[117] Specifically, SERS biosensing applications have been employed to detect and identify small molecules, nucleic acids, lipids, peptides, and proteins, as well as for in vivo and cellular sensing. SERS is particularly well-suited to these tasks because of the high sensitivity, and the molecular fingerprinting capability. In addition, as mentioned previously water has very weak Raman scattering, which leads to minimal background signal from aqueous samples, which is generally preferred for biological studies.[117]

3.3.3-Electrochemical Surface-Enhanced Raman Spectroscopy (EC-SERS)

The coupling of SERS with an electrochemical cell is referred to as electrochemical surface enhanced Raman spectroscopy (EC-SERS). This technique is used to detect the signal of the analyte present on the metal surface at a chosen applied

voltage, and allows for SERS investigaitons of redox systems. Both chemical and physical enhancements can be influenced to some extent by applying a potential, which makes EC-SERS one of the most complicated systems in SERS.[117] Generally, it has been widely accepted that the SERS enhancement effect is contributed to by both the electromagnetic field enhancement (EM) and chemical enhancement (CE).[59,114] Changing the voltage can have an effect on both the chemical and electromagnetic enhancement by altering parameters such as surface charge, electric field and the Fermi level of the metal.[109]

Since the first SERS (also EC-SERS) report of pyridine adsorption on a roughened Ag surface, many papers have been published on various aspects of SERS and EC-SERS.[109] Van Duyne and coworkers have developed a metal film over nanosphere (MFON) technique to fabricate SERS-active electrode surfaces with nanostructured morphology.[118] The surface roughness produced by vapor deposition of a SERS-active metal on top of a nanosphere arrangement is useful for SERS studies under electrochemical conditions because they are not restricted to specific electrolyte environments during the SERS-active generation. Zhang et al. have shown that silver film over nanosphere electrodes are feasible surfaces for the study of electrochemical surface enhanced Raman scattering spectroscopy because of their stability in both aqueous and nonaqueous electrolytes.[119] This MFON substrate was used for detection of bacterial endospore based on the endospores marker -- dipicolinic acid, where the dipicolinate vibrational features are observed in the SERS spectra.[119] In addition, EC-

SERS plays a significant role in biodetection because of its sensitivity and selectivity for diagnostic techniques in biological and biomedical applications.[120]

Recently, electrochemical surface enhanced Raman spectroscopy (EC-SERS), combining both electrochemistry and surface enhanced Raman spectroscopy (SERS), has been developed for routine spectroelectrochemical analysis. A simple, portable EC-SERS system, consisting of a small benchtop Raman spectrometer, a laptop computer, and a portable USB potentiostat, has been reported by Brosseau et al. for real-time on-site monitoring of patient biomarkers.[156] Zhao et al. used this EC-SERS set-up to detect uric acid, a urine biomarker of preeclampsia.[66] In this work, Zhao et al. were able to obtain quantitative detection of uric acid in both 0.1 M NaF and synthetic urine. The electrode was modified by multilayers of gold and silver to achieve a better enhancement of the SERS signal. Karaballi et al developed an EC-SERS DNA aptasensor for direct detection of tuberculosis DNA hybridization.[70] This system has been used in this thesis research for all the target biomarkers in order to obtain SERS data that would then be compared to data obtained from the SERS-active fabric chip.

Chapter 4 Material and Methods

4.1 Reagents and solutions

Prior to use, all glassware for experimentation was first soaked in a bath of neat sulfuric acid overnight, followed by careful rinsing with Millipore water, (>18.2 MΩ cm). All solutions were prepared using Millipore water. Sodium citrate (99%), citric acid (99.9%), sodium fluoride (99%), 4,4'-bypiridine (99%), 4-aminothiophenol (4-ATP) (97%), levofloxacin (≥98%), 2-Deoxyguanosine monohydrate (99-100%) and guanine (98%) were all purchased from Sigma Aldrich (St. Louis, MO) and used without further purification. Potassium chloride (>99%) was purchased from Chimiques ACP Chemicals (Saint-Léonard, QC, Canada). Sodium borohydride ($NaBH_4$, 99 %) was purchased from Fluka Analytical (Seelze, Germany). Silver nitrate (99.9995%) was purchased from Alfa Aesar (Wardhill, MA, U.S.A). 6-thiouric acid (>98%) was purchased from Toronto Research Chemicals (Toronto, ON). Synthetic urine was purchased from Ricca Chemicals (Arlington, TX). Fabric swatches were purchased from Pickering International, Inc. San Francisco, USA. The fabric substrates that have been chosen in this research were: (100% organic cotton, 100% bamboo, 100% hemp, 100% dyed cotton, and blend fabric (37% silk, 35% hemp, 28% org.cotton)). Achira Labs, in Bangalore, India, supplied fabric-based electrode samples. Silver conductive ink and carbon conductive ink were purchased from Applied Technologies, Inc (Exton, PA, USA).

4.2 Instrumentation

4.2.1 Electrochemistry

All EC-SERS measurements were conducted using either the screen printed electrode (SPEs), or the fabric based electrode (both electrodes are shown in Figure 4.2.1). The former was purchased from Pine Research Instrumentation. Built into the SPE is a 5 mm x 4 mm (20 mm^2 surface area) rectangular carbon working electrode, a Ag/AgCl reference electrode, and a carbon counter/auxiliary electrode. The latter was supplied from Achira Labs (Bangalore, India), and was made by integrating the three electrodes (carbon working electrode (WE), silver/silver chloride (Ag/AgCl) reference electrode (RE), carbon counter electrode (CE) into a piece of silk fabric. Each electrode was coupled to the Raman spectrometer and the potentiostat. A Pine Research Instrumentation portable USB Wavenow potentiostat / galvanostat (Durham, NC, U.S.A.) was used for conducting electrochemical measurements. The electrochemical software was Aftermath Data Organizer (version 1.2.4843), also produced by Pine Research Instrumentation. For EC-SERS measurements, the laser was focused onto the working electrode of a modified SPE or fabric-based electrode in an electrochemical small-volume cell as shown in Figure 4.2.2. SERS spectra were collected at each applied voltage. Usually the signal was first collected at open circuit potential (OCP), and then from 0.0V to -1.0V (cathodic scan) in increments of 0.1V for a time interval of 30 seconds, and then returned from -1.0V to 0.0V (anodic scan) in increments of 0.1V for 30 seconds. Hence, for the silver electrode, all applied voltages were negative, and positive voltages were not explored in order to prevent oxidation of the silver surface. SERS spectra were always

collected in a darkened room so as to reduce interference from room light. The electrochemical set up is shown in Figure 4.2.3

For the majority of the EC-SERS measurements, the supporting electrolyte was deaerated 0.1M NaF. The SPE was placed in a special USB adapter for the cell vial, which was connected to the USB potentiostat. Before adding the electrolyte, the SERS signal was collected in air first to ensure that the laser was focused on the electrode surface. Once focused, electrolyte was added, and voltages were applied and the corresponding SERS spectra were collected.

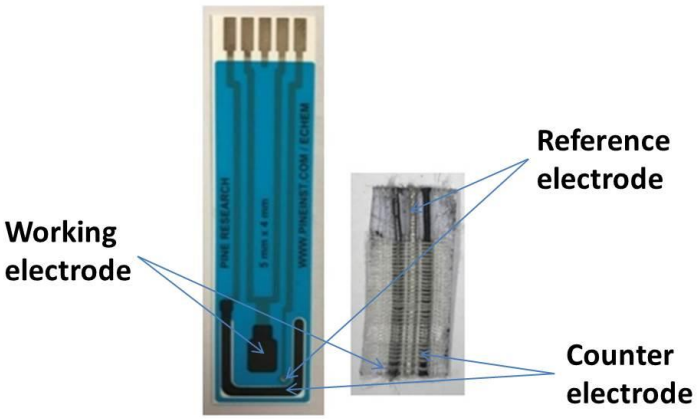

Figure 4.2.1: Screen-printed electrode (left), and Achira fabric-based electrode (right)

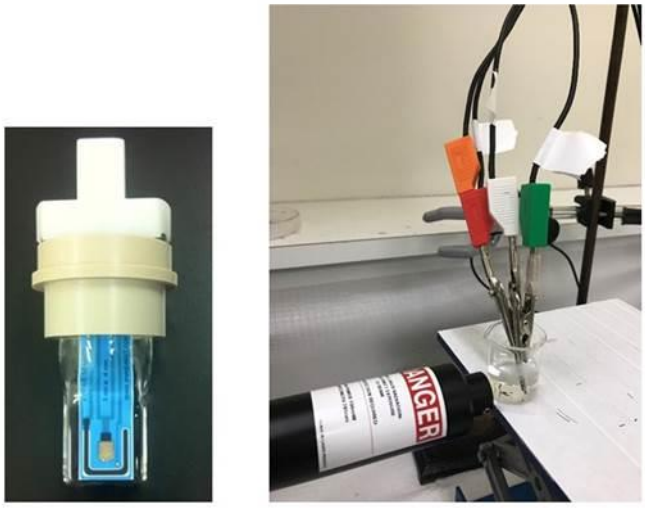

Figure 4.2.2: Photo of the setup used for EC-SERS, including the flat-walled vial, AgNP-modified screen-printed electrode, and USB connector (left), and Achira fabric-based electrode in an electrochemical cell.

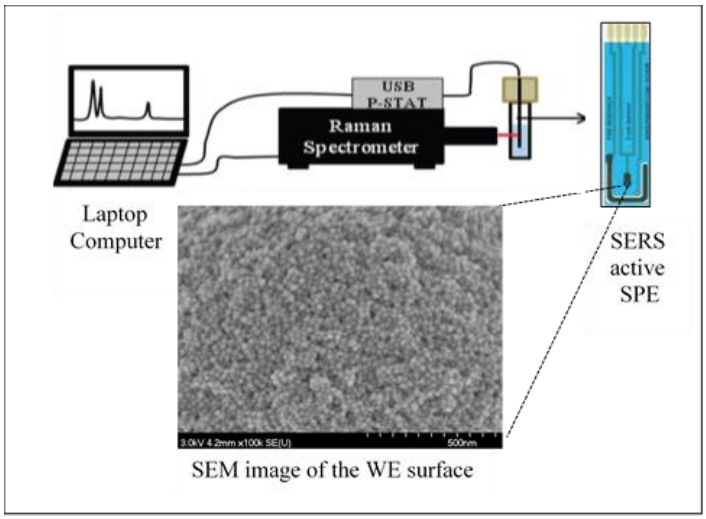

Figure 4.2.3: Schematic setup of the electrochemical surface enhanced Raman spectroscopy setup. The inset shows an SEM image of the Ag deposited onto the working electrode of a disposable screen printed electrode.[54]

4.2.1.1 Preparation of a sustainable fabric-based electrode

In addition to the fabric electrode supplied by Achira Labs, homemade fabric electrodes using the blend fabric were also explored. Blend fabric sample was cut into 15 X 40 mm strips. The first step was to force the conductive silver ink through a patterned stencil, which was then allowed to dry at 120 C˚ for 30 min. Silver ink was used as a conductive layer and as a reference electrode. After the first layer was applied, a second layer of a conductive carbon ink was added using another stencil, which was then dried at 70 C˚ for 30 min as seen in Figure 4.2.4.

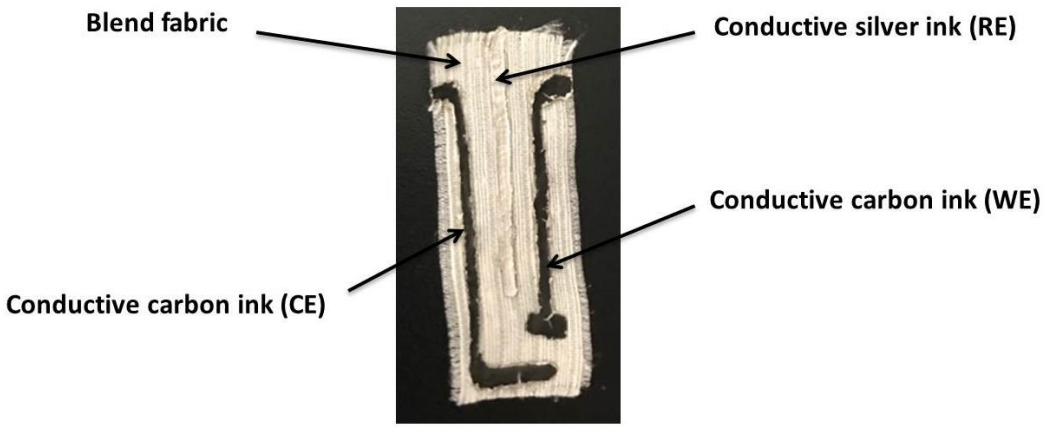

Figure 4.2.4: Sustainable fabric-based electrode.

4.2.2 Raman Spectrometer and SERS setup

All Raman experiments in this research were conducted using a DeltaNu (Intevac Photonics) benchtop dispersive Raman spectrometer equipped with an air-cooled CCD, and connected to a laptop computer which uses NuSpec software for signal processing and the setting of spectral parameters. The software was also produced by DeltaNu. This

spectrometer is equipped with a laser excitation wavelength 785 nm diode laser and an optics extension tube as well as a right angle attachment. All the SERS and EC-SERS spectra on the fabrics were collected at power and acquisition times typically 22.3−55.9 mW and 30−60 s, respectively. The spectrometer resolution was 4 cm^{-1}.

All fabric samples were placed on a glass slide and placed under the laser. For spectral processing and data analysis, the software program Origin 9.0 (OriginLab Corporation, Northampton, MA, U.S.A.) was used on a standard PC. All data measured were corrected for acquisition time and laser power and also smoothed using the adjacent-averaging smoothing method (8 points).

4.2.3 UV-VIS spectrophotometry

UV-visible spectrophotometry measurements were made using a Cary 50 Bio UV-visible spectrophotometer produced by Varian (Palo Alto, CA, USA) with a Xenon flash lamp which can optimize light thoughput at 500 nm using the Align application module in the Varian Cary WinUV™ Bio software. This instrument was used to record the extinction spectra for the colloidal sols. A sample of the sol was placed in a quartz cuvette and irradiated using a UV-visible deuterium light source.

4.3 Selection of Fabric for Sensor Platform

Five different types of fabrics were selected for use as a sensor platform including: 100% white cotton, 100% dyed cotton (blue), 100% bamboo, 100% hemp, and blend (37% silk, 35% hemp, 28% cotton). These fabrics were selected because they have a high moisture absorption, are commonly used, and are sustainable and naturally

sourced. All the SERS experiments were conducted on all these fabrics in order to determine the optimal fabric.

4.4 Modification of fabric for SERS

Fabric samples (3.0-6.0 mg, approximately 5-8 mm^2) were treated with silver nanoparticles, as described below. For SERS measurements, 40 μL of 1.0 mM aqueous stock solution of the target analytes (4,4'-bypyridine, 4-ATP, 6-TUA, levofloxacin, 8-deoxyguanosine, and guanine) was deposited on the modified fabric samples and allowed to air-dry prior to the SERS measurement.

4.4.1 AgNP synthesis and characterization

Silver nanoparticles were prepared according to the method by Zhao et al. method.[66] This method utilizes a three-necked, flat-bottomed round flask. Solutions of $AgNO_3$ (1.00 mL, 0.10 M), sodium citrate (3.40 mL, 0.17 M) and citric acid (0.60 mL, 0.17 M) were added to 95ml water, and stirred under reflux. $NaBH_4$ (0.20 mL, 0.10 mM) was added to this mixture, which was then heated to boiling. After 1 hour of boiling, the colloidal suspension was removed from the heat and allowed to cool to room temperature for 1 or 2 hours. To concentrate the AgNPs, 1.4 mL aliquots of the AgNP suspension were added to 14 Eppendorf tubes and centrifuged at 8000 rpm for 20 minutes. The supernatant was then removed and discarded, and collected the NP pellets were collected into two centrifuge tubes for another round of centrifugation. Finally, after removing and discarding the supernatant, the AgNP "paste" was obtained.

4.4.2 Modification of fabric with AgNPs

Once the AgNPs were prepared, 10 μL of the AgNP paste was drop cast onto the surface of each fabric sample and allowed to air-dry. In initial experiments, 1 layer of 10 μL was deposited, and in most subsequent experiments, 3 layers of 10 μL were added. Once the third layer dried, the fabric sample was incubated in 0.5 M potassium chloride solution for 30 min. This step was conducted for most of the experiments in this research in order to remove the interfering citrate from the surface via displacement with chloride ions, due to the strong specific adsorption of chloride on silver.

For the SPEs, 3 layers of 5 μL of the AgNP paste was added and allowed to dry. For the fabric-based electrode, 3 layers of 2 μL was added; the amount of AgNPs was less than the previous experiments because of the small size of the working electrode. KCl treatment also was conducted on these electrodes.

4.4.3 Characterization of plasmonic fabric-based sensor

The untreated and treated fabric samples as well as the fabric-based electrods were imaged using a TESCAN Mira3 LMU field emission SEM (Warrendale, PA, U.S.A). This FE-SEM has a tungsten electron gun and is fitted with both a back scatter and a secondary electron detector. Energy dispersive X-ray spectra (EDS) were collected using an INCA X-max 80 mm^2 EDS system that uses a silicon drift detector (SDD). The SERS performance of the modified fabric was also investigated, both for common Raman probe molecules as well as the three target biomarkers

Chapter 5 Results and Discussion

5.1 Nanoparticle characterization

5.1.1 UV-vis spectroscopy

UV-vis spectroscopy is commonly used for the characterization of nanoparticles because it can provide information concerning size-dependent properties through peak broadening and shifts in the extinction profile. Figure 5.1.1 shows the UV-vis extinction spectrum for the AgNP colloid used in this work. Normally an extinction maximum is observed in the spectrum (λ_{max}), which corresponds to the localized surface plasmon resonance (LSPR); the AgNPs use in this thesis work exhibited a LSPR peak at 390 nm. In addition, the LSPR peak was observed to have a low FWHM, indicating that the colloid sample was likely near-monodisperse in terms of nanoparticle size and shape.

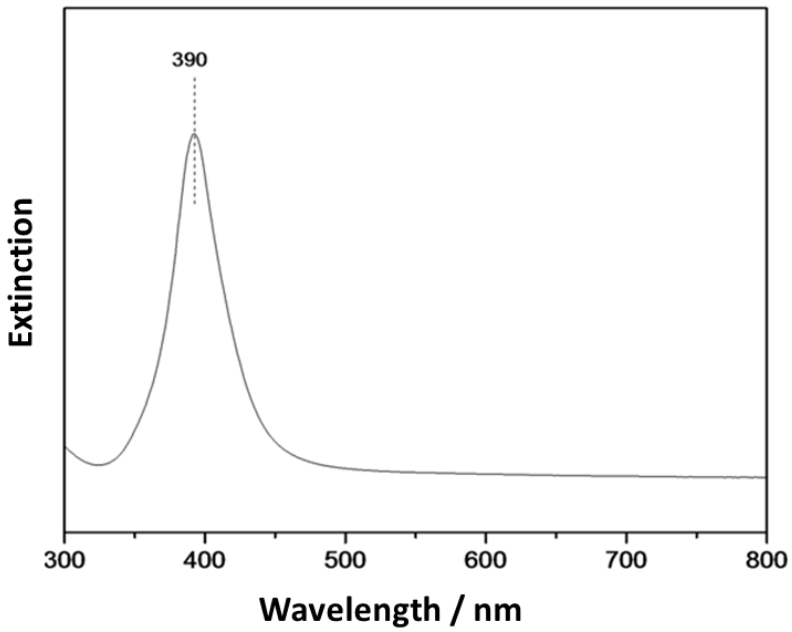

Figure 5.1.1: UV-vis spectrum of AgNP colloidal sol

5.1.2 SEM and TEM of silver nanoparticles

AgNPs were also characterized by SEM and TEM imaging as shown in Figure 5.1.2a and b, respectively. From the TEM image, it was determined that the approximate size of these NPs was 25±6 nm, using ImageJ software available from National Institutes of Health. These images indicated that the nanoparticles were indeed near-monodisperse and of an appropriate size to support efficient SERS enhancement.

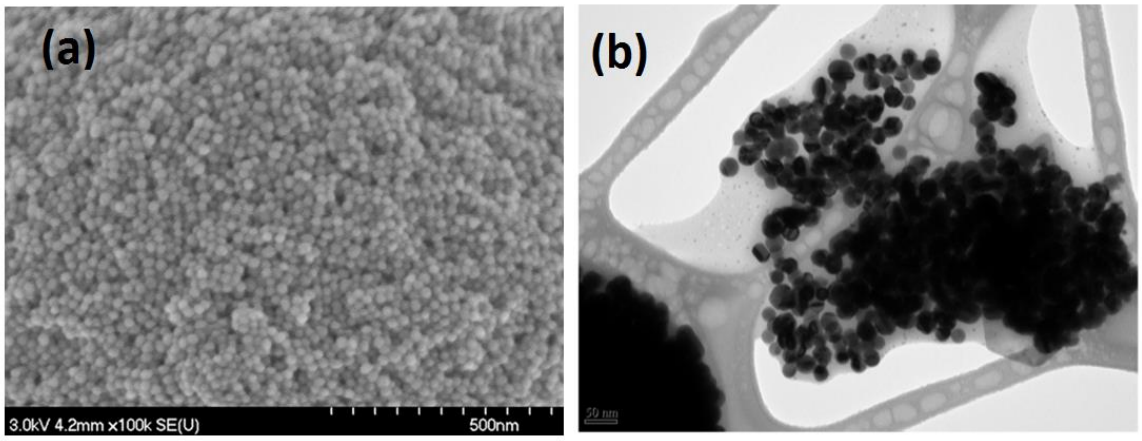

Figure 5.1.2: (a) SEM image of silver nanoparticle (b) TEM image of silver nanoparticle

5.2 Electrochemical SERS (EC-SERS) investigation of target biomarkers

5.2.1 Introduction

This section includes all the EC-SERS results for the four biomarkers (6-thiouric acid (6-TUA), levofloxacin, guanine, and 2-deoxyguanosine) on the screen-printed electrode. EC-SERS is used to detect the signal of the analyte present on the metal surface at a chosen applied voltage. Electrochemical SERS can be useful in detecting the

signal of the analyte in relevant biological environments, and to observe potential-dependent changes in the conformation or orientation of an analyte.[110]

This system has been used in this thesis research for all the target biomarkers in order to obtain SERS data that could then be compared to data obtained from the SERS-active fabric chips.

5.2.2 EC-SERS of biomarkers of interest

5.2.2.1 EC-SERS of 6-thiouric acid on SPE

The normal Raman spectrum of 6-TUA powder is shown in Figure 5.2.1 a, with a strong background fluorescence clearly present. As a result of the significant fluorescence, a background correction was applied (Figure 5.2.1 b). A band assignment for 6-TUA is provided in Table 1.

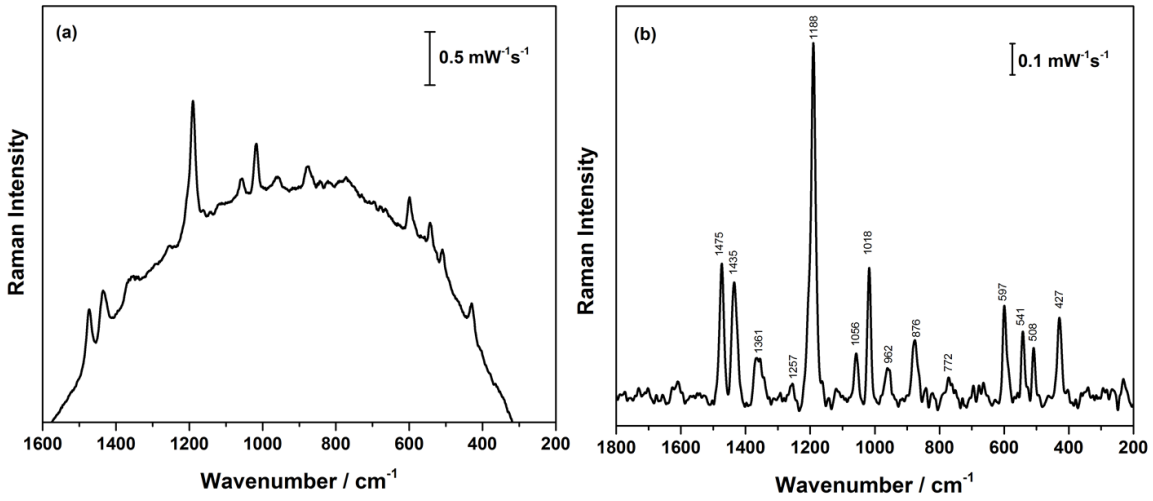

Figure 5.2.1: Normal Raman spectrum of 6-TUA powder, collected for 30 seconds at 785 nm excitation, laser power was 55 mW (a) before (b) after baseline correction.

Table 1. Vibrational mode assignments for both the normal Raman spectrum and the SERS spectra for 6-thiouric acid. Assignments were made based on calculated frequencies as well as reported literature values.

Raman peak / cm^{-1}	**SERS peak / cm^{-1}**	**Assignment**
430	--	
509	516	
542	--	δ(NCS)
600	602	ν(C-S)
--	692	ν(CNC), ip def
772	781	ring def
879	880	ring def
959	943	ν(C=S), ν(C-N)
1018, 1058, 1191	1006, 1081, 1196	Mixed ring def, NH def
--	1272	δ(=NH)
1437	--	NH ip def
1474	--	NH ip def
--	1529	ν(C=C-C), ν(C=C-N)
--	1618	ν(C=C-N), δ(NH)
--	1653	ν(C=C), δ(NH)

Electrochemical SERS (EC-SERS) measurements of 6-TUA were conducted on screen-printed electrodes after the carbon working electrode had been modified with three layers of AgNPs, according to a previously established approach from the Brosseau lab.[54] One major issue with this synthesis is that the nanoparticles are left with a layer of citrate on the surface, which functions as a capping agent, preventing nanoparticle aggregation. Unfortunately, this can limit the use of these nanoparticles for SERS since the citrate molecules give rise to a significant SERS background signal, and limit surface adsorption

of target analytes due to both electrostatic repulsion and reduced surface coverage. Therefore, the electrode was immersed in 0.5M KCl for 30 min, rinsed with deionized water and allowed to air dry prior to the EC-SERS measurements. This is demonstrated in Figure 5.2.2, where the citrate peaks are initially present (Figure 5.2.2a) and then removed after chloride treatment (Figure 5.2.2b). In this case, the chloride ion displaces the citrate ions from the surface of the silver. Studies have shown that Cl^- has a strong specific adsorption on Ag and is able to displace adsorbed citrate, leaving a layer of AgCl on the nanoparticle surface.[4] The chloride is small compared to citrate and is not as Raman active; only the ν(Ag-Cl) band is typically observed at ~230 cm^{-1}. Since the SERS enhancement is distance dependant, the closer the target molecule is to the surface, the more SERS enhancement can be observed. Therefore, the advantages of using this citrate removal step include reduction in citrate spectral interference and improved enhancement of the SERS signal. This enhancement of the signal was clearly observed when the EC-SERS measurements of 6-TUA was performed on both chloride-treated and chloride-untreated electrodes as shown in Figure 5.2.3. This pre-treatment step is necessary for many analytes for improved surface adsorption and thus improved signal intensity. Modification of the SERS surface in this manner has little to no effect on the magnitude of the SERS signal enhancement.

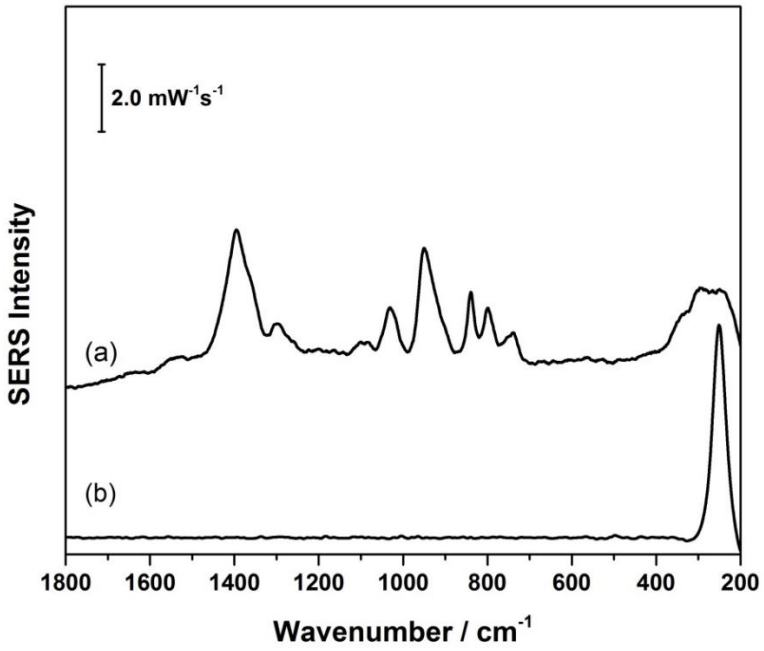

Figure 5.2.2: (a) SERS spectrum, recorded in air (30 second acquisition, 785 nm excitation) for an untreated AgNP electrode (b) SERS spectrum of electrode in (a) after incubation in 0.5 M KCl for 30 minutes, followed by rinsing with distilled water.

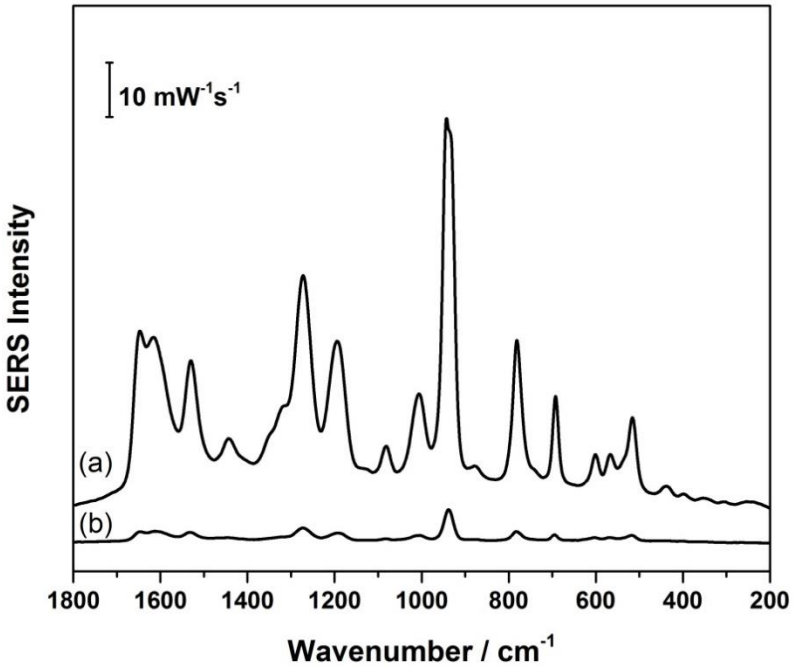

Figure 5.2.3: EC-SERS spectra obtained for 1.0 mM 6-TUA at an applied voltage of -1.0 V vs Ag/AgCl for (a) AgNP electrode treated with potassium chloride and (b) untreated AgNP electrode. Acquisition time was 30 seconds at 785 nm excitation.

Electrochemical surface-enhanced Raman spectroscopy (EC-SERS) data were collected first at open circuit potential (OCP), and then were collected from 0.0 V to -1.0 V vs Ag/AgCl in 100.0 mV increments, in both the cathodic and anodic directions. Figure 5.2.4 shows the EC-SERS data collected for OCP and the then for a few selected potentials in the cathodic direction for 1.0 mM 6-TUA prepared in 0.1 M NaF. The signal at OCP is clearly detectable, with peaks due mainly to the bending and stretching vibrations associated with the N-C═S and N-C═O moieties. As the potential is made more negative, the observed SERS signal increases in intensity, such that at -1.0 V, the signal has increased by over an order of magnitude. This increase of the 6-TUA signal is clearly seen for the 943 cm^{-1} peak, which is attributed to ν(C=S) and ν(C-N) modes, and the peaks at 1196 cm^{-1} and 1272 cm^{-1}, attributed to mixed ring modes and N-H deformations, respectively. These results indicated that 6-TUA was present in the thioketone form in aqueous solution. Ab-initio calculations (not shown) confirmed that this is the most stable species of 6-TUA.

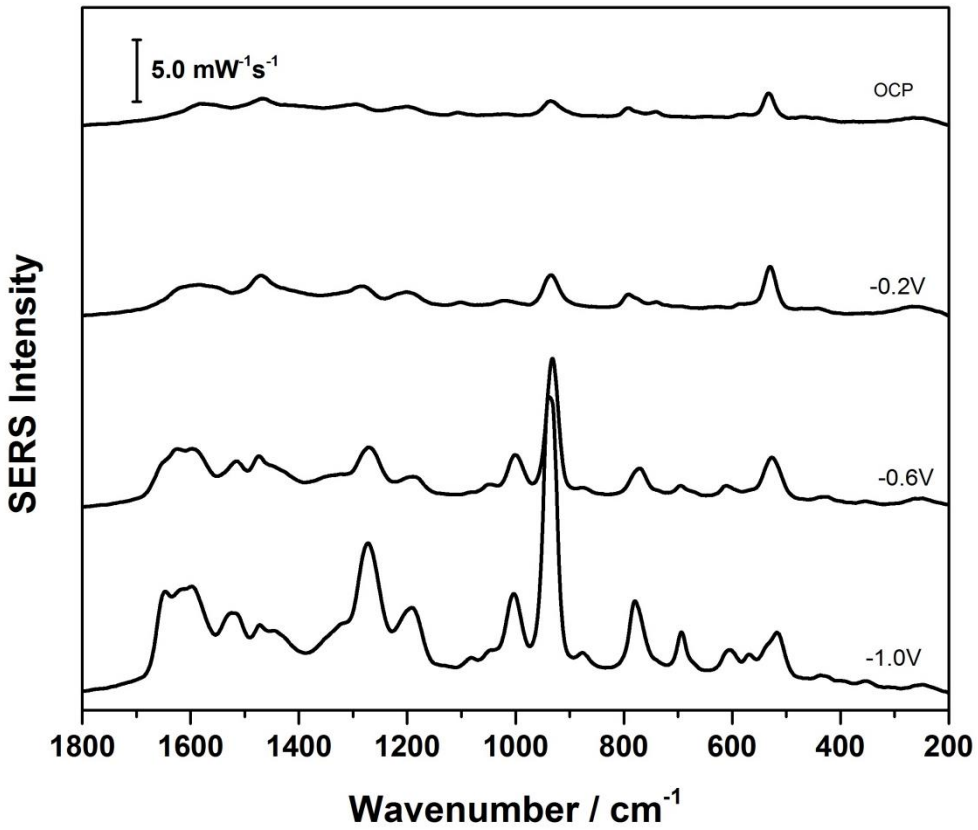

Figure 5.2.4: EC-SERS spectra for 1.0 mM 6-TUA at open circuit potential and three selected applied potentials. Each spectrum acquisition time was 30 seconds at 785 nm excitation. Laser power was 46.5 mW. Supporting electrolyte was deaerated 0.1M NaF.

Once the EC-SERS studies were completed using 0.1 M NaF as an electrolyte, it was important to test EC-SERS using synthetic urine. Figure 5.2.5 shows the EC-SERS spectra of 1.0 mM 6-TUA prepared in synthetic urine as supporting electrolyte at selected applied potentials. The 6-TUA signal was clearly detectable, and increased with increasing applied voltage. From the EC-SERS comparison at -1.0V in Figure 5.2.6, it is clear that there is a significant signal reduction for the study conducted in synthetic urine; however the SERS signal could still be readily obtained.

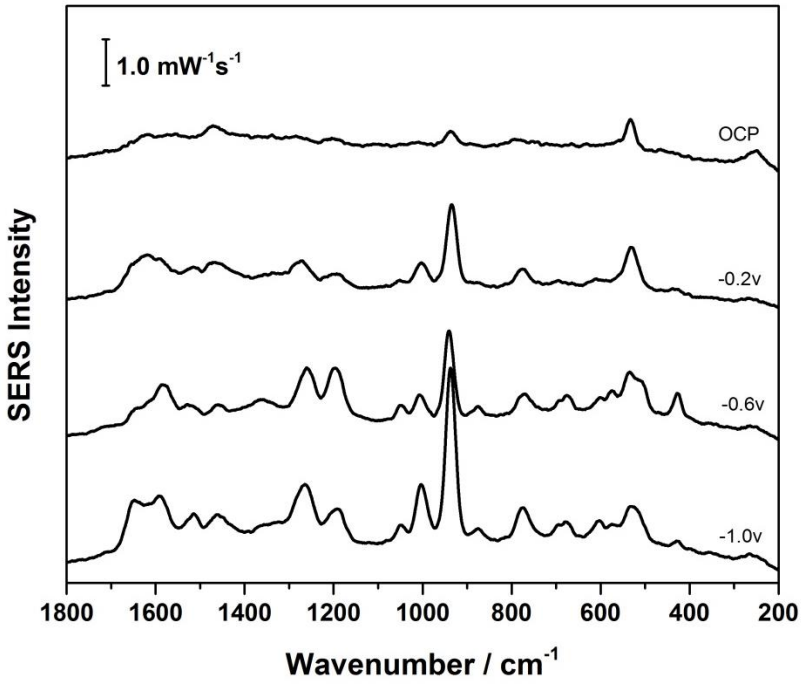

Figure 5.2.5: EC-SERS spectra of 1.0 mM 6-TUA in synthetic urine at open circuit potential and several selected applied potentials. Each spectrum acquisition time was 30 seconds at 785 nm excitation.

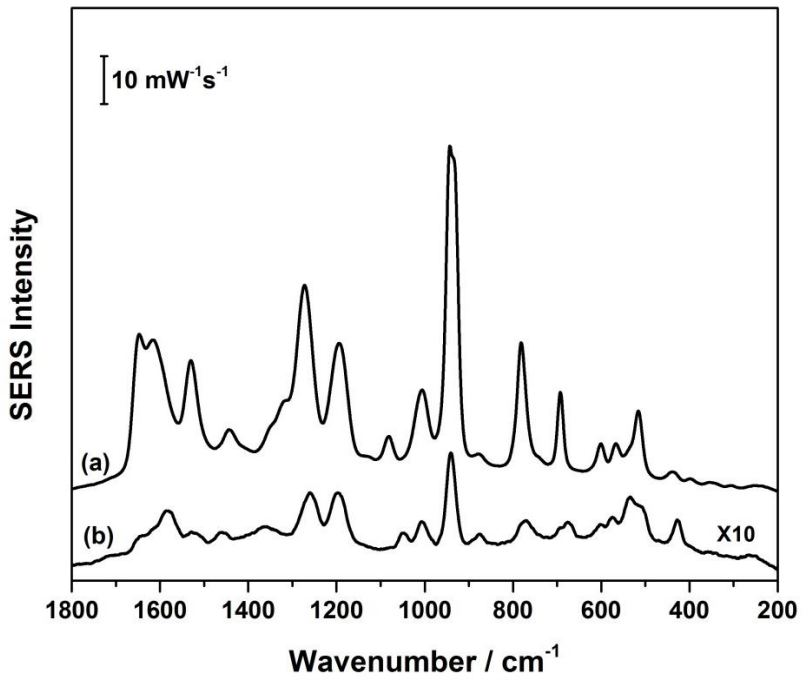

Figure 5.2.6: Comparison of EC-SERS signal for 1.0 mM 6-TUA at an applied potential of -1.0 V vs Ag/AgCl for (a) 0.1 M NaF as supporting electrolyte and (b) synthetic urine

as supporting electrolyte. Each spectrum acquisition time was 30 seconds at 785 nm excitation.

The last test attempted using EC-SERS for this biomarker was to detect 1.0 μM of 6-TUA in synthetic urine; this concentration is clinically relevant. Current methods which are being explored for the detection of 6-TUA generally report detection limits in the μM range.[121,122] In this study, detection of 1 μM 6-TUA using EC-SERS was attempted. Figure 5.2.7 shows the comparison of the EC-SERS signal obtained for 1 mM 6-TUA and 1 μM 6-TUA, both in synthetic urine, at an applied voltage of -1.0 V vs Ag/AgCl. Clearly there is a significant reduction in signal, however the peak at 940 cm^{-1} is still detectable. As a result, with further optimization of this system, routine detection of 6-TUA at clinically relevant concentrations should be possible.

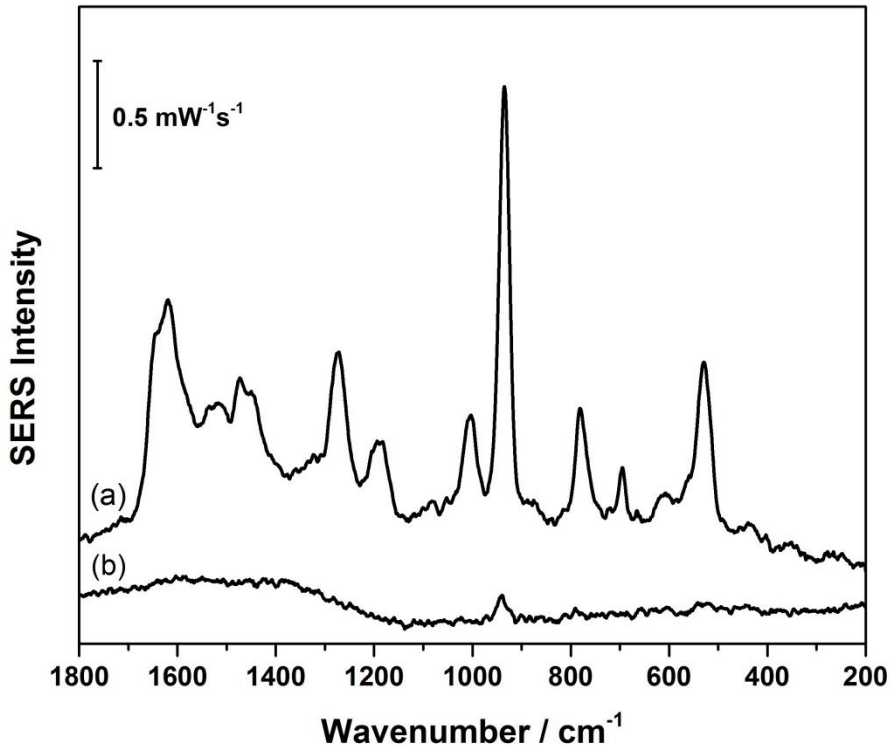

Figure 5.2.7: Comparison of EC-SERS signal obtained at -1.0 V vs Ag/AgCl in 0.1M NaF as supporting electrolyte for (a) 1.0 mM 6-TUA and (b) 1.0 mM 6-TUA. Each spectrum acquisition time was 30 seconds; laser power was 46.5 mW at 785 nm excitation.

5.2.2.2 EC-SERS of levofloxacin on SPE

The normal Raman spectrum of levofloxacin powder was collected as shown in Figure 5.2.8. All the peaks for levofloxacin were readily identified, and the band assignments are provided in Table 2. An EC-SERS study for levofloxacin was conducted using the modified SPE, using the same procedure as outlined previously for 6-TUA. The KCl treatment was applied for all the EC-SERS measurements, and 1.0 mM levofloxacin was measured in both 0.1 M NaF and synthetic urine. Looking at Figure 5.2.9a, the signal is gradually increased by applying an increasingly negative voltage (cathodic direction), and the signal then decreases as the potential returns in the anodic direction

(Figure 5.2.9b). The characteristic Raman vibrational modes for levofloxacin, located at 1401 and 1620 cm^{-1} were clearly detectable with the more enhanced signal at -1.0 V. Figure 5.2.10 shows a comparison between the SERS signal at OCP and the EC-SERS signal at -1.0V. The observable peaks are consistent with the normal Raman peaks as shown in Figure 5.2.11.

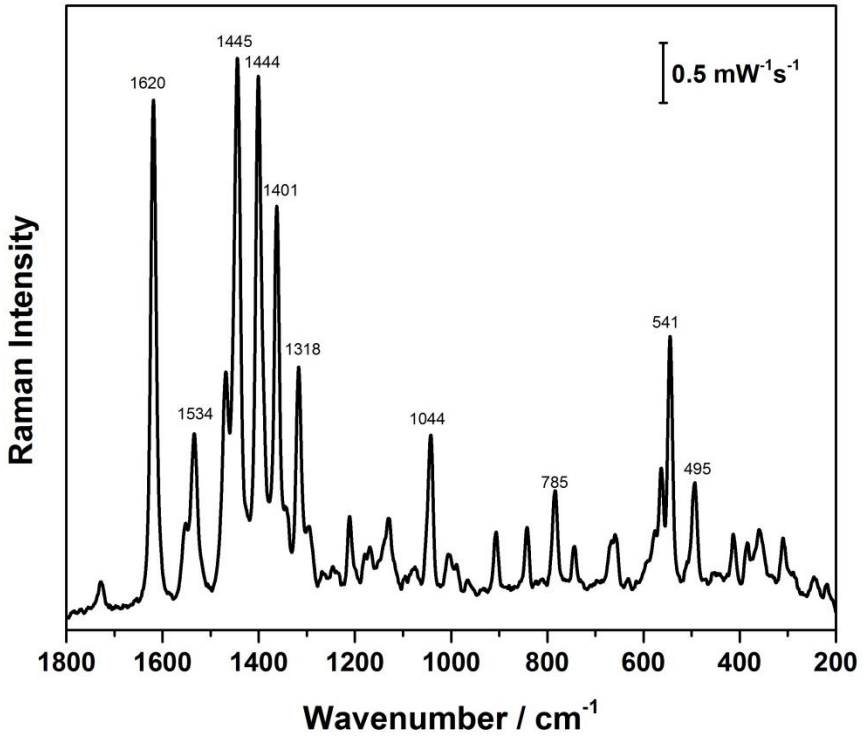

Figure 5.2.8: Normal Raman spectrum of levofloxacin powder. The spectra were measured at 22.3 mW for a time interval of 30 seconds using 785 nm excitation.

Table 2. Vibrational mode assignments for both the normal Raman spectrum and the SERS spectra for levofloxacin.[123]

Raman peak / cm^{-1}	**SERS peak / cm^{-1}**	**Assignment**
495	500	(C-N-C-CH_3) bending, mixed ring def
541	549	Ring def, O-H in-plane bending, CH_2 rocking
785	750	Ring stretching, C=O-O-H bending, C-C bending
1044	900	Ring stretching, CH_3 rocking
1318	1310, 1340	δ CH_2
1401	1380	CH_3 twisting, CH_2 in-plane rocking, O-H bending
1444	1400	CH_3 twisting, CH_2 in-plane rocking
1445	1450	$\upsilon(CH_3)$ υ(C-F) γ(C-H)
1534	1560	δ (C-H) δ (CH_2)
1620	1620	ν (C=C) ν (C=O) γ (O-H)

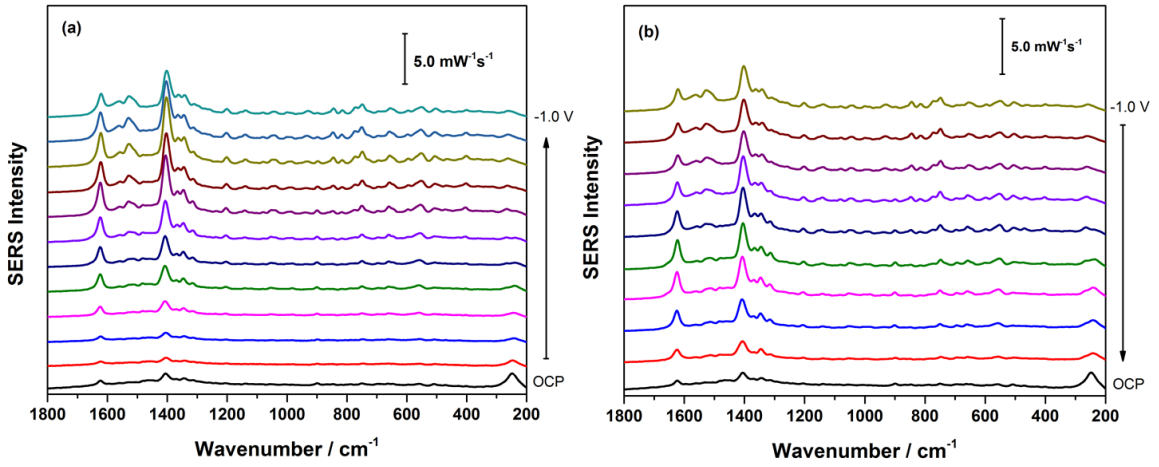

Figure 5.2.9: EC-SERS spectra for 1.0 mM levofloxacin at open circuit potential and applied potentials. Each spectrum acquisition time was 30 seconds at 785 nm excitation. Supporting electrolyte was 0.1 M NaF. Laser power was 46.5 mW.

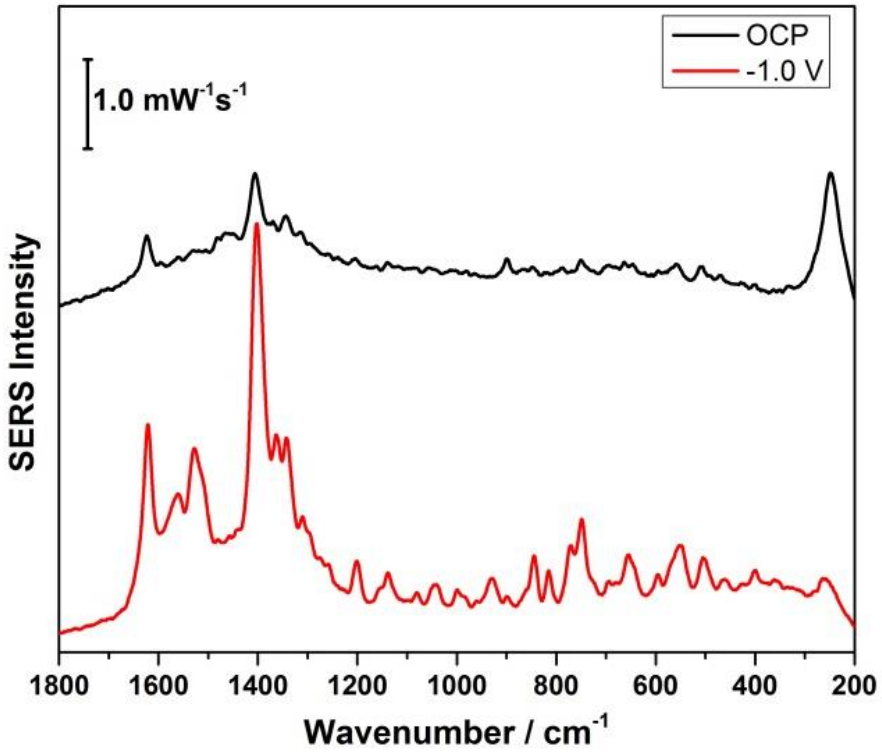

Figure 5.2.10: EC-SERS of 1.0 mM levofloxacin at OCP and at -1.0V. The spectra were measured at 46.5 mW for a time interval of 30 seconds using 785 nm excitation.

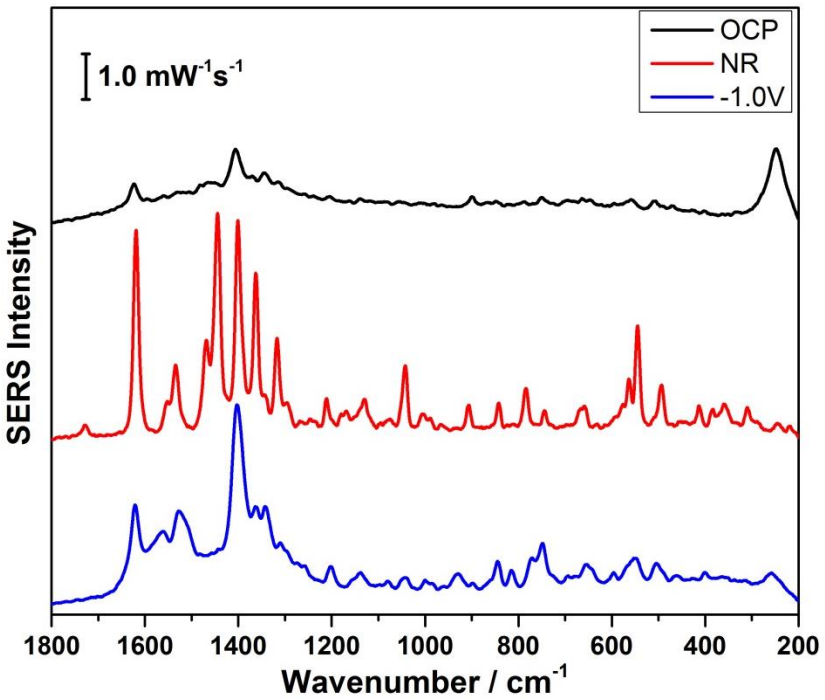

Figure 5.2.11: EC-SERS of 1.0 mM levofloxacin at OCP (black), normal Raman (red), and at -1.0V (blue). The spectra were measured at 46.5 mW for a time interval of 30 seconds using 785 nm excitation.

5.2.2.3 EC-SERS of guanine on SPE

The normal Raman spectrum was first collected for guanine powder (Figure 5.2.12), followed by EC-SERS measurements using the same approach as was used for the previous two biomarkers. The band assignments for prominent vibrational modes are given in Table 3. EC-SERS spectra of 1.0 mM guanine solution were recorded at OCP, and over the potential range of 0.0 to -1.0V (-1.0V increments) vs. Ag/AgCl. The intensity of these peaks gradually increased by applying a negative voltage as seen in the cathodic direction Figure (5.2.13a), and then slightly decreased upon a return to OCP as seen in Figure 5.2.13b. Looking at Figure 5.2.14, it is evident that the signal at -1.0V was very strong and was consistent with the normal Raman peaks.

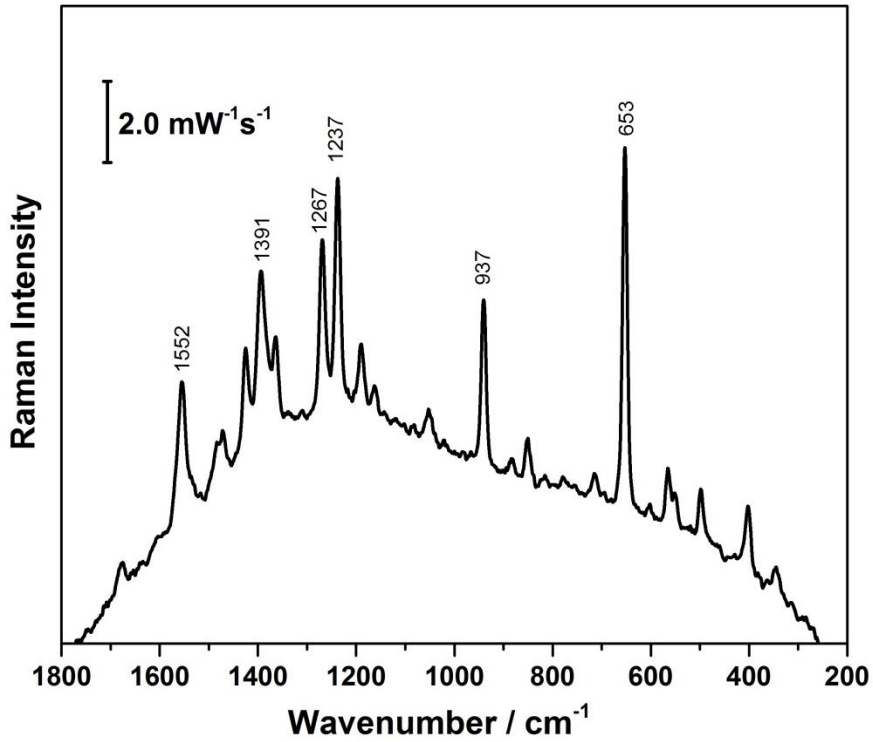

Figure 5.2.12: Normal Raman spectum of guanine powder. Spectra were measured at 10.6 mW for a time interval of 30 seconds using 785 nm excitation.

Table 3. Band assignment for the normal Raman and SERS spectra of guanine.

Raman peak / cm^{-1}	**SERS peak / cm^{-1}**	**Assignment**[124,125]
397	-	
494	-	
544	-	
561	-	N-C=N bending
653	650	Ring breathing
847	860	-
937	970	ν(C-C backbone)
1084	1034	ν(N-C), NH_2 rocking
1186	1140	-
1237	1220	ν(C=N)
1267	1263	Amide III, arising from the coupling of C-N stretching and N-H bonding.
1359	1340	ν(C-N—C-C)
1391	1385	ν(C-N + C-N—C=C), C-H rocking
1421	-	–
1465	1465	δ(CH)
1548	1530	ν(C=C-N), δ(NH)
1674	1690	ν(C=C), δ(NH)

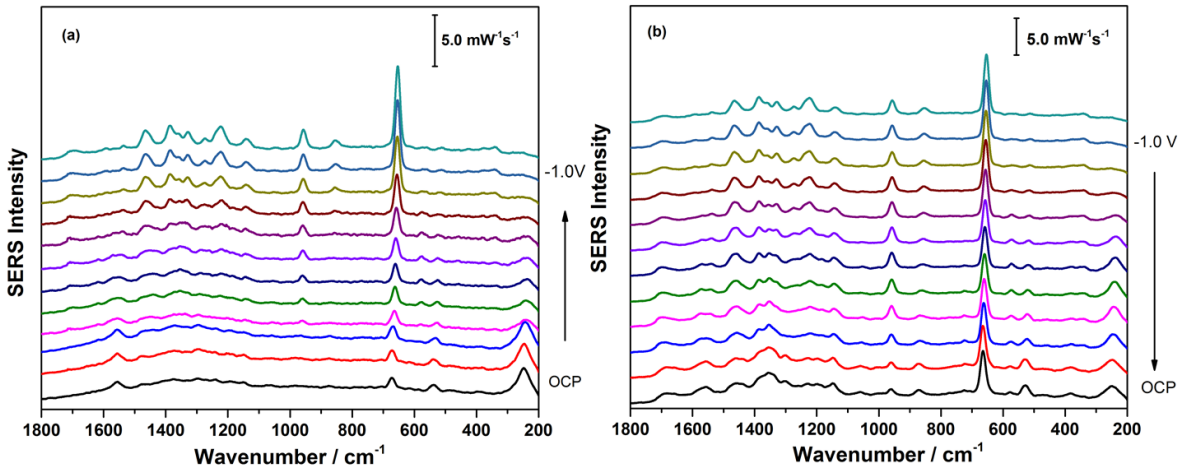

Figure 5.2.13: EC-SERS spectra for 1.0 mM guanine at OCP and applied potentials. Each spectrum acquisition time was 30 seconds, 46.5 mW laser power, at 785 nm excitation. Supporting electrolyte was 0.1 M NaF.

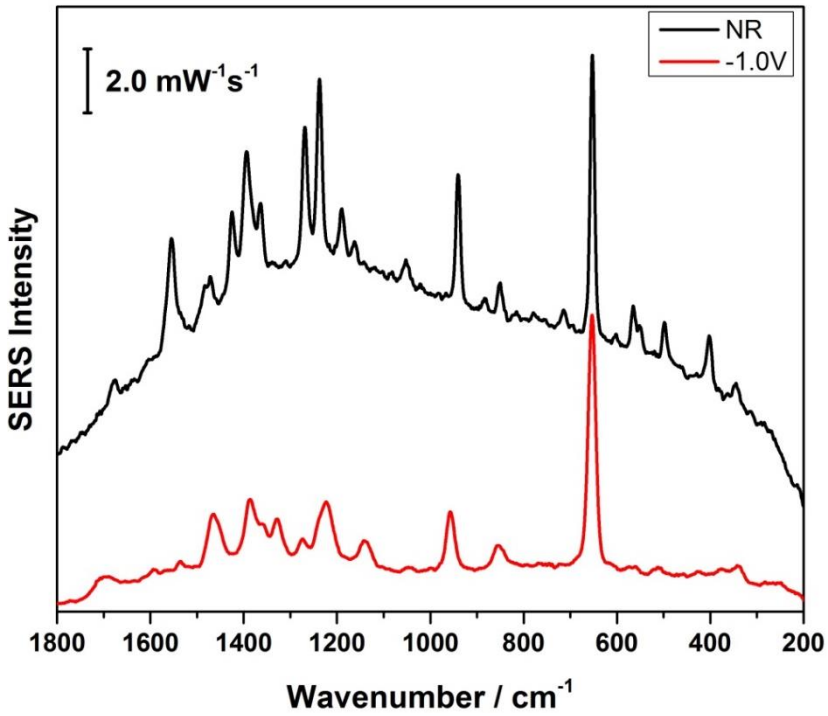

Figure 5.2.14: Comparison between normal Raman spectra of guanine powder (black) and EC-SERS spectrum of 1.0 mM guanine solution at -1.0V (red). Each spectrum acquisition time was 30 seconds, 46.5 mW laser power, at 785 nm excitation.

5.2.2.4 EC-SERS of 2-deoxyguanosine on SPE

The normal Raman spectrum was collected first for 2-deoxyguanosine (powder), the corresponding peaks were readily observed as shown in Figure 5.2.15, and the peak assignments are shown in Table 4. EC-SERS was performed on 1.0 mM 2-deoxyguanosine using the exact same procedure as used for the other biomarkers. It was noticed that the signal at OCP was weak and noisy, and upon application of a negative voltage, the SERS signal increased. The best signal was collected at -0.7V as seen in Figure 5.2.16, and then the signal disappeared and did not return upon returning to more positive voltages. By looking at the overlaid spectra of 2-deoxyguanosine in Figure 5.2.17, it is shown that the signal at -0.7 V was consistent with the normal Raman signal of the powder, although quite low in intensity.

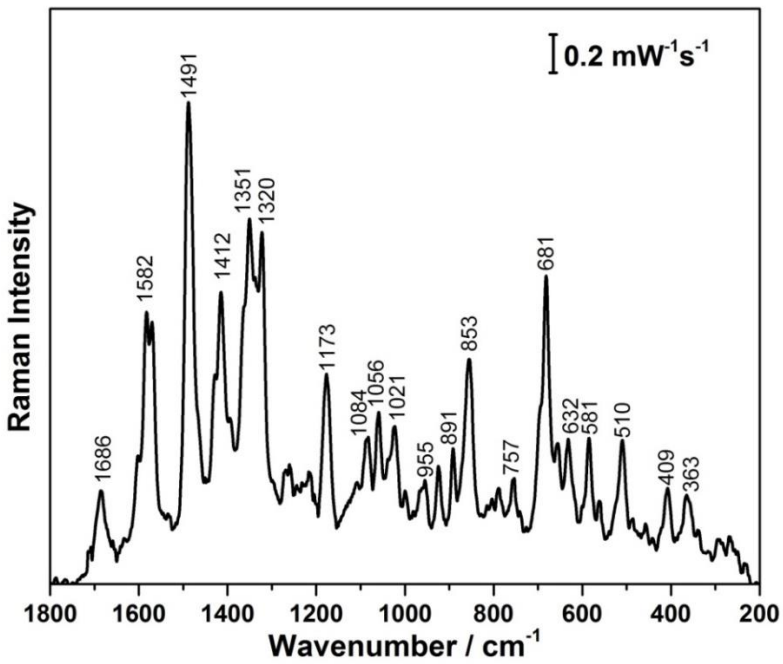

Figure 5.2.15: Normal Raman spectrum of 2-deoxyguanosine. The spectra were measured at 22.3 mW for a time interval of 30 seconds using 785 nm excitation.

Table 4. Vibrational mode assignments for both the normal Raman spectrum and the SERS spectra for 2-deoxyguanosine.

Raman peak / cm^{-1}	**SERS peak / cm^{-1}**	**Assignment**[126]
363	-	-
409	-	Raman deformation
510	520	-
581	570	-
632	673	(CNC), ip def
681	692	NH_2 rocking and N-H bending on guanosine ring
757	-	-
853	860	ν(N-C), NH_2 rocking
891	-	C-C stretching
955	-	ν(C-N)
1021, 1056, 1084	-	Mixed ring def, NH def
1173	1190	N-H and C-H bending in guanosine moiety
1320	1285	δ(=NH)
1351	1340	C-N stretching
1412	-	–
1491	1460	ν(C=N) and NH_2 scissoring in guanosine moiety, C=C stretching
1582	1570	ν(C=C-C), ν(C=C-N)
1686		ν(C=C), δ(NH)

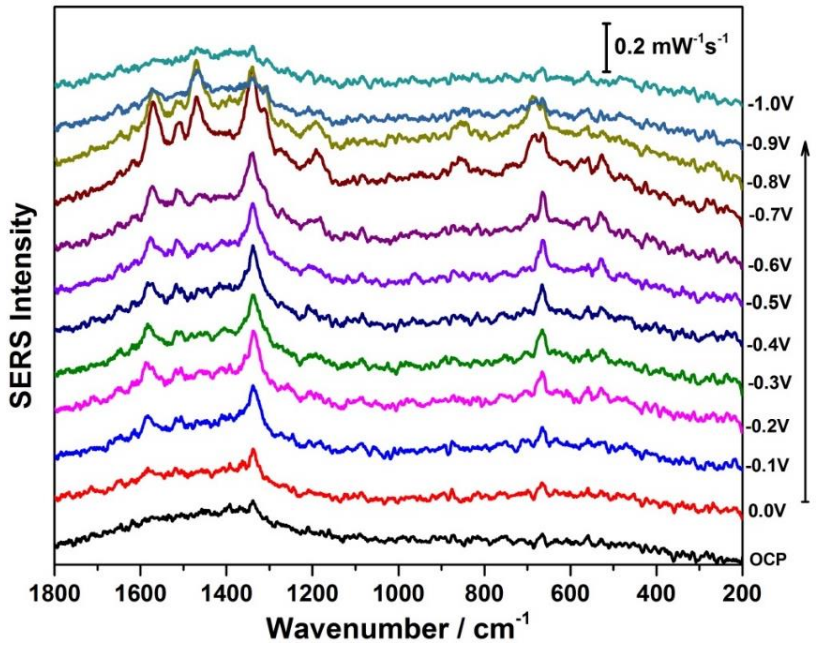

Figure 5.2.16: EC-SERS spectra for 1.0 mM 2-deoxyguanosine at OCP and applied potentials (0.0V to -1.0V). Each spectrum acquisition time was 30 seconds, 46.5 mW laser power at 785 nm excitation. Supporting electrolyte was 0.1 M NaF.

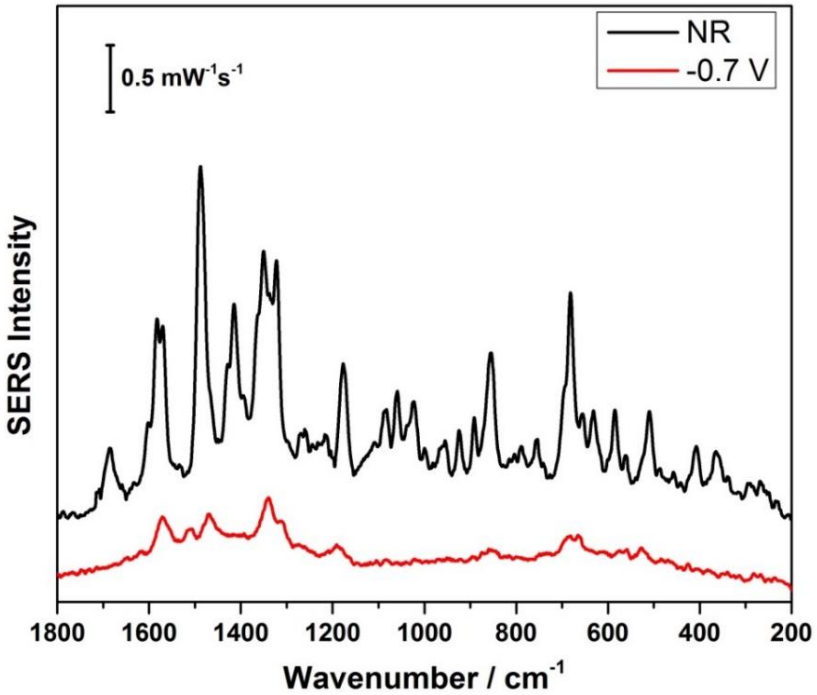

Figure 5.2.17: Comparison between the normal Raman of 2-deoxyguanosine powder (black) and the EC-SERS signal at -0.7V (red). Both spectra were collected at 46.5 mW for a time interval of 30s using 785 nm excitation.

5.2.3 Conclusion

EC-SERS studies were performed for all the biomarkers using a modified screen-printed electrode. These biomarkers were successfully detected and SERS signal was improved by applying a voltage; as the potential was stepped negatively the peaks became stronger. This is due in part to the decreasing surface charge on the surface of the silver as the potential of zero charge is approached.[117] By applying a potential, the molecule is able to come closer to the surface, which causes an increase in the SERS signal. Since the SERS signal strongly depends on the electrode potential, the change in the electrode potential may result in a change in the coverage or the adsorption orientation of the molecule; leading to a change in the SERS intensity.[117] There are two factors may mainly account for this phenomenon: the change of the bonding interaction of the molecule with the surface and the photon-driven charge transfer mechanism.[117] When the bonding strength is changed, the geometry and electronic structure will change as well, which eventually leads to a change in the spectral features of the molecule. The effect of photon-driven charge transfer can occur in two charge transfer directions, metal to molecule or molecule to metal, which depends on the electronic structure of both the adsorbed molecules and the electrode materials.[117] The next part of this thesis work was to investigate the extent to which these same biomarkers could be detected using a fabric-based SERS substrate.

5.3 Fabric-Based SERS

5.3.1 Introduction

This section includes the fabric selection and their characterization, as well as the SERS results for the probe molecules (4,4'- bipyridine and 4-ATP) as well as SERS results of the four biomarkers.

5.3.2 Fabric selection and characterization

The fabrics selected for exploration in this thesis work are shown in Table 5. These fabrics were selected because they have a high moisture absorption which make them ideal to absorb the bodily fluids, and also these fabrics are considered sustainable fabrics, derived from renewable resources.

Normal Raman spectra was collected for each untreated fabric sample in order to observe any background Raman peaks related to the fabric itself. Figure 5.3.1 shows the normal Raman spectrum of the blend fabric sample, it is clear that there are no peaks detected, although there is some background fluorescence. That indicates there would be minimal spectral interference when the SERS signal is collected for the probe molecules. SEM was used to characterize all the fabric samples before and after the AgNP deposition. Figure 5.3.2 shows the SEM image of the white cotton sample prior to modification with nanoparticles. As the fabric is not conductive, significant static charging was observed, causing the image to blur upon higher magnification.

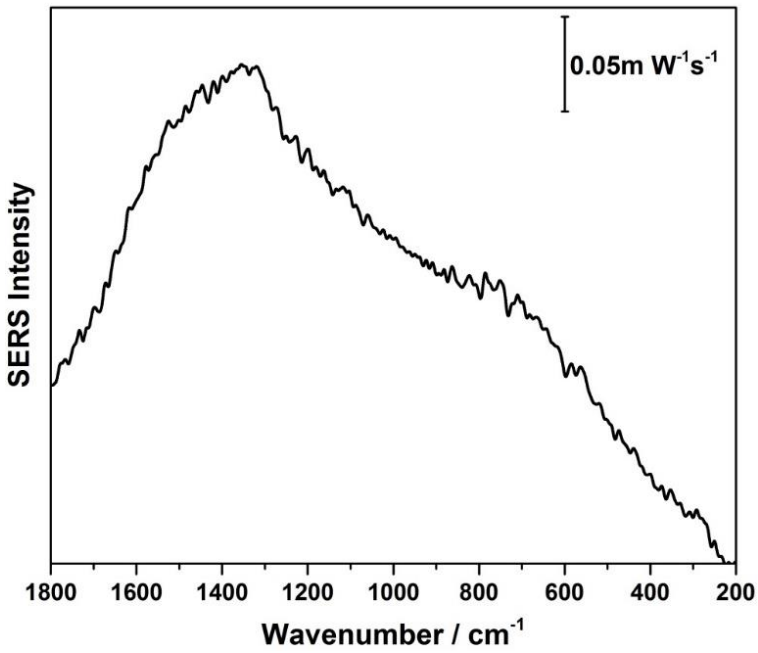

Figure 5.3.1: Normal Raman of untreated blend fabric. The spectrum was collected at 46.5mW, for a time interval of 60 seconds using 785 nm excitation.

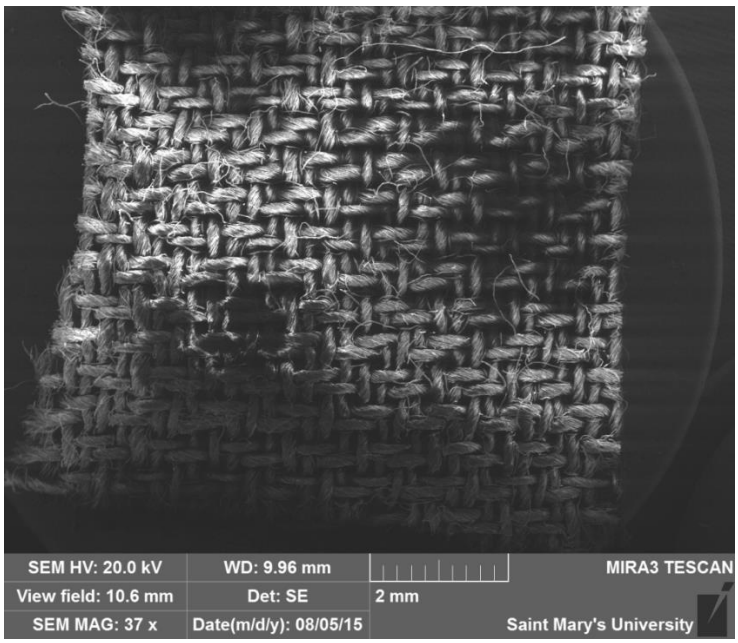

Figure 5.3.2: SEM image of white cotton fabric untreated with silver nanoparticles

Table 5. Type of fabrics and their compositions.

Type of fabric	**Composition**
Cotton	100%
Dye cotton (blue)	100%
Bamboo	100%
Hemp	100%
Blend	37% Silk, 35% Hemp, 28% Organic cotton

5.3.3 Evaluation of SERS performance for 4,4'-bipyridine

5.3.3.1 Normal Raman of 4,4'-bipyridine (4,4'-bipy)

The normal Raman signal of 4,4'-bipy (Figure 5.3.3) was collected prior to conducting the SERS measurement in order to identify the prominent Raman bands for this molecule. 4,4'-bipy displays a strong Raman signal, and is frequently used to investigate the SERS activity of novel plasmonic substrates.[127] The strong Raman signal for 4,4'-bipy is predominantly due to the extensive conjugated system of the pyridyl rings and the presence of two active nitrogen atoms, which enable electron transport as well as energy transfer processes.[127]

The band assignment for the normal Raman signals of 4,4'-bipy is shown in Table 6. The most intense bands, at 1617, 1306, and 1018 cm^{-1} correspond to C-C ring stretching vibrations. Other prominent bands include 1512 cm^{-1} and 1229 cm^{-1} corresponding to C-H i.p bending and ring stretching and C-H i.p. bending, respectively.

Table 6. SERS Band assignments for 4,4'-bipyridine.[128]

Raman peaks / cm^{-1}	SERS peaks / cm^{-1}	Band Assignment
388	-	-
576	-	-
665	-	pyridyl ring deformation
767	742	γ(C-H) + γ(C-C) + γ(C-C)int + γ(C-N)
886	870	γ(C-H)
1006	1018	γ(C-H) + δ(C-C) + δ(C-N) + ν(C-C) + ν(C-N)
1082	-	δ(C-H) + δ(C-C) + δ(C-N) + ν(C-N)
1234	1229	ν(C-C) + ν(C-N)
1306	1306	δ(C-H) + ν(C-C)
1518	1512	δ(C-H) + ν(C-C) + ν(C-C)int + ν(C-N)
1620	1617	δ(C-H) + ν(C-C) + ν(C-C)int + ν(C-N)

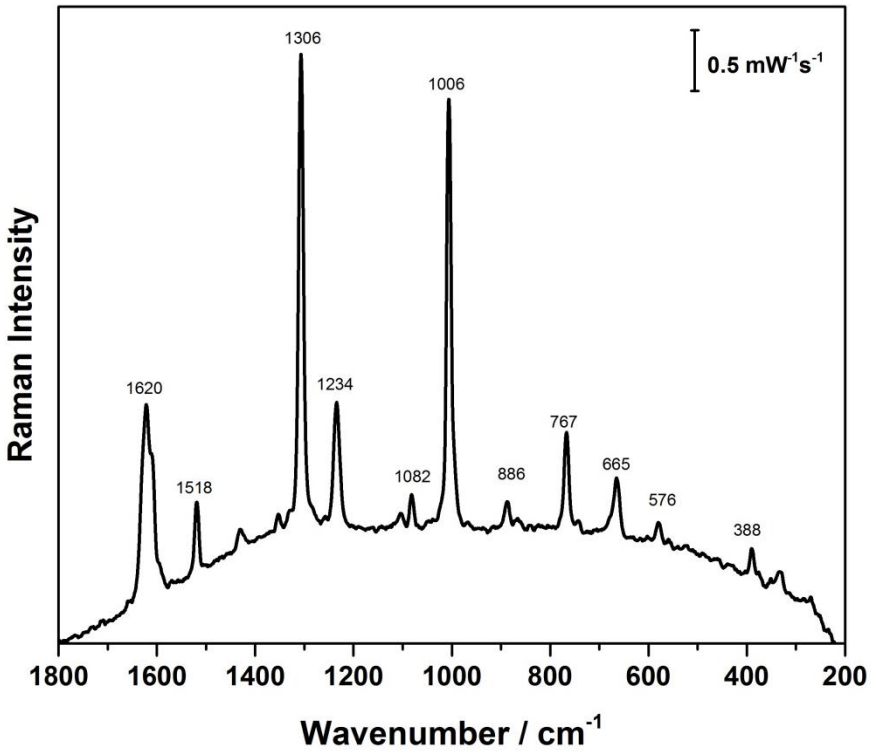

Figure 5.3.3: Normal Raman spectrum for 4,4'-bipy powder. The spectrum was collected at medium power (10.6 mW) for a time interval of 30 seconds using 785 nm laser line.

5.3.3.2 SERS of 1.0 mM 4,4'-bipy, one layer AgNPs on the selected fabrics.

In the initial studies of characterizing the fabric samples modified with AgNPs, 1 layer of AgNP paste was drop coated onto the surface of each fabric sample. The SERS results of the Raman reporter molecule 4,4'-bipy was relatively weak and significant spot to spot signal variation was observed as seen in Figure 5.3.4a-e . These spectra revealed that the signal was highly variable on the fabric, which indicated that the surface coverage was not uniform. In most spectra, strong Raman bands at 1610, 1293, and 1000 cm^{-1} were present.

From all the spectra in Figure 5.3.4 which represents the 10 different spots for each type of fabric; there is clear signal variation from fabric to fabric which is due to the different morphology of each fabric sample. For example, the white cotton fabric had the highest moisture absorption of the selected fabrics, and would therefore be ideal for monitoring biomarkers in bodily fluids. However due to the poor AgNP coverage, the SERS signal of 4,4'-bipy on white cotton was very weak as shown in Figure 5.3.4a, and the corresponding SEM (Figure 5.3.5) highlights the poor coverage. The SERS result for hemp, as seen in Figure 5.3.4b was a little stronger than the white cotton spectrum and the 4,4'-bipy peaks are prominent. However, the SERS signal was still relatively weak and there was significant spot to spot variation.

The SERS result for the bamboo fabric (Figure 5.3.4c) were very weak and noisy, and it was hard to identify the peaks for 4,4'-bipy; only citrate peaks were present. Since citrate is used as the reducing agent and capping agent, it is present on the AgNP surface. The blue cotton also showed a weak signal as shown in Figure 5.3.4d with significant spot to spot variation of signals. The blend fabric (Figure 5.3.4e) also showed a weak SERS signal of 4,4'-bipy, with some strong citrate peaks.

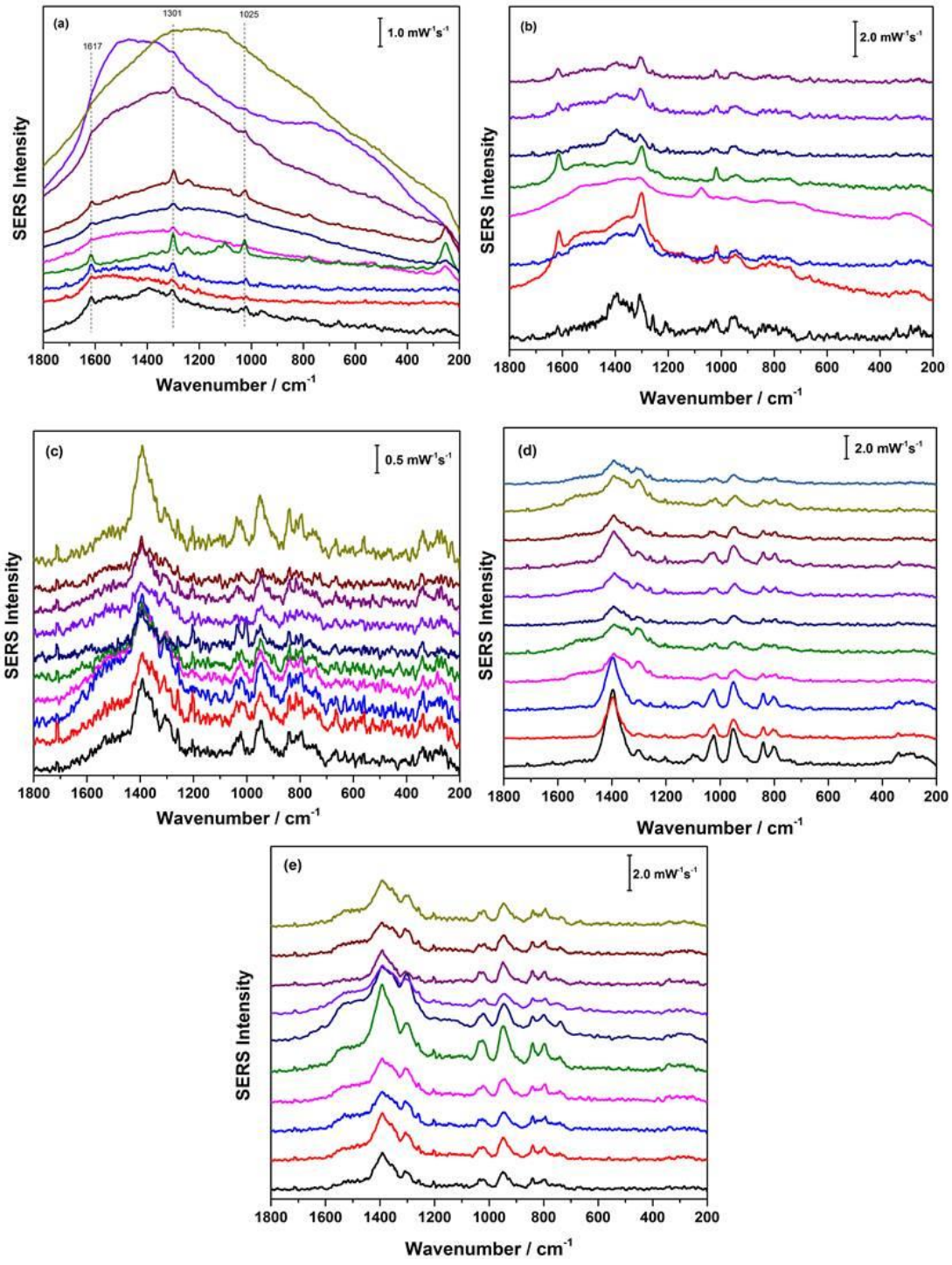

Figure 5.3.4: SERS of 1.0 mM of 4,4'-bipy, 1 layer AgNPs, 30s on (a) white cotton, (b) hemp, (c) bamboo, (d) blue cotton, (e) blend (37% silk, 35% hemp, 28% organic. cotton). Laser power was 10.6 mW, all spectra were collected in a time of 30s.

5.3.3.3 SEM of fabrics modified with one layer of AgNPs

As none of the fabric samples treated with one layer of AgNPs gave reliable SERS signal, scanning electron microscopy (SEM) was used to investigate the quality of the AgNP deposit. Figure 5.3.5 shows images of the modified fabric samples at low and high magnification. It is clear that the AgNP coverage on the fabric surface was poor, which resulted in weak and irreproducible SERS signals. This finding suggested that one layer of AgNPs was not sufficient to provide uniform coverage of AgNPs on the fabric surface.

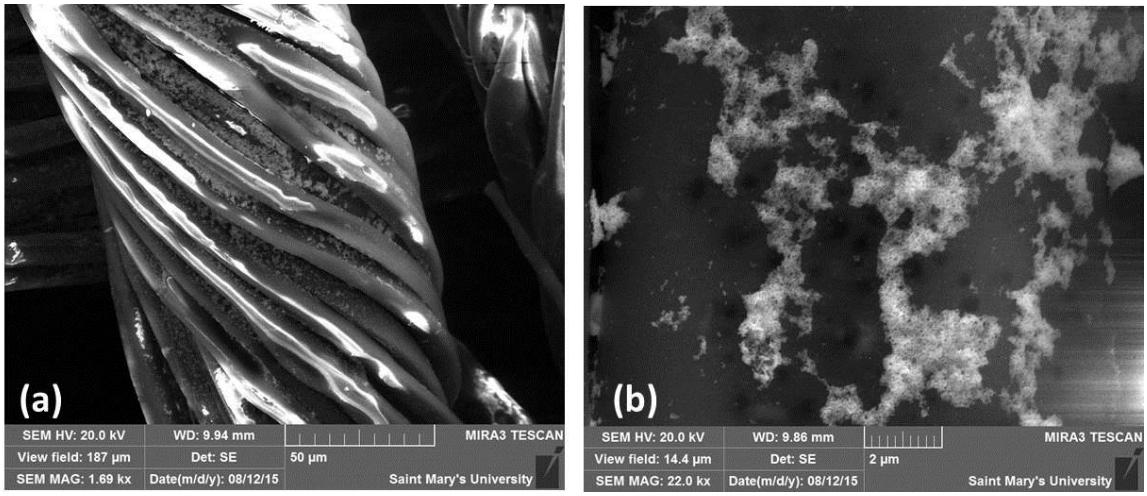

Figure 5.3.5: Scanning electron microscopy (SEM) of fabric modified with one layer of AgNPs under (a) low and (b) high magnification. SEM images were conducted using Tescan MIRA3 LMU Field Emission SEM under high vacuum mode at 10 kV, and at a scanning speed of 32.00 µs / pixel.

5.3.3.4 SERS of 4,4'-bipy on fabric samples modified with 3 layers of AgNPs

In the next study, three layers of AgNPs were added to the fabric samples. After the addition of a layer of AgNPs, the layer was allowed to dry completely prior to addition of the next layer. As shown in Figure 5.3.6, the SERS signal of 4,4'-bipy on the

blue cotton was strong and all the marker peaks were observed, (1610, 1293, and 1000 cm^{-1}), however, the signal was not uniform. The best SERS signal was collected from the blend fabric (Figure 5.3.6a), which gave superior SERS enhancement compared to the other fabric samples. Also, the SERS spectra from hemp, blend, and white cotton (Figure 5.3.6 b,c,d), respectively, were relatively strong, and also there was spot to spot variation for each fabric sample. The broad peaks at 1400 cm^{-1} and 960 cm^{-1} are corresponding to the citrate which are assigned to ν(C-COO) and ν_s(COO), respectively.[129] As noticed previously, citrate can be a major interference for both the adsorption and detection of analytes via SERS as it is directly present on the AgNP surface. Since superior signal was observed for the fabric samples coated with three layers of AgNPs, this number of layers was used for all subsequent fabric samples. In general however, the SERS signals were still fairly weak, and so another common Raman probe was investigated, 4-aminothiophenol (4-ATP). Since 4-ATP is a thiol, it can form a self-assembled monolayer on the nanoparticle surface through the formation of a strong Ag-S bond, and thus should provide a stronger SERS signal. In addition, the chloride treatment strategy used in the previous EC-SERS studies was also explored for the fabric-based sensors in an effort to enhance detection of non-thiol molecules.

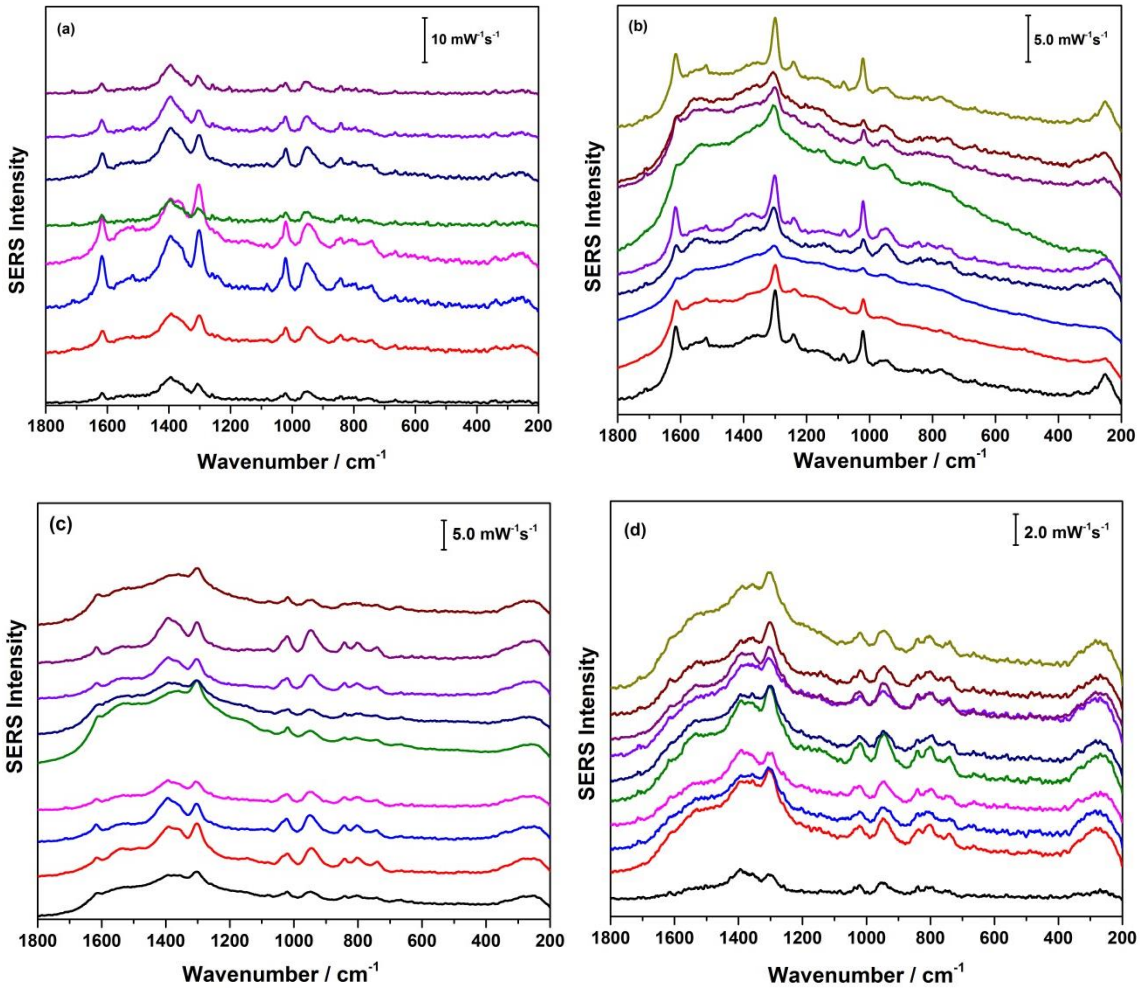

Figure 5.3.6: SERS of 1.0 mM of 4,4'-bipy, 3 layers of AgNPs, 10.6 mW, 30s (a) blend, (b) hemp, (c) blue cotton, (d) white cotton. (Drop coating 10µL of AgNPs).

5.3.3.5 SEM of fabrics modified with 3 layers of AgNPs

The SEM images of the modified fabric samples are shown in Figure 5.3.7a-d. It is clear that with three layers of AgNPs the surface was well covered with NPs. The high magnification image (Figure 5.3.7d) showed the near-monodisperse quality of these NPs.

The dense coverage of the fabric substrate with AgNPs in this case was responsible for the improved SERS signals.

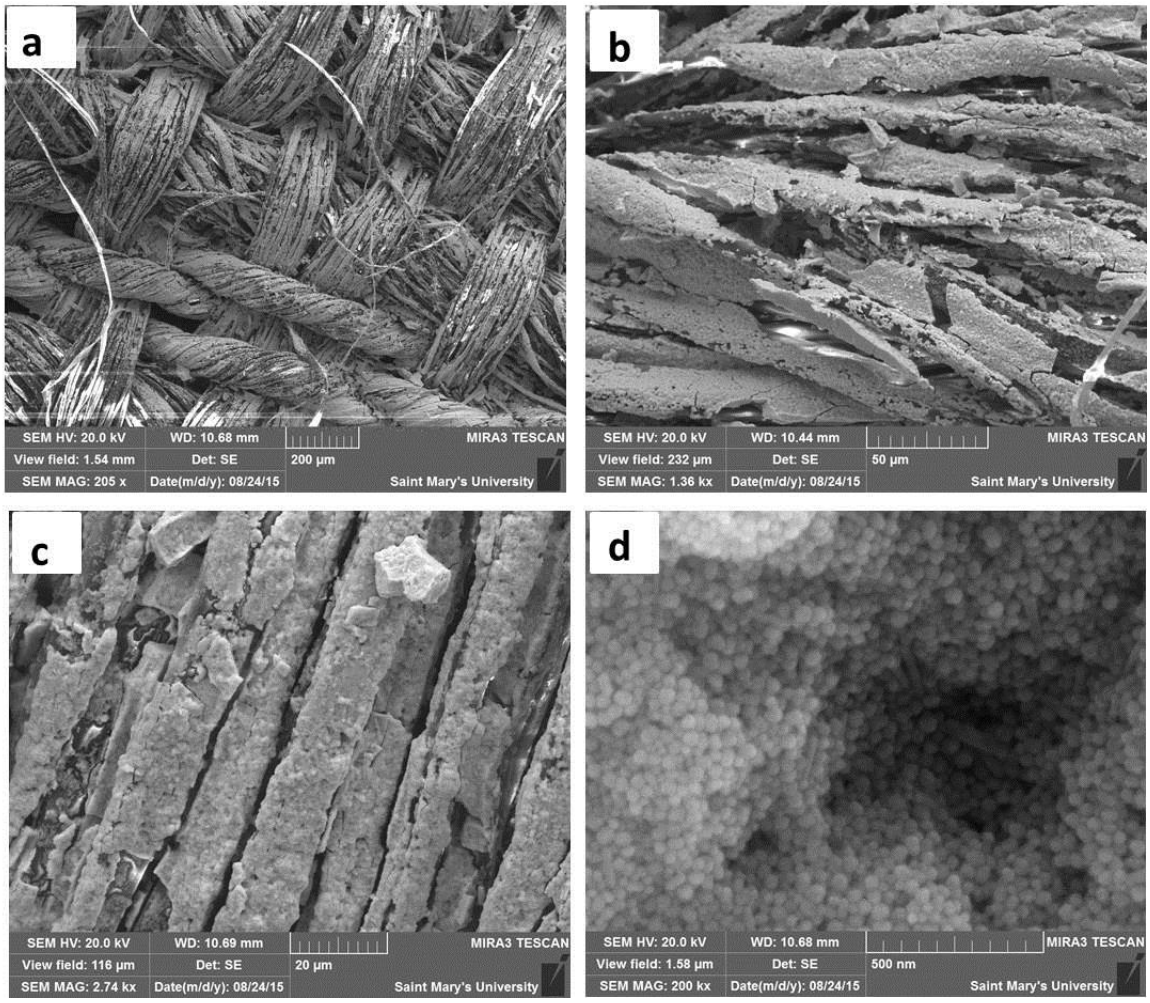

Figure 5.3.7: SEM images of blend fabric samples modified with 3 layers AgNPs at (a - c) low and (d) high magnification. SEM images were conducted using Tescan MIRA3 LMU Field Emission SEM under high vacuum mode at 10 kV, and at a scanning speed of 32.00 µs / pixel.

5.3.4 Evaluation of SERS performance of 4-ATP

5.3.4.1 Normal Raman of 4-ATP

4-aminothiolphenol (4-ATP) is one of the most commonly used Raman reporter molecules, and was utilized in this thesis work to evaluate the fabric-based SERS substrate. The sulfur atom in 4-ATP can bind very strongly to silver and in the process

can displace the citrate capping agent.[109] Therefore, this property is beneficial for obtaining a SERS response for thiolated probe molecules or any biomarker that have a thiol group. As shown in Figure 5.3.8, a Raman spectrum for solid 4-ATP was successfully obtained and different vibrational modes were observed. Table 7 provides the band assignment for p-ATP.

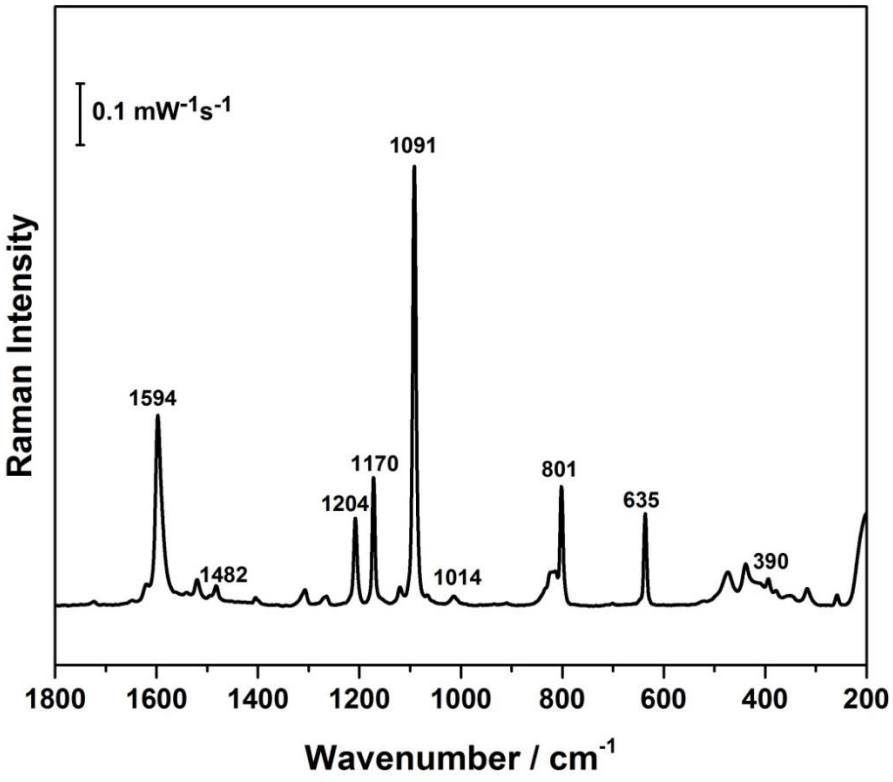

Figure 5.3.8: Normal Raman of 4-ATP powder. Spectrum was collected at 22.3 mW laser power for 30s at 785 nm excitation.

Table 7: SERS peaks for p-ATP on silver substrates.[130]

Raman peaks / cm^{-1}	SERS peak / cm^{-1}	Peak assignment
390	400	$v(C\text{-}S)+ \delta_{ip}(C\text{-}C)_{Ar}$
635	650	$\delta_{ip}(C\text{-}C)_{Ar}+ v(C\text{-}S)+ \delta_{ip}(C\text{-}H)_{Ar}$ v(S-S) from oxidative product
-	715	$\gamma(C\text{-}C)_{Ar}$
801	825	$\delta_{ip,as}\ (C\text{-}C)_{Ar}$
1014	1002	$\gamma_{as}(C\text{-}H)$
1091	1050	$\delta_{ip}(C\text{-}H)_{Ar}$
1170	1190	$\delta_{ip}(C\text{-}H)$
1204	-	$v(N\text{-}N)+ \delta_{ip,s}(C\text{-}H)$
1482	1400, 1444, 1500	$\delta_{ip}(C\text{-}C)_{Ar}+ \delta_{ip,s}(C\text{-}H) + v(C\text{-}N)$
1594	1600	$v(C{=}C)_{Ar}$

5.3.4.2 SERS of 4-ATP on the selected fabric samples

In the next set of experiments, the signal for a monolayer of p-ATP was collected for the fabric samples modified with three layers of AgNPs. Figure 5.3.9 shows the SERS spectra for the all modified fabric platforms with 4-ATP as the reporter molecule (each spectrum represents the SERS of 10 different spots). In this case, the SERS signal was much more intense than for 4,4'-bipy. However, citrate peaks were still observed to be an interference. Since citrate was observed to be a significant interference due to its strong

surface adsorption and resulting SERS signal, steps were taken in the next section to remove citrate from the NP surface.

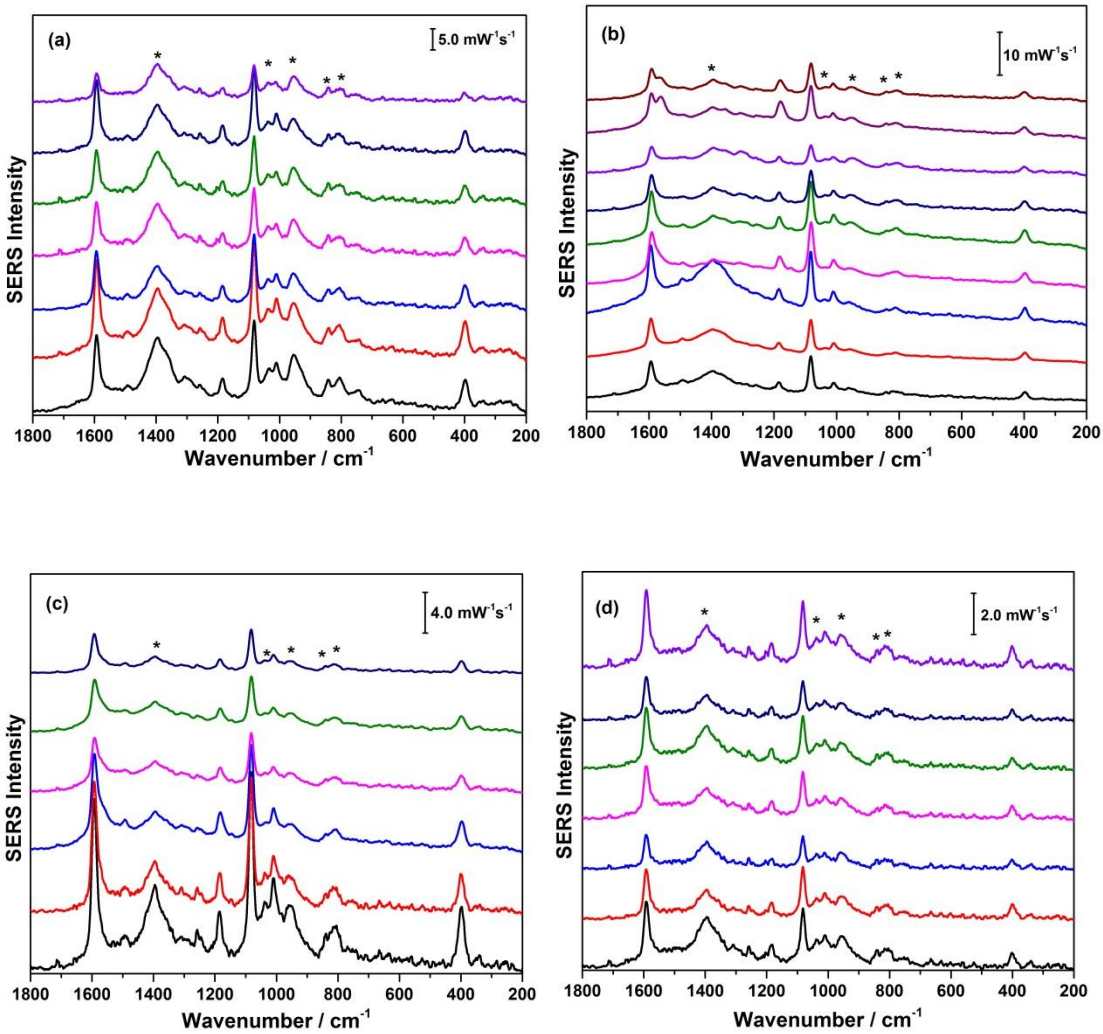

Figure 5.3.9: SERS spectra of 1mM 4-ATP drop coated on fabric samples (a) blend, (b) blue-cotton, (c) bamboo, (d) white-cotton. Peaks due to citrate are labelled with an asterisk (*).

5.3.4.3 SERS of 1.0 mM 4-ATP, 3 layers of AgNPs with KCl treatment (5 fabrics)

3 layers of 10µL AgNP paste was drop coated on all 5 fabric samples and then the fabric sample was immersed in 0.5M KCl for 30 min and rinsed with water and allowed to air dry prior to the SERS measurements. 20 µL of 1.0 mM p-ATP was drop coated onto the modified fabric chip prior to the measurement, and 10 different spots were collected for each sample. The SERS spectra for all the fabric samples were very strong. Moreover, the citrate peaks disappeared and only the 4-ATP signal was observed. Figure 5.3.10 shows the comparison of the SERS spectra for 4-ATP for the chloride-treated and chloride-untreated fabric. For the treated fabric (Figure 5.3.10a), the SERS signal is clearly very strong and only peaks from 4-ATP were observed, while for the untreated fabric (Figure 5.3.10b), the 4-ATP peaks were weaker and citrate peaks appears at 1400 cm^{-1} and 960 cm^{-1} were present. Clearly, once treated with chloride ion (Figure 5.3.10a), the citrate signal is completely removed, and the only observable signal is related to the adsorbed 4-ATP. Hence, for all remaining studies the citrate removal step was employed.

Figure 5.3.11 shows the SERS spectra for 10 different spots on the treated fabrics (each spectrum represents the 10 different spots in the same fabric). After citrate removal, the 4-ATP signal was observed to be strong for all the fabrics, especially from blend (Figure 5.3.11a), bamboo (5.3.11b), and blue-cotton (Figure 5.3.11c). Some spectra for white-cotton (Figure 5.3.11d) were strong and others were weak, such signal non-uniformity is undesirable. The hemp sample (Figure 5.3.11e) also provided non-uniform SERS signals.

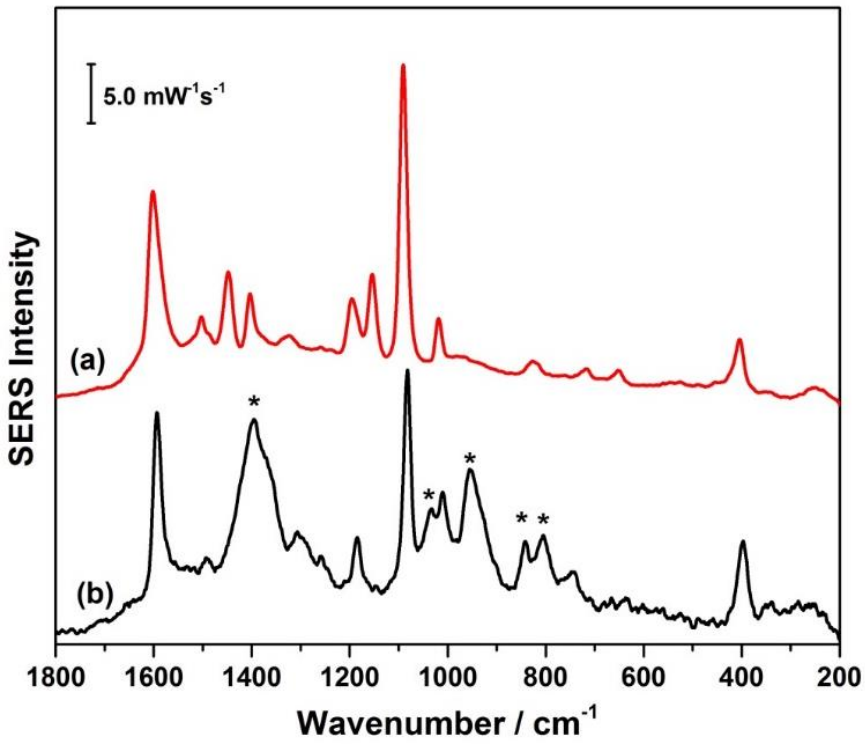

Figure 5.3.10: SERS spectra obtained for 1.0 mM 4-ATP on blend fabric substrate (a) fabric substrate treated with potassium chloride and (b) untreated fabric. Acquisition time was 30 seconds at 785 nm excitation. Asterisks denote peaks due to citrate.

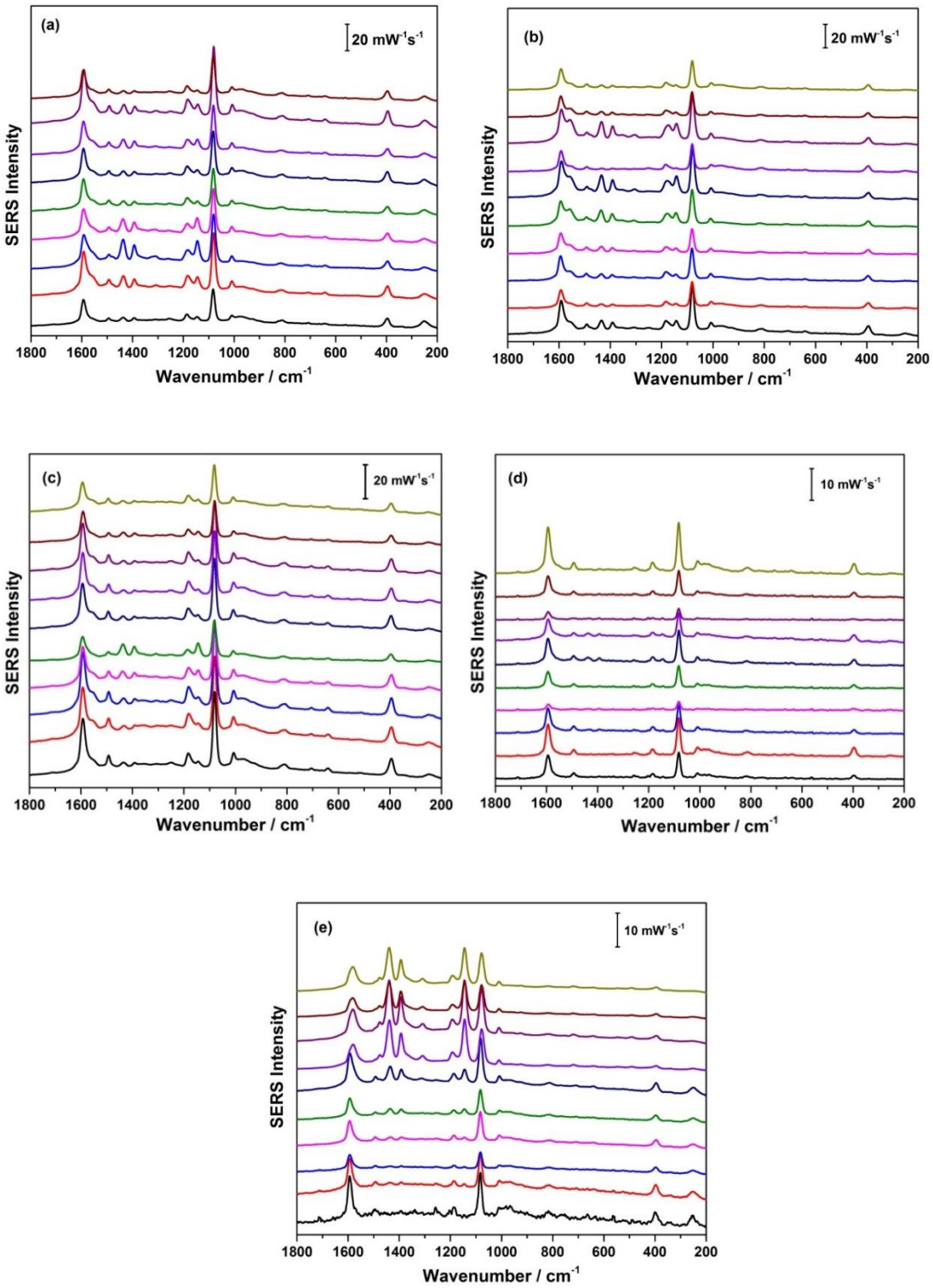

Figure 5.3.11: SERS spectra of 1.0 mM 4-ATP on (a) blend (b) bamboo (c) blue-cotton (d) white-cotton, (e) hemp, all with KCl treatment. Each spectrum acquisition time was 30 seconds at 785 nm excitation, power at the sample was 22.3 mW.

In order to determine which of the 5 fabric platforms gave the strongest SERS response, the SERS signal average of 10 spots for each fabric sample was calculated, and these spectra were overlaid (Figure 5.3.12a). In addition, Figure 5.3.12b shows the standard deviation of the SERS intensity for the 1600 cm^{-1} peak for each of the five fabrics. Careful examination of Figures 5.3.12a and 5.3.12b show that the blend fabric has both the strongest SERS enhancement and the lowest SERS signal deviation. Bamboo and blue cotton also showed promise at this stage. As a result, these three fabric samples were carried forward for further evaluation.

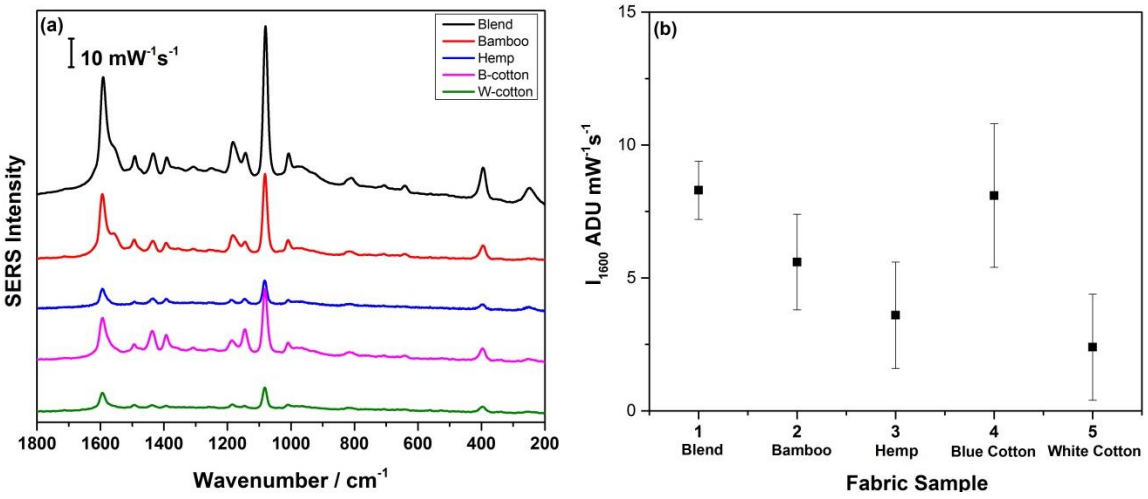

Figure 5.3.12: (a) SERS of 1.0 mM 4-ATP on fabric platforms treated with 0.5M KCl, using a 785nm laser line (30 s, 10.6 mW). Each spectrum is the average of 10 spectra collected from 10 different spots on the same SERS substrate (b) peak intensity at 1600 cm^{-1} for all 5 fabrics.

5.3.4.4 SERS of 1.0 mM 4,4'-bipy; 3 layers of AgNPs with KCl treatment

Once the three top performing fabrics were chosen, the next step was to evaluate their SERS enhancement for a non-thiol probe molecule. This is important because the

majority of the target biomarkers are not thiolated molecules and it was important to ensure that this SERS-based fabric sensor could detect non-thiolated molecules. For this work, 4,4'-bipyridine (4,4'-bipy) was used as a model of a non-thiolated Raman-active molecule. KCl treatment was performed on the selected three fabrics, and comparison between untreated and treated fabric is shown in Figure 5.3.13. SERS enhancement was noted for treated fabric only, and the citrate peaks were not observed (Figure 5.3.13a). Without the chloride treatment, only peaks due to citrate were observed. Clearly, the chloride treatment strategy is necessary for development of a useful SERS-active substrate where detection of non-thiolated molecules is the goal.

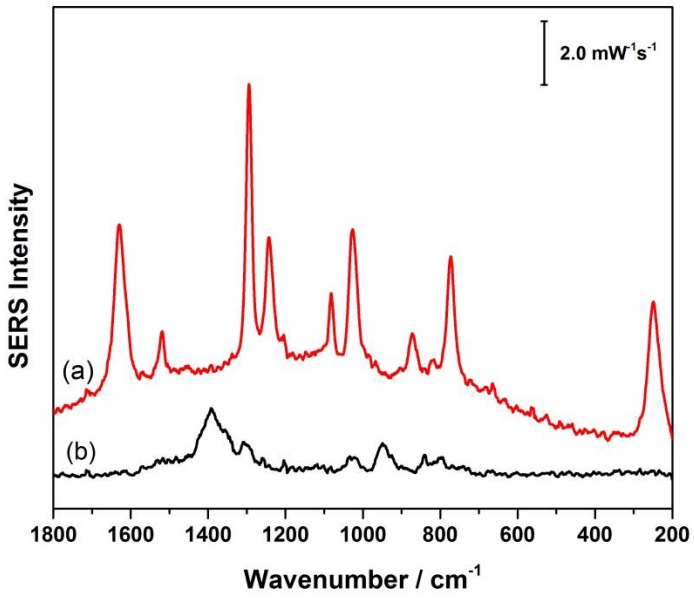

Figure 5.3.13: SERS spectra of 1.0 mM 4,4'-bipy on blend fabric (a) treated with KCl, (b) untreated with KCl. The spectra were measured at 10.6 mW for a time interval of 30 seconds using 785 nm excitation.

SERS results of 4,4’-bipy on the three fabrics are shown in Figure 5.3.14 (a-c); strong signals were detected for the three fabrics with a variation in the SERS intensity. In order to determine which of the 3 fabric platforms gave the strongest SERS response, the SERS signal average of 10 spots for each fabric sample was calculated, and these spectra were overlaid (Figure 5.3.15a). In addition, Figure 5.3.15b shows the standard deviation for each of the three fabrics of SERS signal samples, which indicated that the blend fabric has both the strongest SERS enhancement and a moderate SERS signal deviation. Hence, the blend fabric was deemed the most promising fabric, and all future investigations focused on the blend fabric.

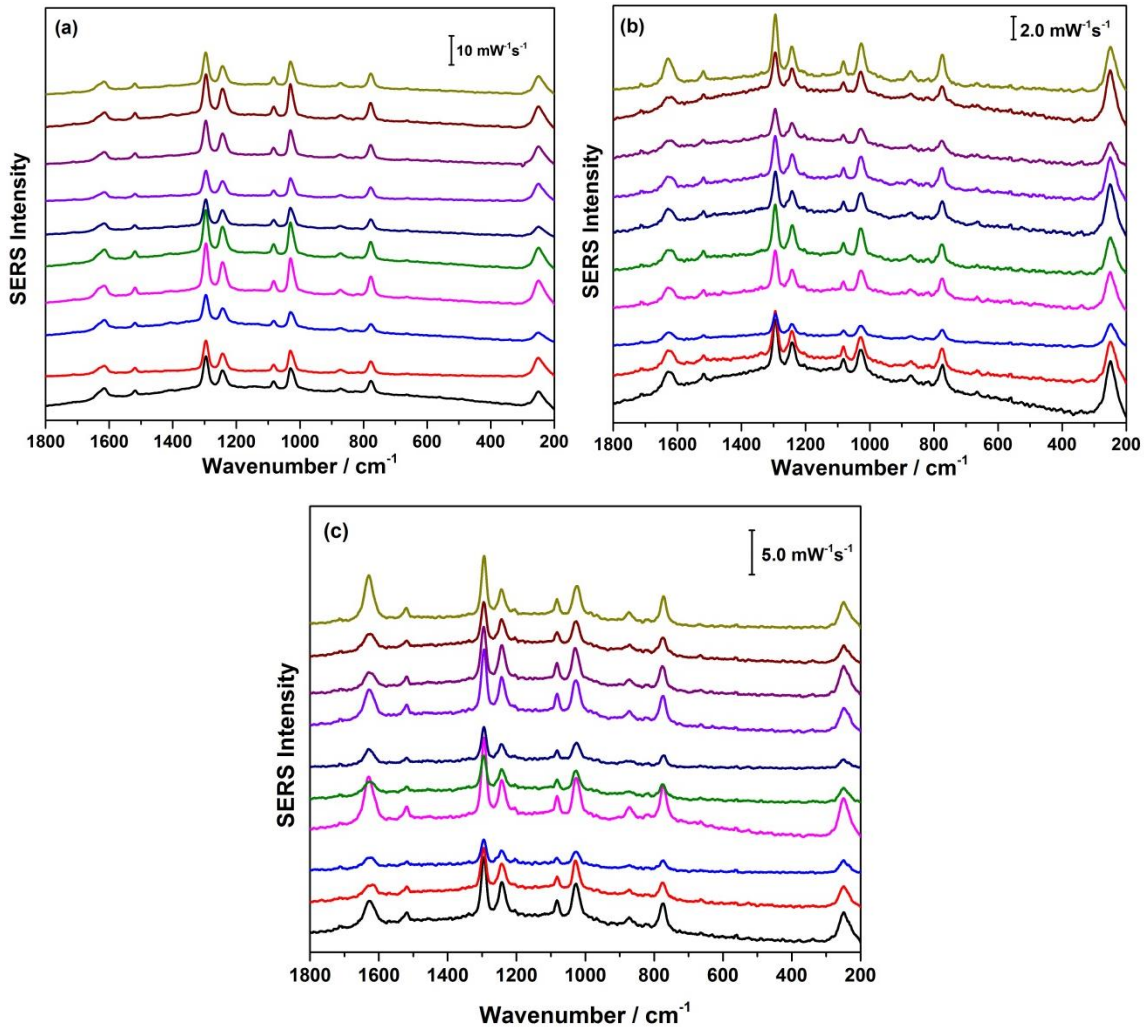

Figure 5.3.14: SERS spectra of 1.0 mM 4,4'-bipy on (a) blend, (b) bamboo, (c) blue-cotton after KCl treatment. Each spectrum acquisition time was 30 seconds, laser power was 22.3 mW, at 785 nm excitation.

.

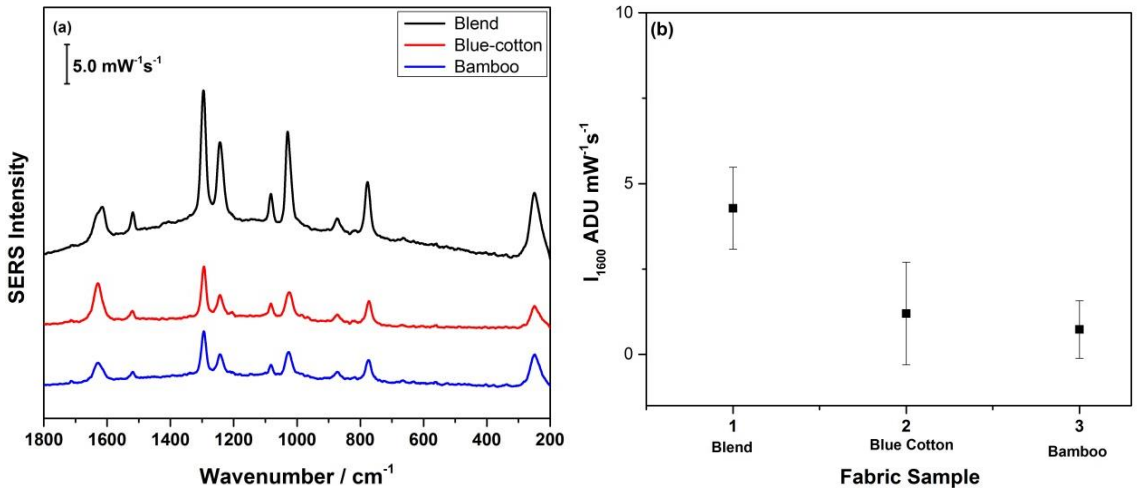

Figure 5.3.15: (a) SERS of 1.0 mM 4,4'-bipy on fabric platforms treated with 0.5M KCl, using a 785nm laser line.(30 s, 10.6 mW) Each spectra is the average of 10 spectra collected from 10 different spots on the SERS substrate b) peak intensity at 1600 cm^{-1} for all three fabrics.

5.3.4.5 Comparison between blend fabric and silk-based "Fab-Chip"

In order to evaluate the SERS intensity of the blend fabric, the SERS measurement for 4-ATP was conducted using the same procedure as reported for the silk-based "Fab-Chip", previously investigated by Robison et al. Figure 5.3.16 shows the comparison of SERS spectra between the blend and the Fab-chip. It was clear that the blend fabric shows the strongest SERS signal (Figure 5.3.16), and thus would be a promising material to investigate further, and represents a significant improvement over the silk used for previous fab-chip work.

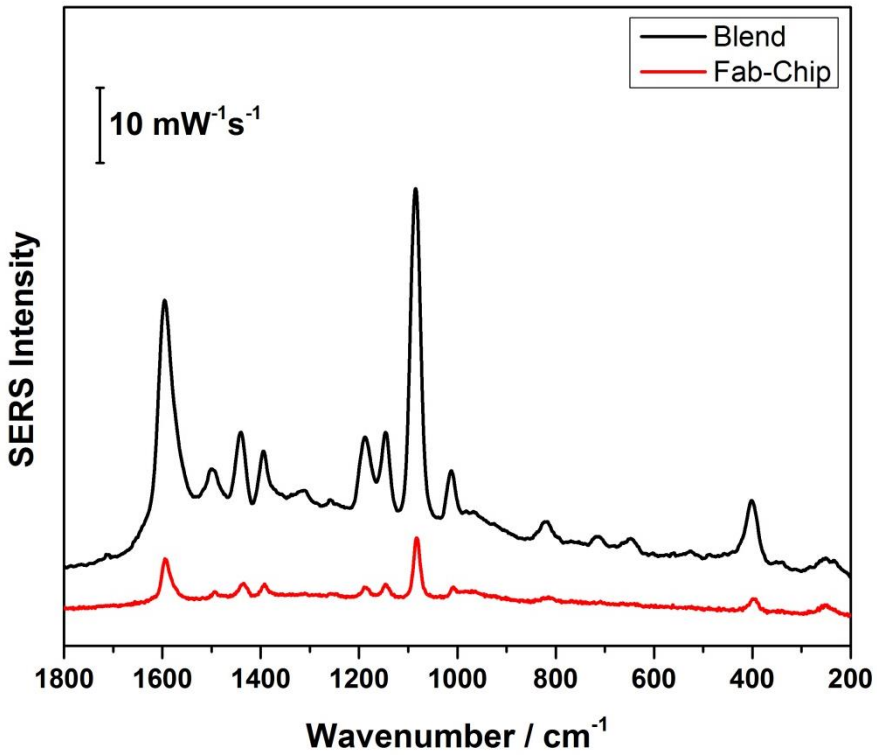

Figure 5.3.16: SERS of 1.0 mM 4-ATP on blend fabric and fab-chip. The spectra were measured at 10.6 mW for a time interval of 30 seconds using 785 nm excitation.

In summary, this part of the thesis research investigated different fabric samples for their SERS performance after modification with AgNPs. From all the SERS measurements and resulting comparisons, the blend fabric was the most promising fabric, provided that a chloride treatment was used prior to analysis in order to remove interfering citrate ions. The blend fabric was selected to continue investigation of the biomarkers in this thesis, as reported on in the next section.

5.3.5 SERS of biomarkers on modified blend fabric

Once the evaluation of the fabrics was complete, and the blend fabric was chosen as the optimal fabric, SERS measurements on the four biomarkers were conducted on this

modified blend fabric. This section includes all the SERS results for the biomarkers on blend fabric samples.

5.3.5.1 SERS of 6-thiouric acid on blend fabric

A 1.0 mM solution of 6-TUA was prepared in synthetic urine, and 20 µL was drop coated onto the blend fabric modified with AgNPs and treated with 0.5 M KCl. 10 different spots were collected to evaluate the SERS intensity. The dominant peak of 6-TUA was clearly observed at 932 cm^{-1} in all 10 spots with some variation in signal intensity as shown in Figure 5.3.17.

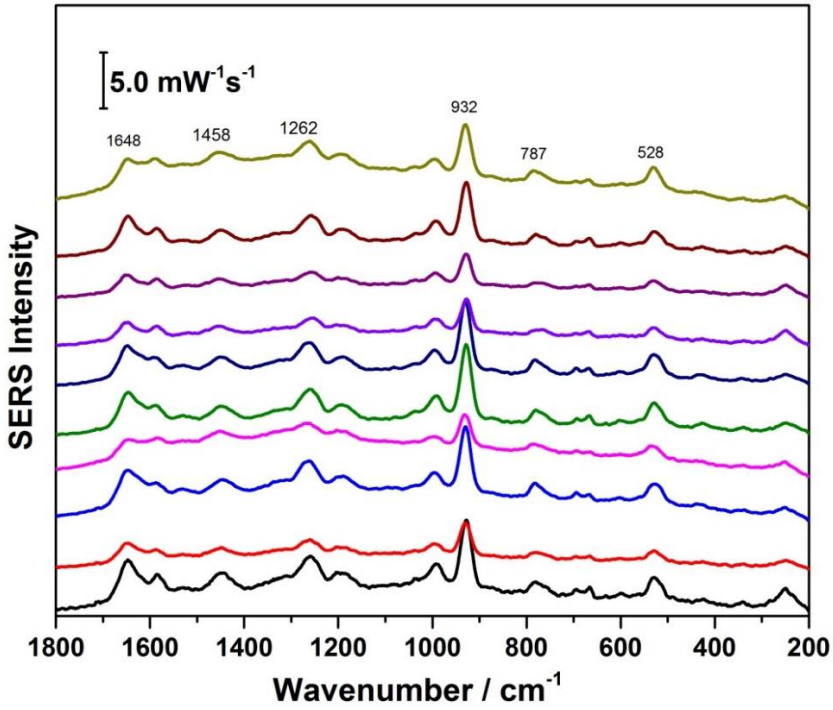

Figure 5.3.17: SERS of 1.0 mM 6-TUA drop coated on blend fabric. The spectra were measured at 22.3 mW for a time interval of 30 seconds using 785 nm excitation.

A central goal of this research was to detect biomarkers at biologically relevant concentrations. For 6-TUA, this would be 1.0 µM as opposed to 1.0 mM, as discussed

earlier. After conducting the SERS measurement on 1.0 mM 6-TUA for the blend fabric, SERS of 1.0 µM was conducted as well with a successful result (Figure 5.3.18). Even though there was some variation in the signal, the corresponding peaks for 6-TUA were observed and easy to identify. However, detection of 6-TUA at 1.0 nM concentration was unsuccessful as shown in Figure 5.3.19, the only observable signal is the strong ν(Ag-Cl) stretch at ~250 cm^{-1}, [131] and the peak at 990 cm^{-1} which is due to the C-N stretching vibration of urea which is present in the synthetic urine.

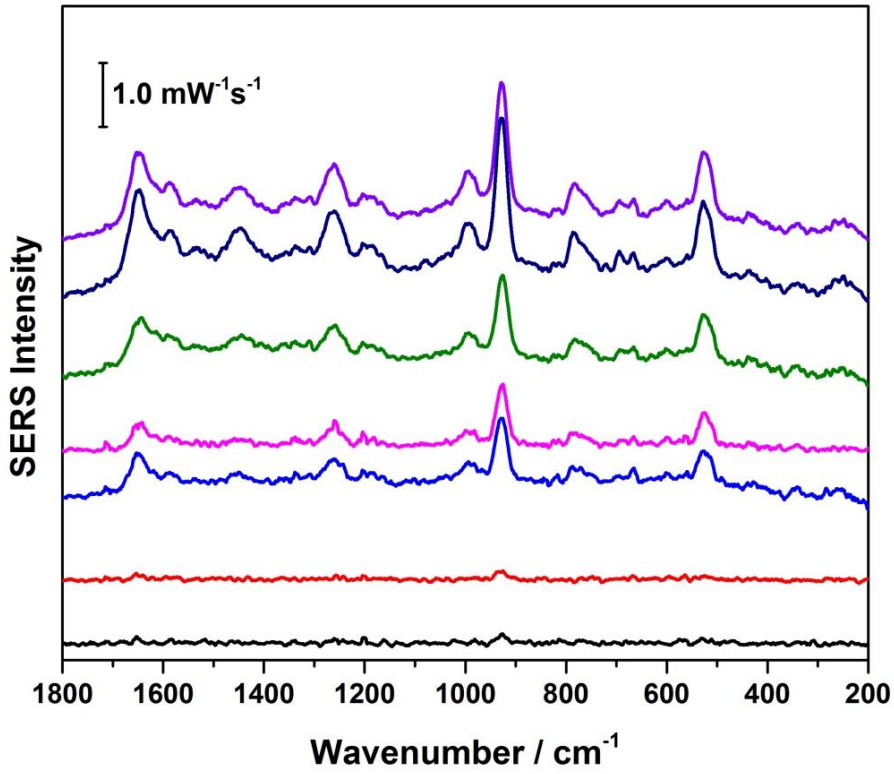

Figure 5.3.18: SERS of 1.0 µM 6-TUA drop coated on blend fabric for seven different spots. The spectra were measured at 22.3 mW for a time interval of 30 seconds using 785 nm excitation.

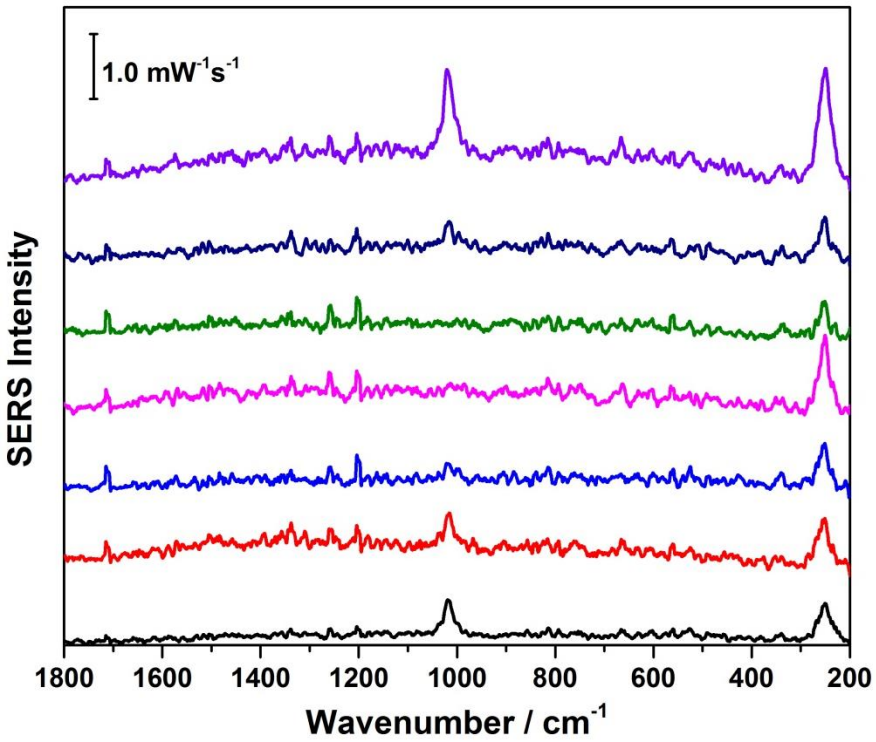

Figure 5.3.19: SERS of 1.0 nM 6-TUA drop coated on blend fabric for seven different spots. The spectra were measured at 22.3 mW for a time interval of 30 seconds using 785 nm excitation.

In order to determine the limit of detection for 6-TUA, different concentrations were prepared and detected by SERS on blend fabric. Figure 5.3.20a shows the overlay of the average of 10 different spots for each concentration tested. The signal was very strong at high concentration, and it is clear that there was a reduction of peak intensity as the 6-TUA concentration is lowered. Based on Figure 5.3.20b, the limit of detection (LOD) was 33.5 µM based on the standard deviation of the blank and the slope.

$$\mathrm{LOD} = \frac{3\sigma\mathrm{blank}}{\mathrm{slope}}$$

$\mathrm{LOD} = 3 \times 1.2\ \mathrm{mW^{-1}s^{-1}} / 107.5\ \mathrm{mW^{-1}s^{-1}mM^{-1}} = 0.0033\ \mathrm{mM} = 33.5\ \mu\mathrm{M}.$

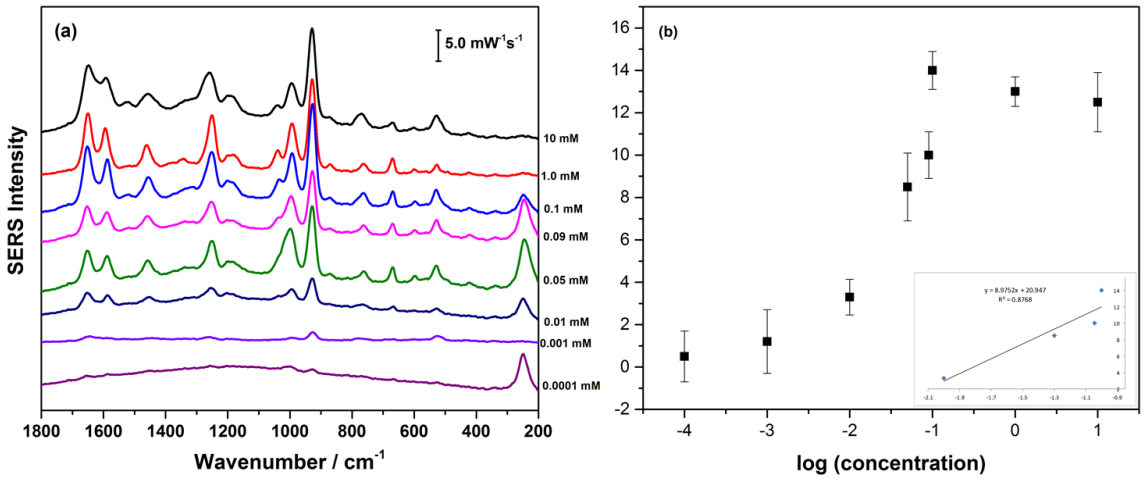

Figure 5.3.20: (a) SERS of different concentrations of 6-TUA drop coating on blend fabric. Each line represents the average of 10 spots, the spectra were measured at 22.3 mW for a time interval of 30 seconds using 785 nm excitation. (b) peak intensity at 930 cm^{-1} for different concentrations.

5.3.5.2 SERS of levofloxacin on blend fabric

The SERS result for 1.0 mM levofloxacin drop coated onto the modified blend fabric after KCl treatment was not successful as shown in Figure 5.3.21a, the only observable signal was the strong ν(Ag-Cl) stretch at ~250 cm^{-1}. [131] A first thought was that the chloride treatment was interfering, and so a trial was conducted using the fabric sample not treated with KCl, and in this case the levofloxacin peaks were still not observed; the only peaks observable were the citrate peaks. This unsuccessful detection of levofloxacin could be due to a weak interaction with the AgNP surface, regardless of whether or not the chloride treatment was applied. Since the EC-SERS investigations of levofloxacin had shown very good signal at negative applied voltage, this is indeed most likely the case.

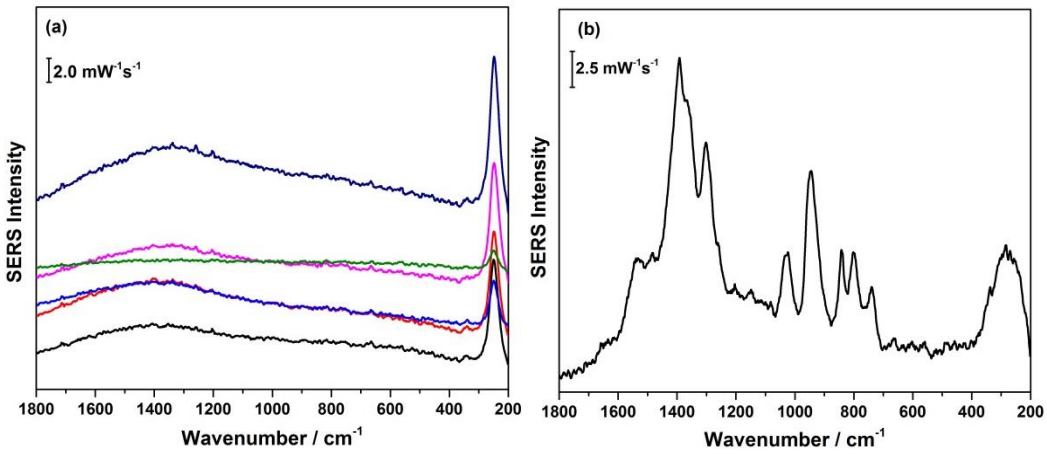

Figure 5.3.21: SERS of 1.0 mM levofloxacin in synthetic urine (a) after KCl treatment, (b) without KCl treatment. Spectra were measured at 10.6 mW for a time interval of 30 seconds using 785 nm excitation.

5.3.5.3 SERS of guanine on blend fabric

SERS measurement of 1.0 mM guanine was conducted on blend fabric that was modified with AgNPs and treated with chloride prior to SERS measurement. As shown in Figure 5.3.22, the SERS signal of 1.0 mM guanine was successfully detected and the dominant peak at 650 cm^{-1} was very strong for each spot. There was some variation in the SERS signals, but the relevant peaks were nevertheless readily detected. Figure 5.3.23 shows the comparison between the normal Raman spectrum of guanine and the SERS spectrum of 1.0 mM of guanine solution on the blend fabric chip; it was clear that all the corresponding peaks were observed which are consist with the normal Raman spectrum.

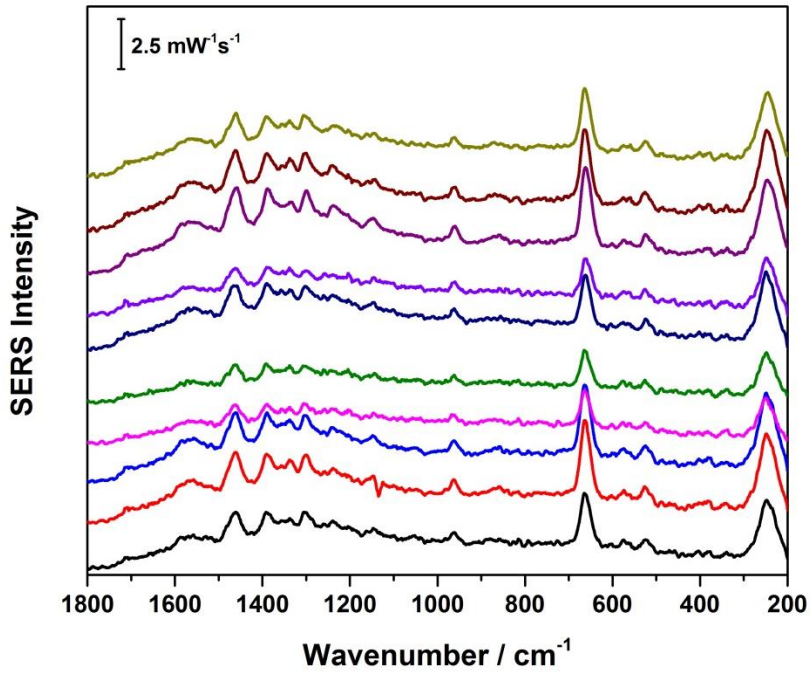

Figure 5.3.22: SERS of 1.0 mM guanine (10 different spots). The spectra were measured at 10.6 mW for a time interval of 30 seconds using 785 nm excitation.

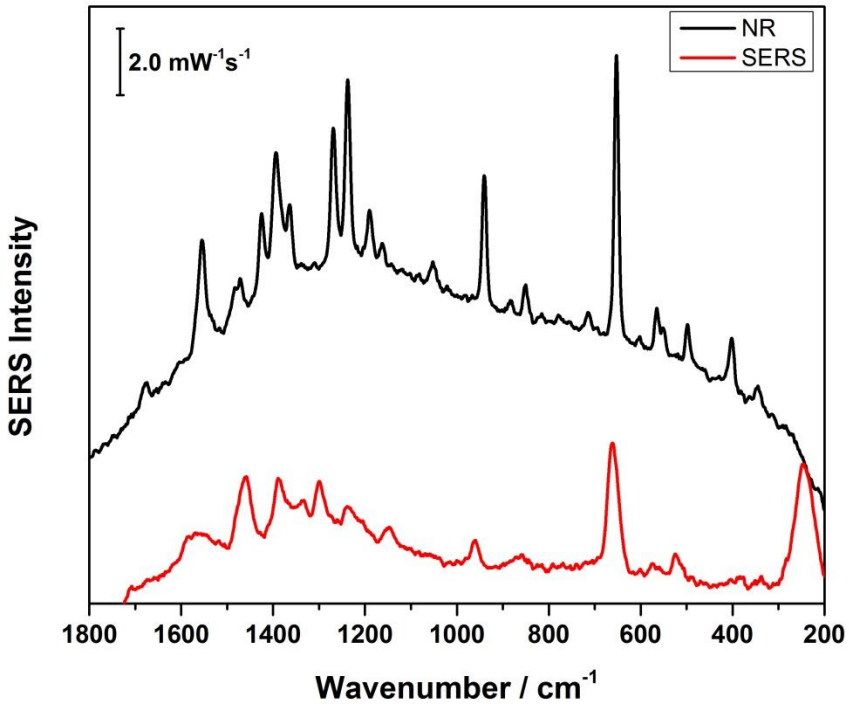

Figure 5.3.23: Comparison between normal Raman of guanine powder and SERS of 1.0 mM guanine on blend fabric.

5.3.5.4 SERS of 2-deoxyguanosine on blend fabric

SERS measurements of 1.0 mM 2-deoxyguanosine were conducted on blend fabric that was modified with AgNPs and treated with chloride prior to SERS measurement. However, the 2-deoxyguanosine peaks were not detected in SERS as shown in Figure 5.3.24, the only observable signal is the strong ν(Ag-Cl) stretch at ~250 cm^{-1}. The poor detection of SERS signal is likely due to surface affinity. Again, since the EC-SERS results had shown signal for 2-deoxyguanosine only at negative applied voltages, this suggests there is weak surface adsorption of this molecule in the absence of an applied voltage.

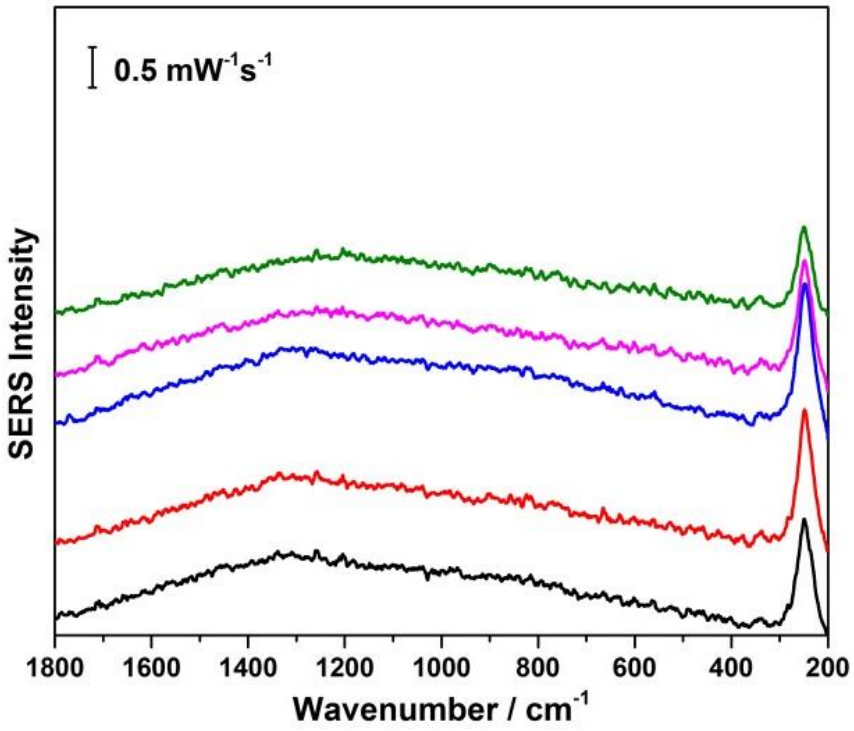

Figure 5.3.24: SERS of 1.0 mM 2-deoxyguanosine. The spectra were measured at 10.6 mW for a time interval of 30 seconds using 785 nm excitation.

5.3.6 Conclusion

Once SERS measurements were conducted on all the biomarkers, it was noticed that the SERS signal of 6-TUA and guanine were easily detected, while the SERS signal of levofloxacin and 2-deoxyguanosine were not observed. However, these signals were previously detected using the screen-printed electrode at applied potential. Clearly, application of a voltage is useful in the detection of these target biomarkers, and as a result the idea of a fabric-based electrode was explored in this thesis work.

5.4 EC-SERS of biomarkers on Fabric-based electrode

This section includes the characterization and the EC-SERS results obtained using fabric-based electrodes. Two types of fabric-based electrodes were studied in this work; one was provided to us by Achira Labs and one was made in-house using the blend fabric and commercial conductive inks.

5.4.1 Achira fabric-based electrode characterization

Once all the SERS and EC-SERS measurements were completed on the four biomarkers using the screen-printed-electrode and on the blend fabric, it was noticed that all these biomarkers could be detected using screen-printed-electrode, since the SERS signal can be rendered much stronger through application of a voltage. This was in stark contrast to the fabric-based SERS substrate, where only two of the four target biomarkers provided a useful SERS signal. However, the main goal of this research was to use fabric as a SERS substrate, which could then be incorporated into clothes to detect biomarkers from bodily fluids. Therefore, incorporating electrodes into a fabric sensor could be

beneficial and allow for more sensitive SERS-based sensing. Fabric-based electrodes were provided by Achira Labs (Bangalore, India). This silk-based electrode has three electrodes woven into the textile (working, reference, and counter electrode) as shown in Figure 5.4.1. These electrodes were prepared using a conductive carbon ink and Ag/AgCl ink. The carbon ink was coated on yarn using a specific instrument to make a counter electrode, and the working electrode was made by coating the carbon ink mixed with potassium ferricyanide on a stainless steel thread. Ag/AgCl ink was coated on the yarn to make the reference electrode.

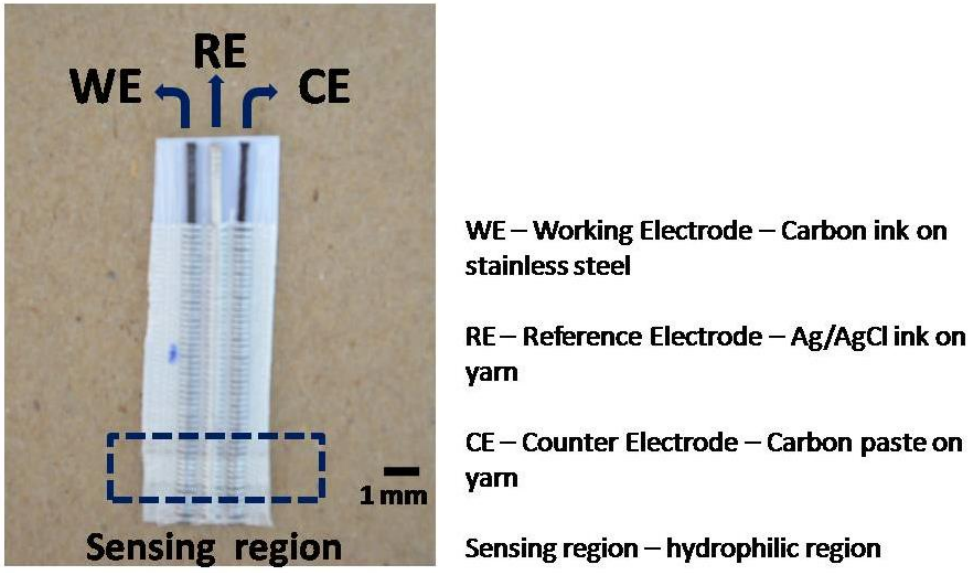

Figure 5.4.1: Fabric based electrode provided by Achira Labs.[133]

Three layers of 2µL silver nanoparticle paste was deposited on the working electrode as shown in Figure 5.4.2, which shows the coverage of AgNPs on the electrode surface. Due to the small size of the electrode, only 2µL was applied.

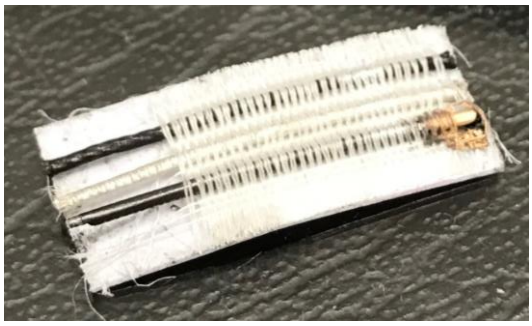

Figure 5.4.2: Achira Labs fabric-based electrode modified with three layers of AgNPs (2µL per layer).

Field emission scanning electron microscopy (FE-SEM) was used to characterize the fabric-based electrode, particularly the modified working electrode. By looking at the image in Figure 5.4.3, it is clear that the surface of the electrode was well covered by the near-monodisperse AgNPs.

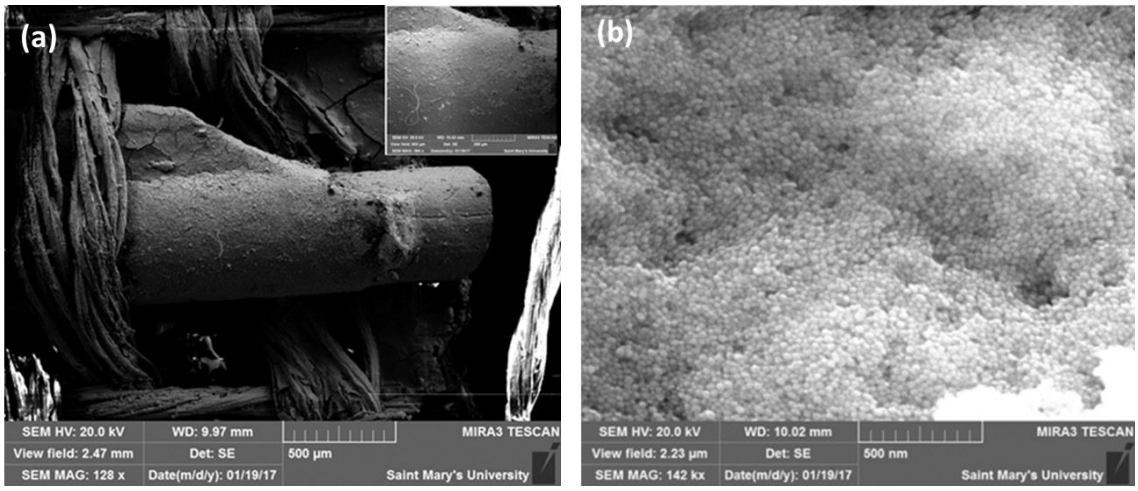

Figure 5.4.3: SEM image of fabric-based-SPE, (a) at low magnification, (b) at high magnification. SEM images were conducted using Tescan MIRA3 LMU Field Emission SEM under high vacuum mode at 10 kV, and at a scanning speed of 32.00 µs / pixel.

5.4.2 EC-SERS of 1.0 mM 4-ATP on Achira fabric-based electrode

In order to evaluate the EC-SERS of the fabric-based-electrode, a study was first conducted using 4-ATP, a strong Raman reporter. Firstly, the SERS signal of 5μL of 1.0 mM 4-ATP drop coated onto the surface at 10 different spots in air was collected as shown in Figure 5.4.4a, and the average of 10 spots is shown in Figure 5.4.4b. From these spectra, it is obvious that 4-ATP was successfully detected even though there was some spot to spot variation in the signal.

EC-SERS measurements of 1.0 mM 4-ATP were then conducted on the fabric-based-electrode after the carbon working electrode had been modified with three layers of AgNPs. After the KCl treatment, 1.0 mM 4-ATP was drop coated onto AgNP electrode, and the EC-SERS measurement was recorded using 0.1 M NaF as a supporting electrolyte. The major observation was that the 4-ATP signal gradually decreased, but the signal was still detectable as shown in Figure 5.4.5. The change in peak intensity with applied voltage suggested that the EC-SERS measurement worked properly, however, the signal was weaker than for the screen-printed electrode. After the EC-SERS study was performed, the modified electrode was prepared for SEM in order to evaluate the surface structure and stability of the AgNP after the EC-SERS measurement. Looking at Figure 5.4.6, it was obvious that AgNPs came off of the electrode surface in some areas, and energy dispersive x-ray spectroscopy (EDX) results confirmed that the black areas were carbon only. This was an important finding since it suggests that the adhesion between the AgNPs and the carbon was poor, and as a result the AgNPs came off during the measurement resulting in a drastic reduction of the SERS signal.

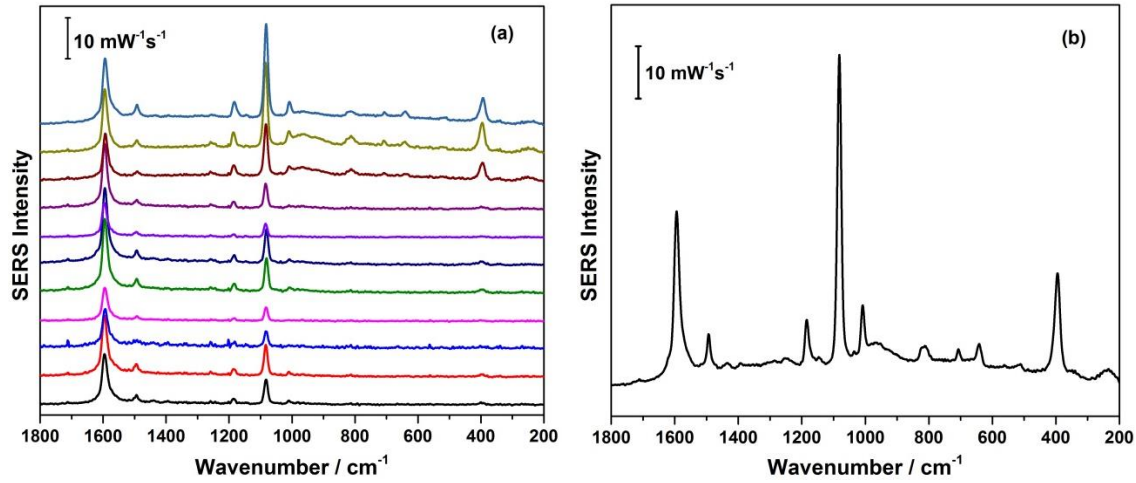

Figure 5.4.4: (a) SERS of 10 different spots 1.0 mM of 4-ATP on Achira fabric-based electrode modified with AgNPs and treated with 0.5 M KCl solution. Spectra were measured at 10.6 mW for a time interval of 30s, using 785 nm excitation. (b) The average of 10 spots.

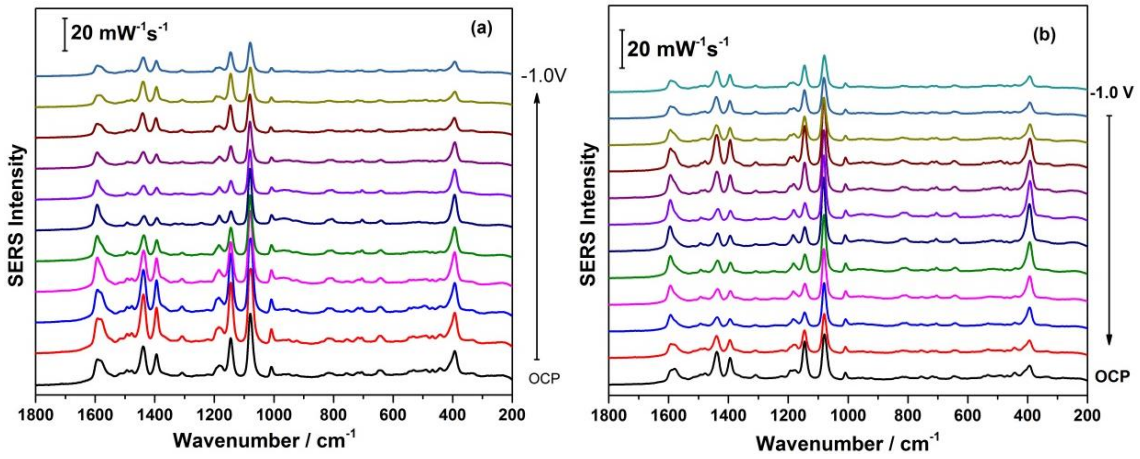

Figure 5.4.5: EC-SERS spectra for 1.0 mM 4-ATP at open circuit potential and applied potentials. Each spectrum acquisition time was 30 seconds at 22.3 mW, and 785 nm excitation. Supporting electrolyte was 0.1 M NaF. (a) cathodic direction, and (b) anodic direction.

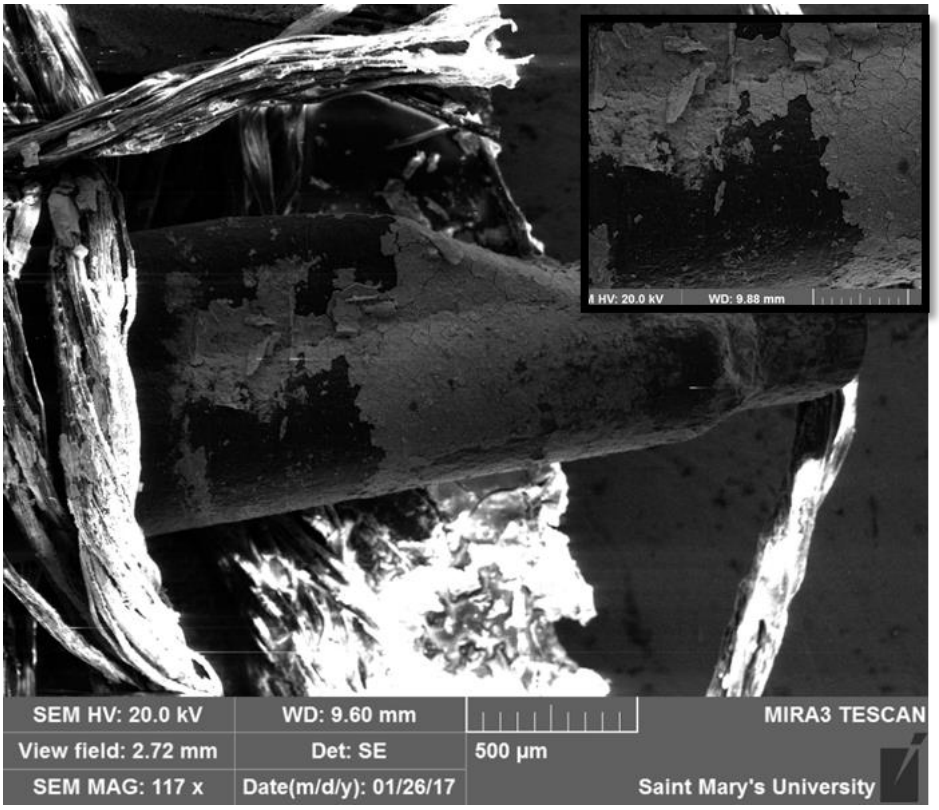

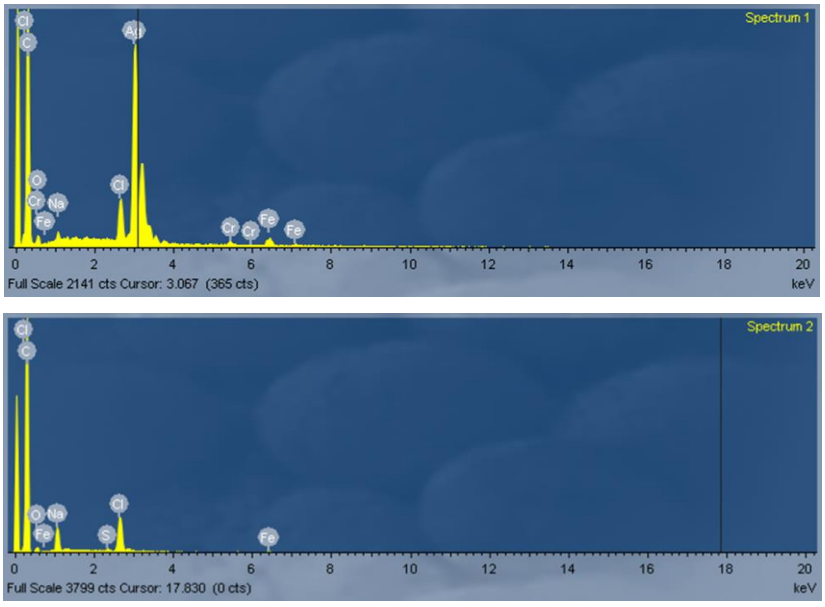

Figure 5.4.6: SEM images and EDX spectra of AgNPs modified fabric-based-SPE after EC-SERS measurement. SEM images were conducted using Tescan MIRA3 LMU Field

Emission SEM under high vacuum mode at 10 kV, and at a scanning speed of 32.00 µs / pixel.

5.4.3 EC-SERS of 6-TUA on Achira fabric-based electrode.

An EC-SERS study was performed on 1.0 mM 6-TUA (5µL was drop coated on the AgNP electrode), and the electrode was treated with KCl prior to EC-SERS measurement. The SERS signal was collected first at OCP and then at applied potentials from 0.0 V to -1.0 V. The signal for 6-TUA was detectable at OCP; however, after applying a negative voltage up to -1.0 V, the peak intensity decreased slightly (Figure 5.4.7a). When the voltage was then stepped back in the anodic direction the SERS signal increased slightly, as shown in Figure 5.4.7b.

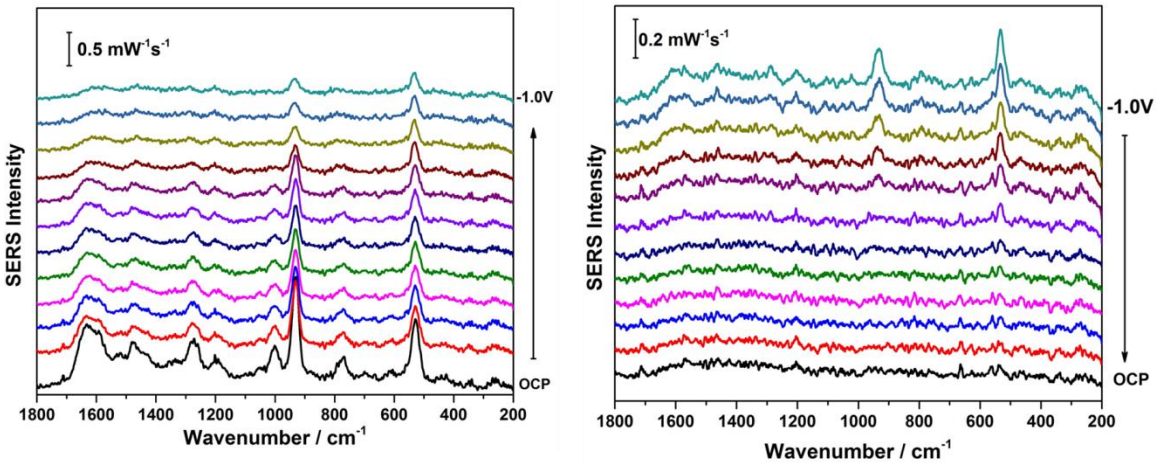

Figure 5.4.7: EC-SERS spectra for 1.0 mM 6-TUA at open circuit potential and applied potentials. (a) Cathodic, and (b) anodic direction. Each spectrum acquisition time was 30 seconds at 46.5 mW and 785 nm excitation. Supporting electrolyte was 0.1 M NaF.

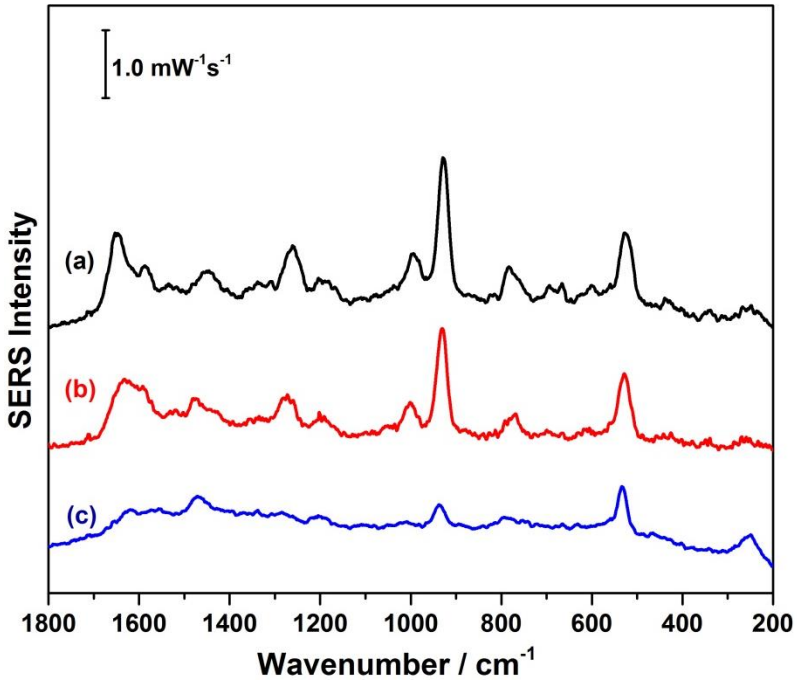

Figure 5.4.8: Comparison between SERS signal of 1.0 mM 6-TUA collected on (a) blend fabric (b) EC-SERS signal at OCP on fabric-based electrode (Achira Labs) and (c) EC-SERS signal at OCP on SPE, using 785 nm excitation, laser power was 46.5 mW.

By looking at Figure 5.4.8, it is clear that the intensity of the SERS signal for 6-TUA at OCP was comparable to the SERS intensity of 6-TUA on the blend fabric. On the screen-printed electrode at OCP, the SERS signal for 6-TUA was slightly reduced. Figure 5.4.9 provides an overlay of the EC-SERS signal for 6-TUA at -1.0 V for both the screen-printed electrode and the fabric-based electrode.

It is obvious that these two electrodes are behaving differently as the applied voltage is changed. One major concern was that there is poor adhesion of the AgNPs to the carbon electrode for the fabric-based-electrode and as a result some of the SERS-active surface coating may be lost during potential application.

Another issue with this electrode was that the size was small and all three electrodes (working, reference, and counter electrode) were close to each other. Due to the close proximity of the three electrodes, only a small quantity (2µL) of AgNPs could be applied to the working electrode at a time. For these reasons, the next step in this project was to make the fabric-based electrode in-house, using the blend fabric which was shown to be optimal for SERS.

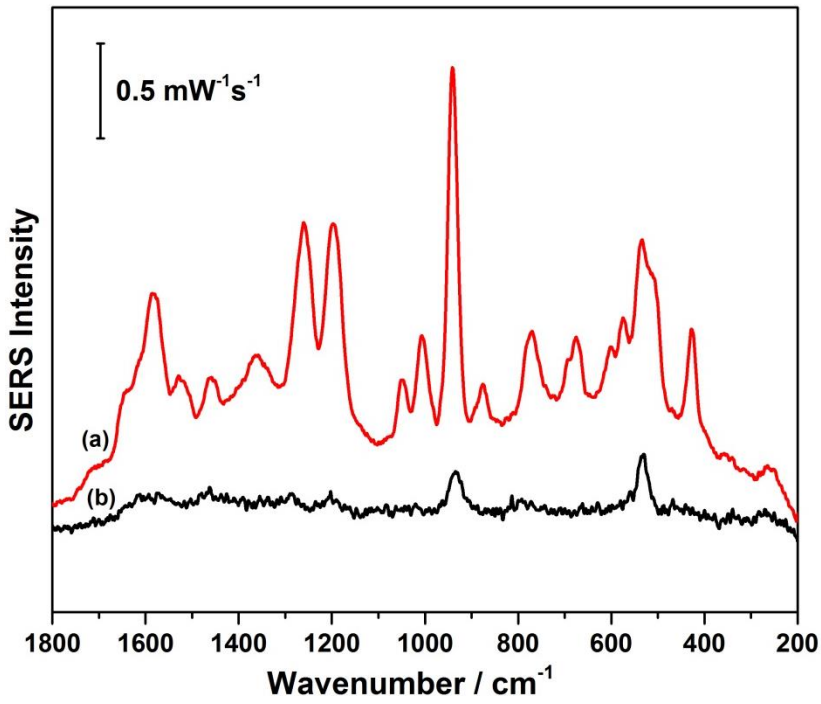

Figure 5.4.9: Comparison between EC-SERS of 1.0 mM 6-TUA at -1.0 V collected from (a) SPE and (b) Achira fabric-based electrode. The spectra were measured at 46.5 mW for a time interval of 30 seconds using 785 nm excitation.

5.4.4 EC-SERS of biomarkers on blend fabric-based electrode

5.4.4.1 Blend fabric-based electrode characterization

This new fabric electrode was made from blend fabric which was shown to be optimal for SERS in this thesis work. This blend fabric electrode was designed in-house

(4 cm x 1.5 cm). Once the conductive inks were applied using a stencil, AgNPs were drop coated onto the working electrode (4 µL x 3 layers) as seen in Figure 5.4.10.

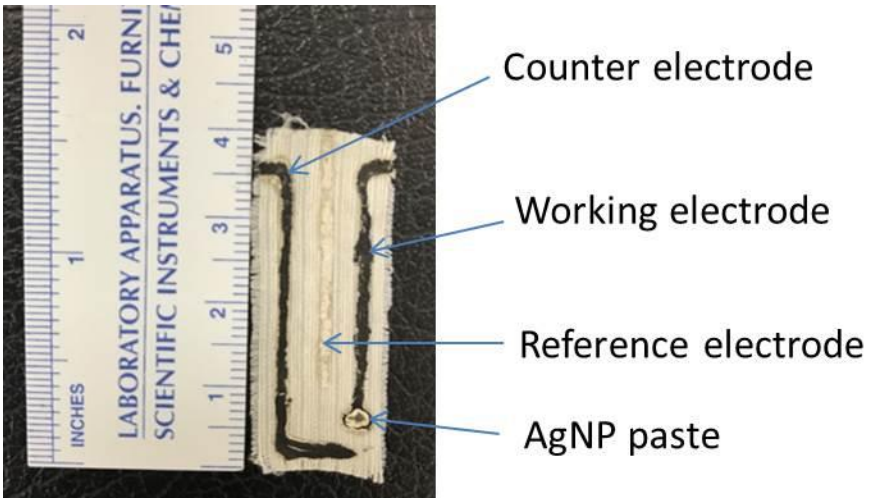

Figure 5.4.10: Blend fabric-based electrode modified with 3 layers of AgNPs.

SEM was performed on the fabric-based working electrode before and after the EC-SERS measurement in order to evaluate the surface coverage of AgNPs on the working electrode. As shown in Figure 5.4.11a, prior to the EC-SERS measurement there were some black areas which indicated that the adhesion of the NPs was not strong, and also after conducting the EC-SERS investigation, more NPs came off of the surface which resulted in a decreased SERS signal.

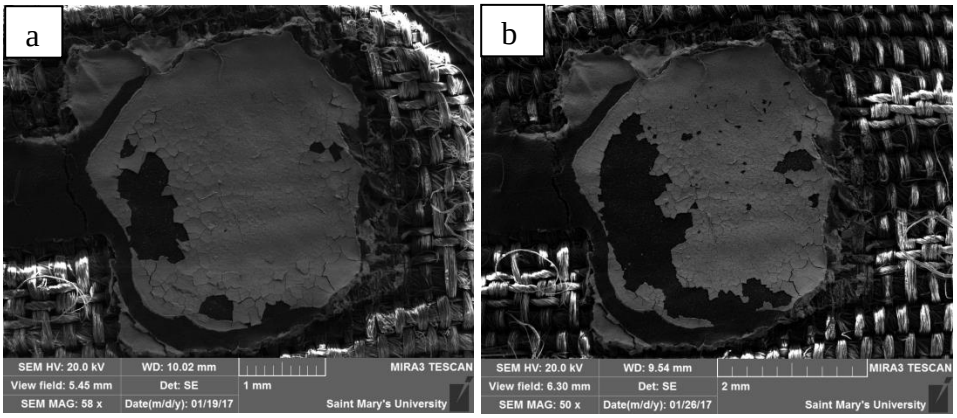

Figure 5.4.11: SEM image of blend fabric-based working electrode modified with AgNP. (a) before EC-SERS (a), and after EC-SERS (b). SEM images were conducted using Tescan MIRA3 LMU Field Emission SEM under high vacuum mode at 10 kV, and at a scanning speed of 32.00 µs / pixel.

5.4.4.2 EC-SERS of 1.0 mM 6-TUA

An EC-SERS study was performed on 1.0 mM 6-TUA in 0.1 M NaF supporting electrolyte, and the signal was collected at OCP and at applied potentials (0.0V to -1.0V). Looking at Figure 5.4.12a, it is evident that the signal was noisy; however, the 6-TUA peaks were present. Moreover, the 6-TUA peaks increased when the potential decreased, this increase of the signal was noted until -0.8V, and then all of the 6-TUA peaks disappeared, and when the voltage was then stepped back in the anodic direction (-1.0 V to 0.0 V), the 6-TUA signal did not return. Again, this suggested that AgNP electrode was not stable.

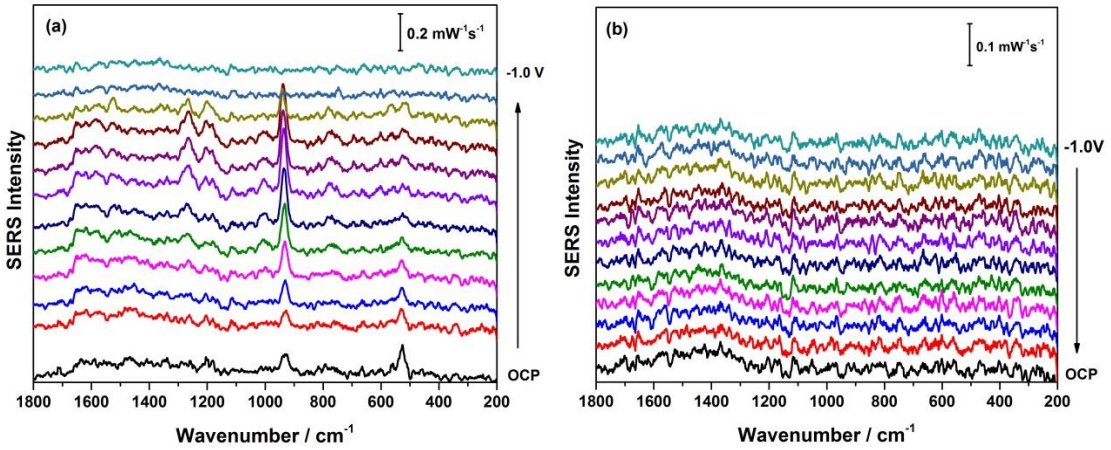

Figure 5.4.12: EC-SERS spectra for 1.0 mM 6-TUA at open circuit potential and applied potentials. Each spectrum acquisition time was 30 seconds (46.5 mW) at 785 nm excitation. Supporting electrolyte was 0.1 M NaF. (a) Cathodic, (b) Anodic.

From the OCP comparison in Figure 5.4.13, the EC-SERS signal from the fabric-based electrode made from conductive inks was comparable to the signal collected from the commercial SPE, although noisier. This observation indicated that this fabric-based electrode was promising. However, upon application of a voltage, the signal decreased as shown in Figure 5.4.14, which indicated that although 6-TUA was initially successfully detected, the adhesion of the NPs was poor, and resulted in a deterioration of the SERS signal upon application of a voltage.

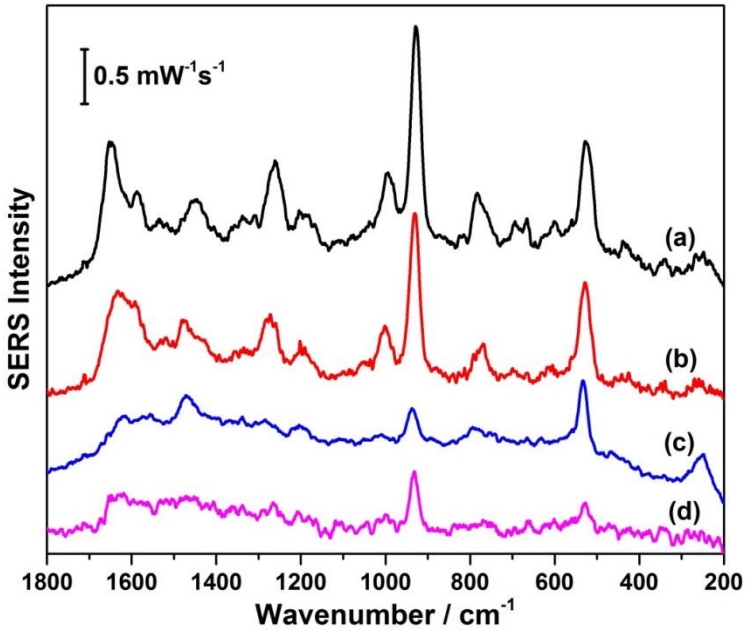

Figure 5.4.13: Comparison between SERS of EC-SERS of 1.0 mM 6-TUA at OCP (a) on blend fabric, (b) on Achira fabric-based electrode, (c) screen-printed electrode and (d) blend fabric-based electrode (made from conductive inks). Each spectrum acquisition time was 30 seconds (46.5 mW) at 785 nm excitation.

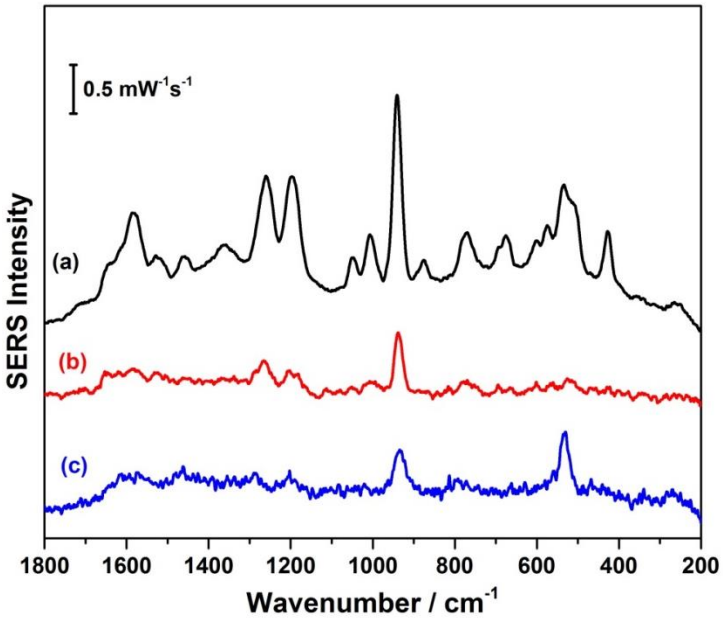

Figure 5.4.14: EC-SERS signal of 1.0 mM 6-TUA at -1.0 V, on (a) screen-printed electrode, (b) fabric-based-electrode (Achira Labs) and (c) blend fabric-based-electrode (made from conductive inks). Spectra were measured at 46.5 mW, in a time interval 30s, using 785 nm excitation.

5.4.5 Conclusion

In summary, the fabric-based electrode has been explored and was promising. A strong SERS signal of 4-ATP was obtained and also for the biomarker 6-TUA. EC-SERS spectra of 1.0 mM 6-TUA on the Achira fabric-based electrode and the blend fabric-based electrode were observable at OCP, however, upon application of a voltage, the SERS signal increased and then disappeared for both fabric-based electrodes. Further study indicated that this was due to poor adhesion between the AgNPs and the carbon electrode, which caused significant loss of some of the SERS-active surface coating during potential application. Further studies should be conducted on improving the adhesion between the AgNPs and the carbon electrode.

Chapter 6 Conclusions and Future work

The demand for new diagnostic techniques for detecting disease biomarkers at the patient point-of-care (POC) has recently increased. POC diagnostics can help to detect disease earlier, leading to more timely and effective treatment. In this work, surface-enhanced Raman spectroscopy (SERS) was explored as a POC detection modality using fabric-based SERS substrates.

Four urine biomarkers (6-TUA, levofloxacin, guanine, and 2-deoxyguanosine) were tested first using electrochemical surface enhanced Raman spectroscopy on commercially available screen-printed-electrodes. These biomarkers were prepared in synthetic urine and drop coated onto the surface of the electrode that was modified with AgNPs. Strong SERS signal was observed for 6-TUA, levofloxacin, and guanine. The SERS signal for 2-deoxyguanosine was weaker, but still detectable. One thing that was noticed in all the SERS and EC-SERS spectra is the presence of the citrate peaks which cause interference with the target analyte. This problem was solved by incubating the electrode in 0.5 M KCl followed by rinsing with ultrapure water. This step was important to displace all surface-adsorbed citrate so as to improve the intensity of the SERS signal.

The main goal of this thesis work was to develop a fabric-based plasmonic sensor. This fabric could then be incorporated into garments such as a head bands, t-shirts, or cloth diapers to detect biomarkers present in bodily fluids of the wearer. Five sustainable fabrics were characterized and evaluated for SERS after modification with AgNPs. Bamboo, hemp, white and dyed cotton, and blend were selected as sustainable fabrics with excellent moisture absorption properties. The fabric samples were characterized first

using Raman spectroscopy and SEM in order to understand the nature of the fabric surfaces. 4,4'-bipy and 4-ATP were used to evaluate the SERS performance of these fabrics. All the fabric samples were tested first using one layer of silver nanoparticles, after which it was clear that three layers were needed to ensure good coverage of the textile fibers with AgNPs, and hence stronger SERS signals could be obtained. KCl treatment of the modified textiles was also found to be necessary for adequate signal detection. From the comparison of the SERS signals on the selected fabrics, it was clear that the blend fabric showed the stronger SERS signal for both 4,4'-bipy and 4-ATP, and therefore the blend was selected as the most promising fabric substrate for this thesis work. Once the fabric selection and characterization was completed, the biomarkers were tested on the blend fabric. 6-TUA and guanine were successfully detected, while levofloxacin and 2-deoxyguanosine were not detected. Since earlier EC-SERS studies had shown success in detecting all four target biomarkers, it was concluded that the ability to apply a voltage to the SERS-active substrate is key, and as a result fabric-based electrodes were then explored as part of this thesis work.

The first fabric-based electrode explored was provided by Achira Labs. The carbon working electrode was modified with AgNPs, and then treated with KCl to remove adsorbed citrate. 4-ATP was first tested as a strong Raman probe, and then 1.0 mM 6-TUA was tested. Strong SERS signal for 4-ATP was obtained, and also strong SERS signal of 6-TUA was observed at OCP. However, upon application of a voltage the signal decreased markedly. Based on SEM investigations, the decrease of the signal was shown to be the result of poor adhesion of the AgNPs on the carbon electrode surface.

When the voltage was applied, the AgNPs came off of the surface, resulting in a significant decrease in the SERS-active surface coating. Similar results were obtained for a fabric-based electrode prepared in-house using the blend fabric.

This thesis work has thoroughly explored the use of sustainable woven textiles for use as SERS-active substrates, with a goal towards eventual integration into wearable sensor technology. While the blend fabric was shown to have the most promise, significant challenges were still observed due to poor interaction between the silver nanoparticle surface and the target molecule. Through the use of electrochemical SERS, it was observed that all biomarkers of interest in this work could be monitored, and hence future explorations in this area should focus on fabric-based electrodes for fabric-based SERS sensing. In order to make progress in this area, future work should focus on improving the nature of the adhesion between the silver nanoparticles and the conductive carbon ink.

Chapter 7 References

1. Choi, S. J., Jiang, Z. W. *Sens. Actuators*. **2006**, 128, 317–326
2. Atalay, O., Kennon, W. R., *Sensors*, **2014**, 14, 4712–4730.
3. Lee, Y. D., W, Y., Chung, W. Y., *Sens. Actuators.* **2009**, 140, 390–395.
4. Windmiller, J. R., Wang, R, J. *Electroanalysis*. **2013**, 25, 29–46.
5. Wu, S. C. Y., Lau, S.K. T., Wallace, B. G., and Diamond, D. *Wearable and Implantable*. **2007**, 13, 1345-1356
6. Calafat, J. A. M., Ye, W. X., Jia, L.T., Hu, S. H., Huttner, R. K., Hauser, R. Environ. *Health Perspect*. **2009**, 117, 639–644.
7. Browne, W. R., McGarvey, J. J., *Coord. Chem. Rev*. **2007**,251, 454-473
8. Foudeh, A. M., Didar, T. F., Veres, T., Tabrizian, M. *Lab on a Chip*. **2012**, 12(18), 3249-3266.
9. Sharma, S., Zapatero-Rodríguez, J., Estrela, P., O'Kennedy, R. *Biosensors*. **2015**, *5*(3), 577-601
10. Tüdős, A. J., Besselink, G. A., Schasfoort, R. B. *Lab on a Chip*, **2001**. *1*(2), 83-95.
11. Gubala, V., Harris, L. F., Ricco, A. J., Tan, M. X., Williams, D. E. *Analytical chemistry*. **2011**, *84*(2), 487-515.
12. Ottiger, C., Gygli, N., Huber, A. R., Fernandez-Tresguerres, B., Pardo, S., Petruschke, T. *Journal of diabetes science and technology*. **2016**, 1932296816638854.
13. Zumla, A., Al-Tawfiq, J. A., Enne, V. I., Kidd, M., Drosten, C., Breuer, J., Mwaba, P. *The Lancet Infectious Diseases*. **2014**, *14*(11), 1123-1135.
14. Wang, J. *Biosensors and Bioelectronics*. **2012**, *21*(10), 1887-1892.
15. St John, A., Price, C. P. *The Clinical Biochemist Reviews*. **2014**, *35*(3), 155.
16. Chin, C. D., Linder, V., Sia, S. K. *Lab on a Chip*. **201**2, *12*(12), 2118-2134.
17. Patel, S., Park, H., Bonato, P., Chan, L., Rodgers, M. *Journal of neuroengineering and rehabilitation*. **2012**. *9*(1), 1.
18. Bourke, A. K., vande Ven, P. W., Chaya, A. E., OLaighin, G.M., Nelson, J. *Conf Proc IEEE Eng Med Biol Soc*. **2008**, 2844-2847.
19. Pantelopoulos, A., Bourbakis, N. G. *IEEE Transactions on Systems, Man, and Cybernetics, Part C (Applications and Reviews)*. **2010**. *40*(1), 1-12.
20. Bonato P. *IEEE Eng Med Biol Mag.* **2010**, 29 :25-36
21. Teng, X.F., Zhang. Y.T., Poon, C.Y., Bonato, P. *IEEE Reviews in Biomedical Engineering.* **2008**, 1:62-74
22. Giansanti, D., Maccioni, G., Morelli, S. *Telemed J E Health.* **2008**, 14, 467-472.
23. Sazonov, E. S., Fulk, G., Sazonova, N., Schuckers, S. *Conf Proc IEEE Eng Med Biol Soc*. **2009**, 2200-2203.
24. Aziz, O., Atallah, L., Lo, B., Elhelw, M., Wang, L., Yang, G.Z., Darzi, A. *Surg Innov*

2007, 14, 83-90.
25. Amft, O., Troster, G. *Artif Intell Med*. **2008**, 42, 121-136.
26. AlertOne medical alert system. http://www.alert-1.com (accessed October 29, 2016).
27. Automatic Fall Detection. http://www.wellcore.com/learn/automatic-fall-detection (accessed November 1, 2016).
28. myHalo. http://www.halomonitoring.com (accessed November 1, 2016).
29. Giansanti, D., Ricci, G., Maccioni G. *Telemed J E Health.* **2008**, 14,1130-1135
30. Lee, Y.D., Chung, W.Y. *Sensors and Actuators B: Chemical*. **2009**, 140(2), 390-395.
31. Chan, L., Hart, L.G., Goodman, D.C. *J Rural Health.* **2006**, 22,140-146
32. Cervinski, M. A., Gronowski, A. M., *Clinical chemistry and laboratory medicine*, **2010.** *48*(7), pp.935-942.D.
33. Choi, S., Zhongwei, J. *Sensors and Actuators A*. **2006**, 128, 317-326.
34. Collins, G. E., Buckley, L. J. *Synthetic Metals*. **1996**, 78, 93-101.
35. Windmiller, J.R., Wang, J. *Electroanalysis*. **2013**, 25: 29-46.
36. Capineri, L. *Procedia Engeering* **2014**, (87), 724-727.
37. Pandian , P. S., Mohanavelu, K., Safeer, K. P., Kotresh,T. M., D. T., Shakunthala, D. T., Gopal, P., Padaki, V.C. *Med. Eng. Phys*. **2008**, 30 , pp.466 -477
38. Coosemans, J.; Hermans, B.; Puers, R. A Phys. **2006**, 130, 48–53.
39. Pelton, M., Bryant, G. W. *Introduction to metal-nanoparticle plasmonics*.**2013,** (5), John Wiley & Sons.
40. Rotello, V. *Nanoparticles: Building Blocks for Nanotechnology*. *Plasmonic Nanomaterials*. Wei. A. University of Massachusetts, Amherst Massachusetts. **2004**
41. Roh, S., Chung, T., Lee, B. *Photonics Asia*. **2010,** (pp. 785303-785303). International Society for Optics and Photonics.
42. Rycenga, M., Cobley, C. M., Zeng, J., Li, W., Moran, C. H., Zhang, Q., Qin, D., Xia, Y. *Chem Rev*. **2011**, 111, 3669-3712
43. Tong, L., Wei, H., Zhang, S., Xu, H. *Sensors*. **2014**, *14*(5), 7959-7973
44. Unser, S., Bruzas, I., He, J., Sagle, L. *Sensors*. **2015**, *15*(7), 15684-15716.
45. Preechaburana, P., Gonzalez, M. C., Suska, A., Filippini, D. *Surface plasmon resonance chemical sensing on cell phones,* Angew. Chem Int'l Ed. **2012**, 51, pp. 11585–11588.
46. Cao, G., Wang, Y. *Nanostructures and Nanomaterials: Synthesis, Properties, and Applications*. 2ndED. University of Washington, USA.**2011**
47. Jeyaraj, M., Sathishkumar, G., Sivanandhan, G., MubarakAli, D., Rajesh, M., Arun, R., Ganapathi, *Colloids and surfaces B: Biointerfaces*. **2013**, *106*, 86-92.
48. Zhang, X. F., Liu, Z. G., Shen, W., Gurunathan, S. *International Journal of Molecular Sciences*. **2016**, *17*(9), 1534.
49. Sondi, I., Salopek-Sondi, B. *Journal of colloid and interface science*. **2004**, *275*(1), 177-182.

50. Rai, M., Yadav, A., Gade, A. *Biotechnology advances*. **2009**, *27*(1), 76-83.
51. Pelletier, M. J. *Analytical Applications of Raman Spectroscopy*, Michigan, USA: Blackwell Science Ltd., **1999**.
52. Movasaghi Z., Rehman S., Rehman I. U. *Appl. Spectrosc. Rev.* **2007**, *42*, 493-541.
53. Harris, D.C., Bertolucci, M. D. *Symmetry and Spectroscopy: An Introduction to Vibrational and Electronic Spectroscopy*; Dove Publication: New York, **1989**, pp 93-97, 151-159.
54. Robinson, A. M., Harroun, S. G., Bergman, J., Brosseau C. L. *Anal. Chem*. **2012**, *84*, 1760-1764.
55. Doering, W. E., Piotti, M. E., Natan, M. J., Freeman, R. G. *Adv. Mater*. **2007**, *19*, 3100-3108.
56. Lyandres, O., Shah, N. C., Yonzon, C. R., Jr. Walsh, J. T., Glucksberg, M. R., Van Duyne, R. P. *Anal.Chem.* **2005**, *77*, 6134-6139.
57. Bantz, K. C., Meyer A.F., Wittenberg A.J., Im H., Kutulus Ö., Lee S.H., Lindquist N.C., Oh S.H., Haynes C.L. *Phys. Chem. Chem. Phys*. **2011**, *13*, 11551-11567.
58. Zhang, X., Shah, N. C., & Van Duyne, R. P. (2006). Sensitive and selective chem/bio sensing based on surface-enhanced Raman spectroscopy (SERS).*Vibrational Spectroscopy*, *42*(1), 2-8.
59. Granger, J. H., Granger, M. C., Firpo, M. A., Mulvihill, S. J., Porter, M. D. *Analyst*. **2013**. *138*(2), 410-416.
60. Kim, I., Lee, M., Lee, S., Lee, E. K., Chang, S. I., & Choo, J .*Journal of Molecular Structure*, **2012**. *1023*, 197-203.
61. Zhang, X., Young, M. A., Lyandres, O., Van Duyne, R. P. *Journal of the American Chemical Society*. **2005**, *127*(12), 4484-4489.
62. Lee, M., Lee, K., Kim, K. H., Oh, K. W., Choo, J.. *Lab on a Chip*. **2012**, *12*(19), 3720-3727.
63. Wen, R., Fang, Y.. *Journal of colloid and interface science*. **2005**. *292*(2), 469-475.
64. Botta, R., Rajanikanth, A., Bansal, C. *Sensing and Bio-Sensing Research*. **2016**, *9*, 13-16.
65. Goodall, B. L., Robinson, A. M., Brosseau, C. L. *Phys. Chem. Chem. Phys*. **2013**, *15*, 1382−1388.
66. Zhao, L., Blackburn, J., Brosseau, C. L. *Anal. Chem.* **2015**, *87*, 441−447.
67. PiĢta, E., Proniewicz, E., Kudelski, A., Olszewski, T. K., Boduszek, B. *Vibrational Spectroscopy*. **2016**, *83*, 115-125.
68. Pergolese, B., Bonifacio, A., Biotto, A. *Phys. Chem. Chem. Phys*. **2005**, 7, 3610.
69. Yigit, T., Akdogan, E., Karagoz, I. D., Kahraman, M. In *SPIE BiOS*. **2016**, 970411-970411
70. Karaballi, R., Nel, A., Krishnan, S., Blackburn, J., Brosseau, C. L. *Phys. Chem. Chem. Phys*. **2015**, *17*, 21356-21363.

71. Robinson, A. M., Zhao, L., Alam, M. Y. S., Bhandari, P., Harroun, S. G., Dendukuri, D., Blackburn, J. and Brosseau, C. L. *Analyst*, **2015**, 140, 779-785.
72. Kim, K., Lee, H. B., Lee, J. W., Shin, K. S. *Colloid Interface Sci*. **2010**, 345, 103–108
73. Ballerini, D. R., Ngo, Y. H., Garnier, G., Ladewig, B. P., Shen, W., Jarujamrus, P. *AIChE J*., **2014**, 60, 1598-1605.
74. Liu, J., Zhou, J., Tang, B., Zeng, T., Li, Y., Li, J., Wang, X. *Applied Surface Science*. **2016**, *386*, 296-302.
75. Kurouski, D., Large, N., Chiang, N., Greeneltch, N., Carron, K.T., Seideman, T., Schatz, G.C. and Van Duyne, R.P. *Analyst*, **2016**.*141*(5),1779-1788.
76. Herberman, R. B., Ortaldo, J. R. *Science.* **1981**, *214*, 24−30.
77. Sorouraddin, M. H., Khani, M. Y., Amini, K., Naseri, A., Asgari, D., Rashidi, M. R. *Bioimpacts*. **2011**, *1*(1), 53-62.
78. Miller, R. W., Young, J. L., Novakovic, B. *Cancer*. **1995**, *75*, 395−405.
79. Lennard, L. *Eur. J. Clin. Pharmacol.* **1992**, *43*, 329−339.
80. Wang, L., Zhang, Z. *Talanta* **2008**, *76*, 768−771.
81. Chrzanowska, M., Flig, E., Krzymanski, M. *Chem. Anal. (Warsaw)* **1992**, *37*,391−397.
82. Chalmers, A. H. A *Biochem. Med. Metab. B.* **1975**, *12*, 234−241.
83. Ensafi, A. A., Karimi-Maleh, H. *Drug Test. Analysis* **2012**, *4*, 970−977.
84. Karadas-Bakirhan, N., Sarakbi, A., Vandeput, M., Ozkan, S. A., Kauffmann, J. M. *Anal. Chem.* **2015**, *87*, 6730−6735.
85. Karimi-Maleh, H., Tahernejad-Javazmi, F., Atar, N. Yola, M. L., Gupta, V. K., Ensafi, A. A. *Ind. Eng. Chem. Res.* **2015**, *54*, 3634−3639.
86. Kalra, S., Paul, M. K., Balaram, H., Mukhopadhyay, A. K. *J. Chromatography*, **2007.** 850(1), 7-14.
87. North, D. S., Fish, D. N., Redington, J. J. *Pharmacotherapy*, **1998**, 18, 915–935.
88. Pote, S., Tiwari, P., D'cruz, S. *Pharmacy Practice (Internet)*, **2007**. *5*(1), 17-20.
89. Hidi, I., Jahn, M., Pletz, M., Weber, K., Cialla-May, D., Popp, J. *The Journal of Physical Chemistry C*, **2016**, *120*(37), 20613-20623.
90. Hidi, I., Jahn, M., Weber, K., Cialla-May, D., Popp, J. *Physical Chemistry Chemical Physics*,**2015**, *17*(33), 21236-21242.
91. Djabarouti, S., Boselli, E., Allaouchiche, B., Ba, B., Nguyen, A.T., Gordien, J.B., Bernadou, J.M., Saux, M.C. and Breilh, D., *Journal of Chromatography B*, **2004**, *799*(1),165-172.
92. Liang, H., Kays, M.B. and Sowinski, K.M. *Journal of Chromatography B*, **2002**, *772*(1), 53-63.
93. Campos, C., Guzmán, R., López-Fernández, E. and Casado, Á. *Life sciences*, **2011**, *89*(17), 655-661.
94. Al-Saleh, I., Abduljabbar, M., Al-Rouqi, R., Elkhatib, R., Alshabbaheen, A.

Shinwari, N. *Biol Trace Elem Res*. **2013**, 153, 145–154.
95. Ding, G., Han, S., Wang, P., Gao, Y., Shi, R., Wang, G. and Tian, Y. *Environmental pollution*, **2012**, *167*,110-114.
96. Wang, H., Lv, S., Li, F., Liu, Q. and Ke, S. *Science of the Total Environment*. **2010**, 408, 6092–6099.
97. Zhang, S., Song, X., Zhang, W., Luo, N. and Cai, L. *Science of the Total Environment*. **2013**, 450-451: 266-270.
98. Kundu, L. M., Loppnow, G. R. *Photochemistry and Photobiology*. **2007**, 83, 600–602.
99. Wang, H., Lv, S., Li, F., Liu, Q. and Ke, S. *Science of the Total Environment*. **2010**, 408, 6092–6099.
100. Ding, G., Han, S., Wang, P., Gao, Y., Shi, R., Wang, G. and Tian, Y. *Environmental Pollution.* **2012**, 167: 110-114.
101. Garratt, L.W., Mistry, V., Singh, R., Sandhu, J.K., Sheil, B., Cooke, M.S. and Sly, P.D. *Free Radical Biology & Medicine.* **2010**, 48, 1460–1464.
102. Darwish, I. A., Wani, T. A., Khalil, N.Y., Aboul-Fadl, T., Kadi, A. A., Al-Majed, A. R. A. *Anal. Methods*, **2013**, 5, 1502–1509
103. Campos, C., Guzmán, R., López-Fernández, E. and Casado, Á. *Life sciences*, **2011**, *89*(17), 655-661.
104. Barregard, L., Møller, P., Henriksen, T., Mistry, V., Koppen, G., Rossner Jr, P., Sram, R. J., Weimann, A., Poulsen, H. E., Nataf, R. and Andreoli, R. *Antioxidants & Redox Signaling*. **2013**, 18, 2377-2391.
105. Jayanth, N., Ramachandran, S. and Puranik, M. *J. Phys. Chem. A.* **2009**, 113, 1459–1471.
106. Wang, J. *Analytical Electrochemistry, 2nd ed.*, New York, USA: Wiley-VCH, **2000**.
107. Bard, A. J., Faulkner, L. R. *Electrochemical methods: Fundamentals and applications, second edition*; John Wiley & Sons, Inc.: New York, **2001**, p 26.
108. Wang, H., Pilon, L. *Electrochimica Acta*. **2012**, *64*, 130-139.
109. Shaw, D. J. *Introduction to Colloid and Surface Chemistry*, Reed Educational and Professional Publishing Ltd., **1992**, pg. 64-96.
110. Zoski, C. G. *Handbook of Electrochemistry, 1st ed.*; Amsterdam, Netherlands: Elsevier, **2007**, pp 22-24
111. Ren, B., Cui, Y., Wu, D.Y., Tian, Z. Q. *Electrochemical SERS and its Application in Analytical, Biophysical and Life Science*, Weinheim, Germany: Wiley-VCH Verlag & Co. **2011**, pp 191-193.
112. Fleischmann, M., Hendra, P. J., McQuillan, A. *J. Chem. Phys. Lett.* **1974**, *26*, 163-166.
113. Jeanmaire, D. L., Van Duyne, R. P. *J. Electroanal. Chem.* **1977**, *84*, 1.
114. M. G. Albrecht, J. A. Creighton. *J. Am. Chem. Soc.*, **1977,** *99*, 5215-5217.

115. Stiles, P. L., Dieringer, J. A., Shah, N. C., Van Duyne, R. P. *Annu. Rev. Anal. Chem*. **2008**, *1*, 601-626.
116. Porter, M. D., Lipert, R. J., Siperko, L. M., Wang, G., Narayanan, R. *Chem. Soc. Rev*. **2008**, *37*, 1001-1011.
117. Haynes, C. L., McFarland, A. D., Van Duyne, R. P. *Anal. Chem*. **2005**, *77*, 338A-345A.
118. Aroca, R. Surface-Enhanced Vibrational Spectroscopy, 1st ed.; Wiley: England, 2006
119. Dick, L. A., McFarland, A. D., Haynes, C. L. and Van Duyne, R. P. *The Journal of Physical Chemistry B*. **2002**, *106*(4), 853-860.
120. Zhang, X., Yonzon, C. R. and Van Duyne, R. P. In *Proc. of SPIE Vol* **2003**, (Vol. 5221, p. 83).
121. Alvarez-Puebla, R. A., Liz-Marzán, L. M. *Small*. **2010**, *6*(5), pp.604-610.
122. Chrzanowska, M., Flig, E., Krzymanski, M. *Chem. Anal. (Warsaw)* **1992**, *37*,391−397.
123. Chalmers, A. H. A. *Biochem. Med. Metab. B.* **1975**, *12*, 234−241
124. Gunasekaran, S., Rajalakshmi, K. and Kumaresan, S. *Spectrochimica Acta Part A: Molecular and Biomolecular Spectroscopy*. **2013**, 112,351-363.
125. Otto, C., van den Tweel, T. J. J., de Mul, F. F. M., Greve, J. *J. Raman Spec*. **1986**, *17*, 289-298.
126. Giese, B., McNaughton, D. *Biopolymers*. **2003**, *72*, 472-489.
127. Singh, S., Srivastava, K., Donfack, P., Schlucker, S., Materny, A.,Asthana, B. P. *Phys. Chem. Chem. Phys.* **2012**, *14*, 14315–14324.
128. Schlucker, S. Surface Enhanced Raman Spectroscopy: Analytical, Biophysical and life Science Applications. *Electrochemical SERS and its Application in Analytical, Biophysical and Life Science.* Ren, B., Wu, Y. C., Tian, Z. University of Wurzburg and Eisingen.**2011**
129. Zhuang, Z., Ruan, W., Ji, N., Shang, X., Wang, X. and Zhao, B. *Vibrational Spectroscopy*. **2009**, *49*(2), 118-123.
130. Liang, E.J., Engert, C., Kiefer, W. *Vib. Spec*. **1995**, 8, 435-444
131. Dendisova, M., Havranek, L., Oncak, M., Matejka, P. *J. Chem. C*. **2013**, 117, 21245-21253
132. Matulaitienė, I., Kuodis, Z., Eicher-Lorka, O., Niaura, G. *J. Electoanal. Chem*. **2013**, *700*, 77-85.
133. Choudhary, T., Rajamanickam, G. P., Dendukuri, D. *Lab on a Chip*, **2015**. *15*(9), 2064-2072.